Winter 2017

UNRAVELING SHORT-TERM VARIATIONS IN TIDEWATER GLACIER FLOW: INSIGHTS FROM TERRESTRIAL RADAR INTERFEROMETRIC STUDIES

Ryan Cassotto
University of New Hampshire, Durham

UNRAVELING SHORT-TERM VARIATIONS IN TIDEWATER GLACIER FLOW: INSIGHTS FROM TERRESTRIAL RADAR INTERFEROMETRIC STUDIES

BY

RYAN K. CASSOTTO

B.S., University of Hartford, 1999

M.S., University of New Hampshire, 2011

DISSERTATION

Submitted to the University of New Hampshire
in Partial Fulfillment of
the Requirements for the Degree of

Doctor of Philosophy

in

Earth and Environmental Sciences

December 2017

This thesis/dissertation has been examined and approved in partial fulfillment of the requirements for the degree of Doctor of Philosophy in Earth and Environmental Sciences by:

Dissertation Director, Margaret S. Boettcher, Associate Professor of Earth Sciences

Mark Fahnestock, Affiliate Research Professor of Earth Sciences

Joseph M Licciardi, Professor of Earth Sciences

Jason M. Amundson, Associate Professor of Geophysics
University of Alaska Southeast, Juneau, AK 99801

Martin Truffer, Professor of Physics
University of Alaska Fairbanks, Fairbanks, AK 99775

On November 2, 2017

Original approval signatures are on file with the University of New Hampshire Graduate School.

DEDICATION

To Megan, Logan, and Julia – Thank you! Your sacrifices helped make this a reality.

ACKNOWLEDGEMENTS

I started this journey several years ago with little more than a handful of ideas, a great deal of motivation, and a healthy dose of optimism. I was quite fortunate to gain the support and encouragement of many people along the way that helped frame this research, and to whom I owe a great debt of gratitude.

I am truly grateful to my committee for their expertise, commitment, and patience. Early on, I was lucky enough to convince Mark Fahnestock, my primary advisor and committee co-chair, to serve as my mentor as I started graduate school as a non-traditional student. He constantly challenged me to explore new and exciting opportunities and to approach solutions to problems by thinking far outside the box. He provided tremendous field experiences in Greenland and Alaska, and generously supported me through various research grants for several years. Mark and Judy welcomed me into their home on several occasions – in New Hampshire, Alaska, and Denmark. I am incredibly grateful to Margaret Boettcher, my UNH advisor and committee chair, who kept an open mind and ventured into glaciology despite her expertise in seismology and rock mechanics. Margaret welcomed me into her geophysics group and was a tremendous supporter and mentor to me throughout my PhD career. She helped me to develop proposal writing skills, and she and Linda provided hospitality in the final days of my defense. Jason Amundson advised me as though I was one of his own students. He tirelessly (and quickly) provided detailed comments and fresh ideas during several iterations of manuscripts. Jason also invited me to collaborate on mélange-related projects with condensed matter physicists; that experience helped frame chapter 3. Martin Truffer readily dispenses simple and yet sound advice – whether it pertains to research,

coursework, field techniques, or just plain old advice to navigate the complexities of life. He possesses the most remarkable ability to guide one through the most complex of problems with ease, all while instilling valuable analytical lessons. Joe Licciardi introduced fundamental glacial principles through coursework in geomorphology, glacial geology, and paleoclimate. Joe also provided detailed and constructive comments that significantly improved my manuscripts.

A variety of organizations provided financial support throughout my PhD career. A NASA Earth and Space Science Fellowship funded the bulk of this research. I was awarded a fellowship through the New Hampshire Space Grant Consortium. Mark Fahnestock generously supported me through various research grants, including the Gordon and Betty Moore Foundation. The Department of Earth Sciences provided financial support through scholarships, teaching assistantships, and the ESCI-EOS student research fund, which helped fund attendance at the International Summer School in Glaciology. The Natural Resources and Earth System Science Program provided a tuition waiver during my last semester. Finally, I received travel support for various meetings and workshops from the National Science Foundation, the International Glaciological Society, and the US Climate Variability and Predictability Program.

I am grateful to the Department of Earth Sciences for the many years of exceptional support and encouragement. I am particularly grateful for conversations with Wally Bothner, Will Clyde, Linda Kalnejais, and Anne Lightbody. I am also grateful to the Earth Systems Research Center, especially Jack Dibb, Cameron Wake, Joe Souney, and Mark Twickler for providing guidance and residency (office space) in the glaciers group; Belinda Camire, Gary Desjardins, and Linda Tibbetts eased clerical and accounting responsibilities. I am also grateful for the many

conversations, insight, and feedback from the members of the UNH Geophysics group – Pamela Moyer, Evangelos Korkolis, Monica Wolfson-Schwehr, Debra Kane, Jiawei Jiang, and Liam Kenefic; Liam digitized hundreds of calving fronts from satellite and terrestrial radar images.

Many colleagues enriched my graduate experience. Roman Motyka provided guidance and expertise in the field, and welcomed me to collaborate on several occasions. Kelly Brunt provided indispensable advice in career planning. Shad O'Neel supported and funding field work at Columbia Glacier. Justin Burton provided a condensed matter physicist's perspective on the granular flow of ice mélange. Colin Meyer suggested initial ideas for modeling of observations at Columbia Glacier. I am grateful to Louis Sass, David Podrasky, Bob McNabb, and Santiago de la Peña for their assistance in the field. The Juneau Icefield Research Program provided me with a tremendous opportunity and my first field experience in glaciology. The International Summer School in Glaciology provided guidance and expertise in addressing glaciological questions.

Finally, this research would not have been possible without the tremendous love and support of my family. My wife, Megan, encouraged me throughout my graduate career – from early, geology 100 level courses to completing this doctoral dissertation. Although she may not have been fully aware of her commitments when I started, she nonetheless provided unwavering support throughout. The sacrifices made by her and our children, Logan and Julia, enabled me to pursue a life-long goal. I am truly fortunate and incredibly grateful!

TABLE OF CONTENTS

LIST OF TABLES

LIST OF FIGURES

ABSTRACT

UNRAVELING SHORT-TERM VARIATIONS IN TIDEWATER GLACIER FLOW: INSIGHTS FROM TERRESTRIAL RADAR INTERFEROMETRIC STUDIES

By

Ryan K. Cassotto

University of New Hampshire, December 2017

Tidewater glaciers are fast-flowing valley glaciers that advect ice from the interior of ice sheets to the ocean. Processes along the submarine boundaries of tidewater glacier termini can trigger a dynamic response in glacier ice that can impact stability along the terminus. Predictions of 21st century sea level rise require a comprehensive understanding of tidewater glacier dynamics over a variety of spatial and temporal scales. Perturbations to the calving front, such as iceberg calving, tidal modulations, changes in proglacial ice mélange strength and rigidity, and the subglacial discharge of meltwater occur on time-scales that exceed temporal resolution of satellite measurements; thus, little is known about the dynamic response of glaciers to these processes. Terrestrial radar interferometry is a relatively new technology that measures millimeter scale surface deformation with a spatial resolution comparable to satellites, but at much higher temporal resolution. Here, I use terrestrial radar interferometers to measure short-term variations in speed and surface elevation along Jakobshavn Isbræ, Greenland and Columbia Glacier, Alaska. I find

that small calving events can trigger large, dynamic changes in speed and ice thickness. I present observations that show that glacier response to calving events is a consequence of two competing feedbacks: (1) an increase in strain rates leads to dynamic thinning and faster flow, thereby promoting destabilization, whereas (2) an increase in flow rates advects thick ice toward the terminus and promotes restabilization. The competition between these feedbacks depends on temporal and spatial variations in the glacier's proximity to flotation. I also present the first field evidence of a granular ice mélange influence on iceberg calving, which has implications for calving rates, the speed and thickness of the terminus, and consequently tidewater glacier stability. Finally, I present observations of a large increase in speed along Columbia Glacier in response to a precipitation event. The results demonstrate the importance that variations in basal hydrology have on sliding along the bed, and more importantly how changes in the subglacial hydrology can affect the response of a tidewater glacier to tidal fluctuations.

1 INTRODUCTION

Dynamic processes along the termini of tidewater glaciers, fast-flowing glaciers that transport ice from the interior of ice sheets to the ocean, can account for more than half of all ice mass loss in Greenland and Antarctica. In the early 2000s, changes that initiated along Greenland's ice-ocean boundary triggered feedbacks in ice dynamics that led to large calving retreats and significant ice mass loss. The changes are ongoing, but predictions for tidewater glacier evolution and the impacts to sea level are limited by a poor understanding of tidewater glacier response to perturbations at the calving front. This dearth of knowledge is due, in part, to an inability to adequately measure rapid, dynamic processes with high temporal *and* spatial resolution. As a result, several major questions remain unanswered, including: (1) How does iceberg calving affect tidewater glacier stability? (2) What effect does ice mélange have on iceberg calving, if any? (3) How do variations in subglacial hydrology and discharge affect speed? and (4) How do variations in ocean and fjord circulation impact frontal ablation? Understanding tidewater glacier response to these perturbations, including the effect of short-term velocity variations on tidewater glacier stability, is paramount for predictions of 21st century sea level rise. Recent advances in terrestrial radar interferometers, instruments that measure surface deformation using fractional changes in electromagnetic wavelengths (phase differences) between acquisitions, allow for these short-period processes to be observed with high temporal and spatial resolution, and thus has motivated the research presented here.

Historically, the study of tidewater glacier flow began in earnest in the 1970s with the conceptualization of the tidewater glacier cycle [*Post*, 1975]. Post hypothesized that tidewater glaciers 1) advance over millennial time scales, 2) reach an advanced position by building and mobilizing a protective moraine at the glacier terminus, 3) undergo rapid retreat on centennial time scales, and then 4) remain at the head of fjord until the cycle repeats. Seminal work by Meier and Post [1987] described the unique geophysical environment of tidewater glaciers that contributes to their fast flow. Specifically, submarine beds and high seawater pressures lead to characteristically high subglacial water pressures at the terminus, which are necessary to drive basal melt water from the system. Consequently, this enhances basal sliding and thus speeds along tidewater glacier termini. Another attribute of their work was the idea that tidewater glaciers are largely insensitive to climate variations, owing to complex fjord geometries, the distribution of mass balance, and the accumulation of eroding sediments. That view has changed in recent years to reflect a rather complex relationship between climate and tidewater glaciers [*Post et al.*, 2011], wherein tidewater glacier sensitivity to climate varies at each stage of the cycle, and is most sensitive when the terminus is in an advanced configuration [*Amundson*, 2016]. Furthermore, recent, concurrent changes along many of the planet's tidewater glaciers suggest a climate-induced trigger for rapid retreat.

Many recent studies have documented rapid changes throughout the cryosphere that implicate a changing climate. For example, increased surface melt *[e.g. Nghiem et al* [2012]*]* and the drainage of supraglacial lakes [*Das et al.*, 2008] have been shown to accelerate speeds along the margin of the Greenland Ice Sheet. An increase in subglacial discharge, coupled with warm ocean currents that reach the termini of tidewater glaciers [*Holland et al.*, 2008; *Rignot et al.*, 2010; *Straneo et*

al., 2010; *Rignot et al.*, 2013b], can create convective freshwater plumes that ablate the submarine fronts of tidewater glaciers [*Motyka et al.*, 2003], which in some cases surpass the calving flux [*Bartholomaus et al.*, 2013]. These climate-induced changes can initiate positive feedbacks within ice dynamics that lead to tidewater glacier thinning [*Pritchard et al.*, 2009], faster flow [*Joughin et al.*, 2010], and rapid retreat [*Moon and Joughin*, 2008] that continue regardless of climate variations [*Amundson*, 2016; *Brinkerhoff et al.*, 2017]. The ability to predict the evolution of tidewater glacier retreat is contingent upon the ability to study and analyze dynamic processes along the terminus. However, these processes - subglacial discharge, iceberg calving, and variations in speed, all occur on spatial and temporal scales that exceed the sampling capabilities of traditional survey techniques.

Early traditional glaciological studies used theodolite and photogrammetric surveys to measure speed. Active seismic campaigns were used to measure ice thickness and the depths of submarine beds (e.g. Clarke and Echelmeyer [1996]). Drilling expeditions measured ice thickness as well as subglacial [*Meier et al.*, 1994] and englacial conditions [*Luthi et al.*, 2002]. These and numerous other studies that characterize glacier flow provided the framework for modern glaciology.

Technological advances have revolutionized glaciological observations and understanding. For example, GPS technology has increased temporal sampling rates. Airborne radar sensors sample bed depths and derive ice thicknesses that are combined with fundamental conservation principles to derive topographic maps of glacier beds (e.g.[Bamber et al., 2000a; 2000b; *Morlighem et al.*, 2014]). The launch of multiple Earth observing satellites has significantly enhanced the spatial resolution of observations. The application of spaceborne radar interferometry allows for fine scale

surface deformation measurements over relatively moderate time scales (weekly to monthly). However, the challenge for tidewater glaciers is to monitor changes with high spatial *and* temporal (sub-daily) resolution – a technological barrier that, until recently, was not possible to cross.

Terrestrial-based radar interferometry was developed more than a decade ago but was limited to the mining and landslide communities. Terrestrial radar interferometers (TRIs) have distinct advantages over spaceborne counterparts, including the ability to deploy and observe areas not viewable by satellites. Their stationary observation position also simplifies post-processing calculations by reducing the number of measured phase displacement components. Perhaps most significant is the high sampling rate (minutes), creating an instrument capable of satellite spatial resolution but with the temporal resolution close to GPS systems. As a result, rapidly deforming surfaces that temporally decorrelate between satellite acquisitions can be observed with TRI (e.g. iceberg calving, ice mélange, rapid dynamic thinning). Recently, TRIs have been deployed to characterize flow along tidewater glacier termini [*Dixon et al.*, 2012; Voytenko et al, 2015a; 2015b; 2015c; *Xie et al.*, 2016]. Here, I use dense TRI observations to create high-resolution time-series of short-term variations in speed and surface elevation along tidewater glaciers in Greenland and Alaska. In particular, I present a novel approach to DEM differencing whereby I use stationary targets in TRI-derived digital elevation models (DEMs) to reduce elevation errors and produce a record of rapid, dynamic thinning (Chapter 2, methods). The results presented herein demonstrate how TRI studies can enhance our understanding of short-term tidewater glacier dynamics, and when coupled with longer records from satellites, can be used to make predictions about the evolution of tidewater glaciers.

The focus of this thesis is to apply TRI technology to investigate the response of short-term perturbations along the termini of two glaciologically significant tidewater glaciers. Since 2000, Jakobshavn Isbræ in West Greenland has retreated ~20km, thinned by more than 100 m [*Motyka et al.*, 2011], and discharged more ice than any other Greenland glacier [*Enderlin et al.*, 2014], which has contributed to a dense proglacial ice mélange. Columbia Glacier in South-Central Alaska has also endured a nearly 40-year, 22 km retreat [*McNabb and Hock*, 2014], experienced a >50% reduction in ice volume [*McNabb et al.*, 2012], and is currently exhibiting very low speeds in late fall. Both glaciers occupy submarine beds, which suggests additional retreat is possible. In the following chapters, we investigate short-term variations in glacier flow in response to: iceberg calving (chapter 2) and precipitation (chapter 4), and short-term variations in ice mélange flow between calving events (chapter 3).

2 NONLINEAR GLACIER RESPONSE TO CALVING EVENTS, JAKOBSHAVN ISBRÆ, GREENLAND

2.1 Introduction

After decades of relative stability [*Sohn et al.*, 1998; *Podlech and Weidick*, 2004], Jakobshavn Isbræ began to destabilize at the turn of the 21st century. Submarine melting of the floating tongue [*Motyka et al.*, 2011], enhanced by the influx of warm ocean currents in the late 1990s [*Holland et al.*, 2008], initiated changes along the glacier terminus. The glacier thinned by more than 100 m [*Krabill et al.*, 2004; *Motyka et al.*, 2010], velocities doubled [*Joughin et al.*, 2004; *Luckman and Murray*, 2005], and the terminus rapidly retreated [*Podlech and Weidick*, 2004; *Moon and Joughin*, 2008]. The rate of retreat peaked in 2003 with the collapse of the glacier's floating tongue [*Thomas*, 2004; *Joughin et al.*, 2012], and the retreat continues to this day. The pattern of accelerating flow and kilometer-scale retreat slowed in 2010 and 2011, but speeds reached record high values in 2012 as the glacier retreated to a new minimum position [*Joughin et al.*, 2014].

Retreat down a reverse bed slope is believed to have triggered the large increase in speed that occurred in 2012 *[Joughin et al., 2014]*. Measurements and numerous bed models show a submarine channel extends far into the interior of the ice sheet [*Clarke and Echelmeyer*, 1996; *Bamber et al.*, 2013; *Morlighem et al.*, 2014]; however, the depth of the channel varies by model. Understanding Jakobshavn Isbræ's response to perturbations along the calving front, including bathymetric influence, is paramount for accurate predictions of tidewater glacier evolution and the resultant impact on sea level.

Variations in ice thickness affect tidewater glacier stability through changes in effective pressure (ice overburden minus subglacial water pressure). A reduction in ice overburden decreases basal friction and enhances flow, creating a positive feedback that propagates upglacier and leads to rapid retreat [*Pfeffer*, 2007]. The recent 15 m yr^{-1} thinning rate [*Joughin et al.*, 2012], 20 year period of fast flow [*Joughin et al.*, 2012; 2014] and ongoing retreat [*Moon and Joughin*, 2008; *Cassotto et al.*, 2015] indicate that positive feedbacks are driving Jakobshavn Isbræ's instability. If sustained, the glacier could retreat far into the ice sheet interior within a few decades [*Joughin et al.*, 2014]. Furthermore, proglacial studies show that the ice sheet margin around Jakobshavn Isbræ has previously responded to terminus variations on centennial time scales [*Briner et al.*, 2011; *Young et al.*, 2011]. Therefore, the continued destabilization of Jakobshavn Isbræ could have profound effects on the drawdown of interior ice, and by direct consequence, sea level rise over the next century.

On shorter time-scales, brief periods of acceleration can influence the seasonal and interannual behavior of Jakobshavn Isbræ [*Podrasky et al.*, 2012]. Here, we use terrestrial radar interferometry (TRI) to assess the influence that short-term perturbations in speed have on long-term glacier dynamics. TRI is a relatively new tool, wherein phase differences between multiple radar passes are used to derive surface deformation and digital elevation models. The portability and high sampling rates of TRI provide tremendous opportunities for geophysical surface studies (e.g. *Caduff et al.,* [2014] and references therein*)*, including tidewater glaciers [*Dixon et al.*, 2012; *Voytenko et al.*, 2015b; *Xie et al.*, 2016]. TRI data collected at Jakobshavn Isbræ in 2012 has already been used to characterize ice mélange motion during calving events [*Peters et al.*, 2015] and towards the development of a 2D velocity field [*Voytenko et al.*, 2017]. The objective of this study is to use the full, high-resolution record of TRI observations to evaluate how short-term

variations in ice flow influenced the 2012 historic change in speed. Specifically, we seek to answer: 1) if calving affected flow along the terminus, 2) if retreat of the terminus downslope of a previously stable location caused the unprecedentedly high velocities as hypothesized by *Joughin et al*. [*2014*], 3) what short-term variations in speed, surface elevation, and tidal forcing indicate about terminus stability, and 4) how these observations compare with the large seasonal acceleration observed in the satellite record?

We present TRI observations of speed and elevation along the terminus of Jakobshavn Isbræ during a transition to peak flow in 2012. We find that a relatively small calving event triggered a step increase in speed that affected ice thicknesses and glacier stability in two competing ways: 1) an initial increase in strain rates dynamically thinned the terminus and reduced coupling at the bed; and 2) an increase in advection subsequently thickened ice and re-stabilized the terminus. Consistent with previous studies [*Rosenau et al.*, 2013; *Xie et al.*, 2016], we find that the terminus of Jakobshavn Isbræ is very close to flotation. Our study emphasizes the glacier's sensitivity to ice thickness variations over short timescales and the consequences of that short-term variability on the glacier's ongoing retreat.

2.2 Methods

We performed an in-situ study along the southern terminus of Jakobshavn Isbræ between 30 Jul and 13 Aug 2012. We deployed time-lapse cameras, a tide gauge, on-ice GPS receivers, and a terrestrial radar interferometer from a bedrock camp (Figure 1) to monitor short-term variations in ice flow and surface elevation.

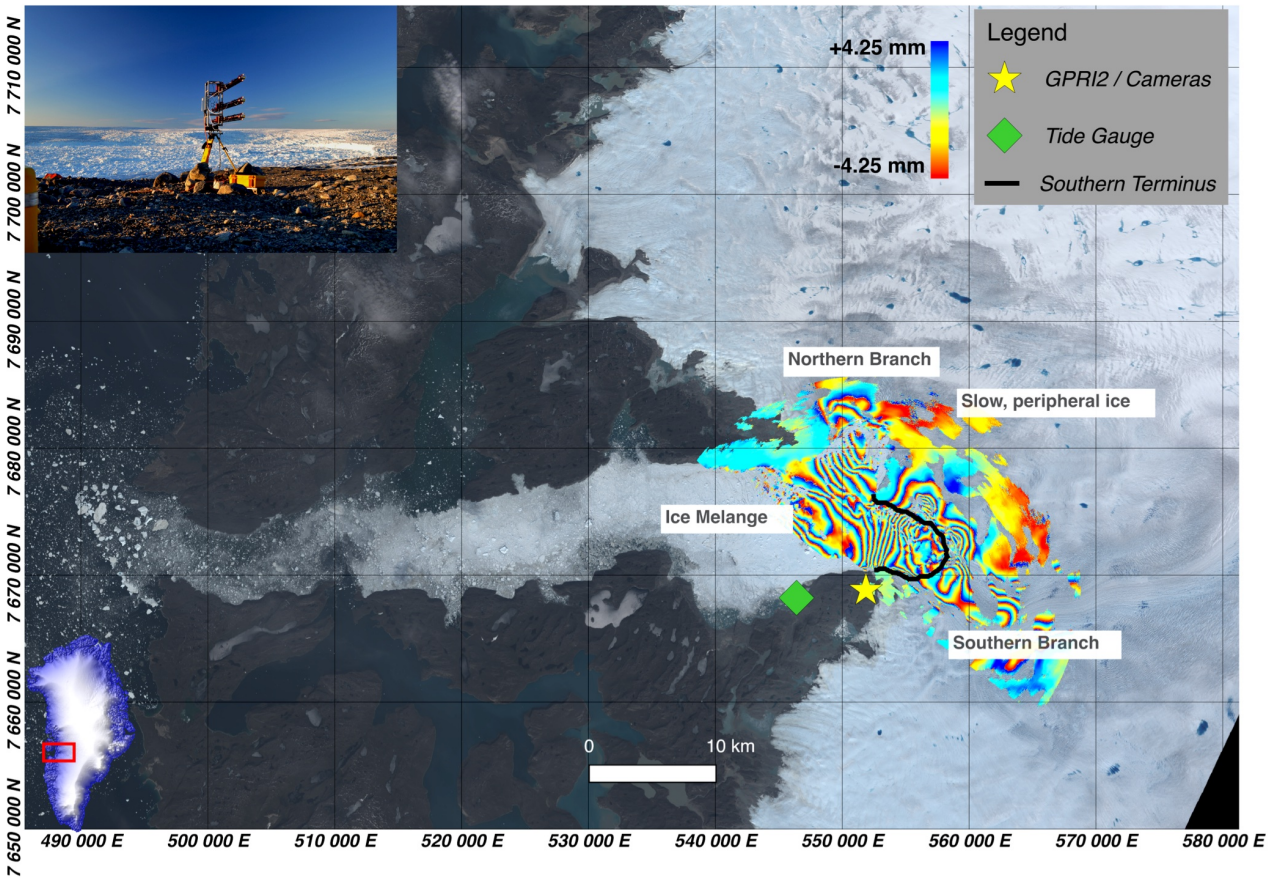

Figure 1: Differential interferogram superimposed on a Landsat 8 image of Jakobshavn Isbræ shows displacement during a 3-minute interval. (Inset) Photograph of the GPRI2 at the study site.

We used Canon EOS DSLR cameras to document the timing of calving events throughout the year. Four cameras photographed the terminus and ice mélange every 15 minutes during the field campaign and every 3 hours throughout the rest of 2012. A fifth, high-rate camera was used during the field campaign to photograph the terminus every 10 seconds. A Global Water WL400 water level sensor was deployed ~10 km downfjord of the calving front and sampled every 30 seconds.

We used a Gamma Remote Sensing Ground-based Portable Radar Interferometer II (GPRI-II) to measure the short-term changes in glacier speed and surface elevation. The GPRI-II is a Ku-band

(λ=1.75 cm), real aperture, rotating radar interferometer capable of measuring surface deformation at a range of up to 16 km. It has a range resolution of 0.75 m and an azimuthal resolution proportional to slant range at a ratio of 8:1000 (8 m at 1 km slant range). We used the TRI to image the terminus and proglacial fjord every 3 minutes for 15 days with limited breaks. We decimated raw radar data by 5 in azimuth to account for oversampling, and then converted it to single-look-complex data (SLC). All SLCs were co-registered to the first image in the record, and multi-looked by 15 in range to reduce noise and generate square pixels along the southern terminus. They were processed to line-of-sight (LOS) displacement and topographic interferograms, and later speeds and digital elevation models (DEMs). All TRI images were reprojected to 15-m Cartesian space in local UTM projection and geolocated using corner radar reflectors surveyed with handheld Garmin GPS receivers. We neglected a terrain correction and kept measurements in native slant range coordinates; the small topographic range (few hundred meters) distributed over the large scan radius (16 km) using a nearly horizontal viewing geometry translates to minor differences in range. The methods used to generate the high-resolution time-series are new and required several additional steps that are described in detail in Sections 2.2.1-2.2.2.

2.2.1 TRI-derived speeds

A total of 5,579 interferograms were used to generate a 15-day record of speed. Most interferograms span 3 minutes, while a small percentage (~2%) span 5 to 6 minutes. Interferograms were smoothed with an adaptive filter (ADF) to minimize noise [*Goldstein and Werner*, 1998]. The filter preferentially favors pixels with high coherence, while penalizing less coherent pixels; we used a 32 x 32 ADF window size, a 7 x 7 correlation window size, and an ADF exponent of 1. We then used *Goldstein et al's* [1988] minimum cost flow method (MCF) to unwrap the ADF

filtered interferograms, converting relative phase differences to true phase displacements. The complicated deformational field along Jakobshavn Isbræ's terminus (e.g., slow moving ice sheet, fast ice stream, and ice mélange with variable speeds, frequent transients, and distinct discontinuities) generates large gradients in phase that are difficult and tedious to unwrap. Consequently, many of the unwrapped interferograms contained erroneous branch cuts that led to 2π phase jumps and discontinuous speeds. Such interferograms are typically excluded from interferometric studies; however, our objective was to maintain a high temporal resolution record of short-term variations. Therefore, additional steps were taken to eliminate these errors.

2.2.1.1 Eliminating branch cuts / unwrapping errors

A series of corrections were made to account for the unwrapping errors. We started with a-priori information and a Johnny Appleseed approach *[Hanssen, 2001]* to generate phase reference maps that contained the correct number of $n2\pi$ integers. These reference maps were created by speckle tracking polar MLI images and then converting the speeds into LOS phase displacements over 3 minutes. Each map was calculated 24 hours before and after a nominal center time to minimize noise for each reference. Four reference maps were generated to reflect the changes in speed over the study: steady flow early in the record, accelerated rates mid-record, and two maps to cover the gradual return to steady flow. The intervals and MLI images used for the reference maps are

Table 1: MLI acquisition times used for target integer maps

Map	Time Interval	MLI Image 1	MLI Image 2	MLI Image 3
1	Jul 30 16:38 - Aug 2 23:10	Jul 30 16:22	Jul 31 16:21	Aug 1 16:22
2	Aug 2 23:10 - Aug 6 00:00	Aug 3 16:21	Aug 4 16:21	Aug 5 16:21
3	Aug 6 00:00 - Aug 8 00:00	Mean of Maps 2 and 4	--	--
4	Aug 8 00:00 - Aug 13 09:00	Aug 7 15:57	Aug 8 16:21	Aug 9 16:21

provided in Table 1; maps 2 and 4 were averaged to define the reference during the transition period (map 3).

The first phase correction compared each interferogram with its respective reference map; pixels more than 1 fringe (2π radians) from the reference were adjusted to keep phase values within the predicted target integer range (yellow in Figure 2). Next, we corrected for ambiguity, and adjusted pixels that were more than half a cycle from the target by 2π (blue in Figure 2). This sometimes led to the rewrapping of phase measurements along the calving front, which re-introduced branch cuts. To account for this, we assumed flow fields were continuous and differences were less than 1 fringe, and made a third correction (black in Figure 2) to ensure the calving front had the same number of integer cycles as the ice a short distance behind it. Finally, we used a smoothing spline

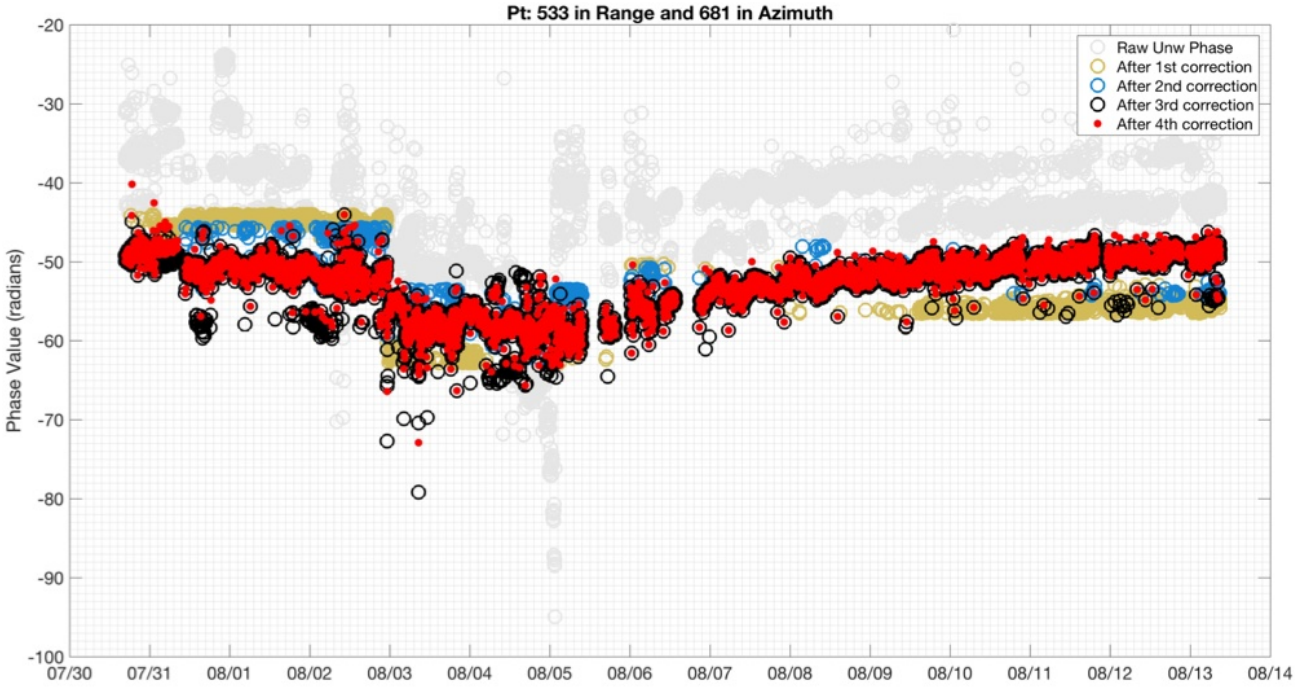

Figure 2: Sample unwrapped phase showing the results after each correction step at a discrete pixel.

to fit a curve to the time series for the fourth and final correction (red in Figure 2); phase values more than 5.5 radians (0.9 integer cycles) from the curve were adjusted by 2π. The entire process generates interferograms with correct LOS phase displacements and few unwrapping errors; remaining residuals were later accounted for during stacking for atmospheric effects.

2.2.1.2 Atmospheric Corrections

Variations in atmospheric pressure and moisture between radar acquisitions can impact the index of refraction, which affects the two-way travel time of the electromagnetic wave and the measured phase. Typically, two atmospheric corrections are made: 1) a linear range correction that accounts for bulk atmospheric changes, and 2) a local correction to account for a heterogeneous atmosphere. We assume that bulk atmospheric variations are negligible over the short duration of our interferograms (minutes) and neglect a range dependent correction. Instead, we focus on the local variations within the radar's viewing geometry, and stack the phase measurements over a 21-minute moving mean. We exclude pixels with phase values >1 standard deviation from the mean, and those with fewer than 5 measurements in the interval.

2.2.1.3 Line-of-sight (LOS) to along-flow motion in UTM coordinates

Polar (azimuth, range), atmospherically corrected interferograms were reprojected to Cartesian coordinates and rotated into local UTM coordinates. Corner reflectors in the radar's viewing geometry were located by handheld GPS receivers and used to coregister the images. No correction was made for slant range because the small vertical look angle (5º below the horizontal) and low topographic relief in the viewing geometry have a negligible effect on ground range values (<0.5%). Next, LOS phase displacements were converted to speed in the direction of flow using PyCORR-derived (speckle-tracked) displacements [*Fahnestock et al.*, 2015]. The component

vectors were used to calculate ξ, the direction of flow, and then θ, the difference between the flow direction and the LOS look angle. Two pairs of MLI GeoTIFFs were used to generate a complete map of θ values. The majority of the map was comprised using data from an 8 Aug 13:45 - 9 Aug 13:45 image pair, a time when the calving front was in an advanced position and velocity variations were minimal. Katabatic winds on 6 Aug induced offsets in azimuth that resulted in the loss of measurements along the southern edge of the ice stream; therefore, component vectors from a 30 Jul 16:22 - 31 Jul 16:21 image pair were used to supplement θ values during this time period. To minimize artifacts due to subtle flow differences between the two-time periods, the hybrid θ map was passed through a 20x20 Gaussian low pass filter using a standard deviation of 2. LOS speeds were then divided by the cosine of θ to calculate speed in the direction of flow in units of m d^{-1}.

2.2.1.4 Error in TRI-derived Speeds

Error sources for the TRI-derived speeds include phase unwrapping, LOS to along-flow conversion, and atmospheric effects. Phase unwrapping errors were minimized using speckle-tracked polar reference images (*see 2.1.1*); this reduced error to within the 1 integer cycle or ~4.08 m d^{-1}. We assumed flow vectors remained constant over the study period and used a single θ map to convert LOS speeds to along-flow. PyCorr-derived velocity fields calculated for 11 of the 15 days reported standard deviations in flow direction of 5 to 8º over time, which translates to errors in speed of 9.0 to 15.6%. Steps were taken to minimize atmospheric phase noise (*see* 2.2.1.2), but estimates of atmospheric phase contribution are difficult to quantify due to a lack of stable reflectors (e.g. exposed bedrock) along the southern terminus.

The values above provide conservative error estimates from individual sources. To provide a more comprehensive estimate, we evaluated the total error by comparing phase-derived speeds with: 1)

on-ice GPS measurements, and 2) speckle-tracked speeds. GPS data provide an independent assessment of speed, and thus are ideal. We calculated a difference of 2.3 – 3.5 m d^{-1} in the mean speed between 3 on-ice GPS sensors and the corresponding pixels in the phase-derived speeds during the last 2.6 days of observations, the time period for which GPS was available. To evaluate the early record, we compared phase-derived speeds with speckle-tracked speeds derived from TRI intensity images, which are not susceptible to atmospheric phase noise and do not require a LOS conversion. Comparisons were made for four different 24-hour intervals with center dates: 31 Jul 4:22, 1 Aug 5:22, 2 Aug 00:22, 9 Aug 00:21; RMSE values for all pixels ranged from 3.26 to 3.99 m d^{-1}. Based on GPS and speckle-tracked comparisons, we adopt a conservative estimate in total error of 3.99 m d^{-1}.

2.2.2 TRI-derived surface elevation changes

The GPRI-II has two receive antennas spaced 25 cm apart vertically (bottom antennas in Figure 1**,** inset). Concurrent measurements from both antennas can be used to generate digital elevation models (DEMs) without the need for atmospheric and phase displacement corrections. We used the dense record of topographic interferograms to generate multiple DEMs following the methods of *Strozzi et al* [2008]. We then differenced the DEMs to track the change in surface elevation over time. To minimize noise, we ADF filter the interferograms, stack for each hour of observation, and exclude pixels with coherence <0.9.

High quality DEMs requires perfect vertical alignment of the TRI instrument. Despite our best attempts to secure the instrument and maintain perfect vertical alignment, the combined effects of wind stress, thermal variability, and the inherent instability of till throughout the region, including the TRI site, led to deviations in vertical alignment over time. As a result, biases in range and

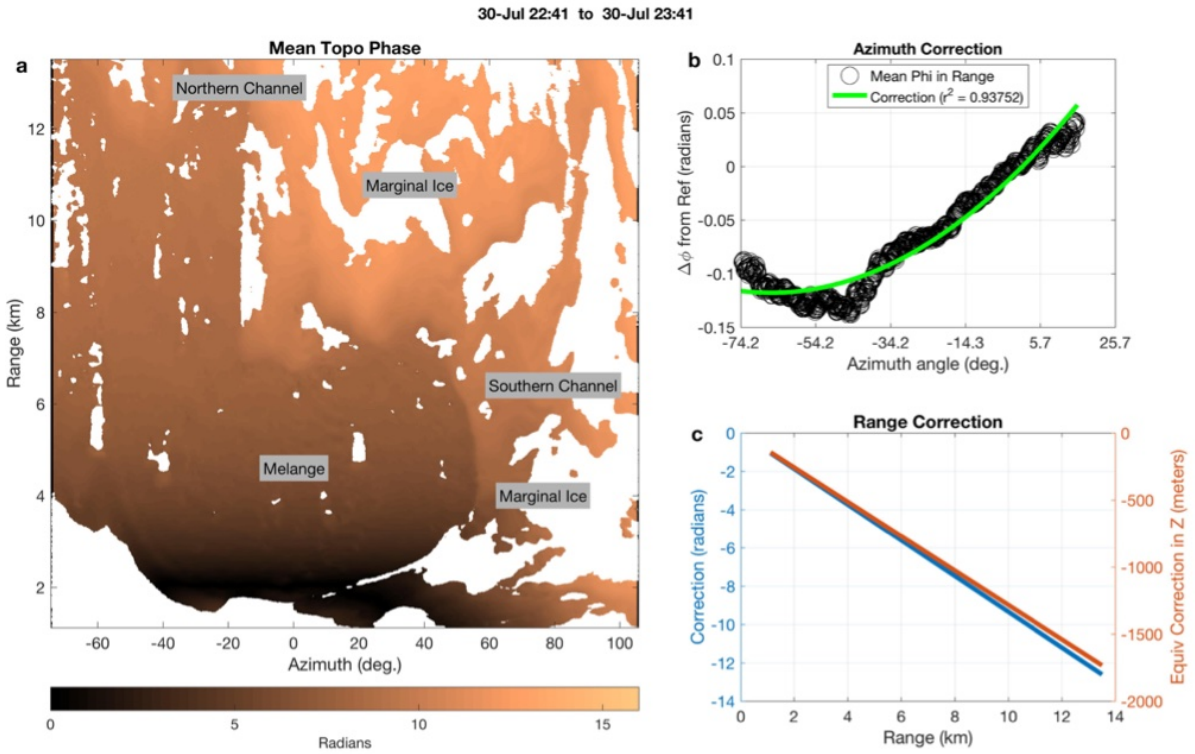

Figure 3: Topographic phase correction for vertical alignment errors. (a) Mean phase for a stack of interferograms on 30 Jul. (b) The azimuth and (c) linear range corrections applied to the mean phase maps.

azimuth were observed in the maps of mean phase (Figure 3b). Two corrections were made to remove the bias in the topographic stacks: a quadratic correction in azimuth to account for the variation in the tilt over 15 days, and a linear correction in range to account for the initial error in vertical alignment. For the non-linear correction, we difference each interferogram stack from the first hour and then calculate the median phase in range along each azimuth step (Figure 3b, black circles); we exclude near and far-field range values and those >1 standard deviation to minimize noise. We then fit a quadratic curve (Figure 3, green curve) to the residuals and use it to correct for the variations in tilt.

To correct for the initial error in vertical alignment, we used a ground control point located at the same elevation as the TRI. Pixels with stable bedrock make ideal ground control points; however, the bedrock points in the radar viewing geometry were all lower than the TRI. Therefore, we

identified a pixel in the slow, peripheral ice that appeared in Google Earth images and the topographic stack. The phase was sampled at the ground control point and added back into the mean phase values to generate the DEMs. The DEMs were adjusted by the GPRI-II elevation and filtered. We used a Gaussian filter to remove high frequency noise, and interpolated for pixels with no data to generate a smooth and continuous DEM. Lastly, the DEMs were converted to GeoTIFFs in local UTM coordinates; all elevations are in height above sea level. Elevations sampled at six locations on stable bedrock near the north channel report standard deviations from 2.5 to 2.9 m. However, these points are >12 km in range, and thus are expected to be significantly higher than values along the southern channel (4 - 7 km in range) due to the linear decrease in spatial resolution with range. A better evaluation of error is the variability within slow moving ice in the near field (2 km range) and in the peripheral ice adjacent to the southern channel (~8 km in range), where changes in surface elevation are primarily due to surface melt and are expected to be minimal over our short observation period. Standard deviations ranged from 0.47 m in the near field to 0.99 m along the peripheral ice; we adopt the latter as the error.

2.2.3 Mapping Calving Events and Terminus Locations from TRI

We used the reprojected radar backscatter intensity images (i.e. MLI) to map terminus locations. The calving front was manually digitized in MATLAB using the techniques of Cassotto et al [2015]. The terminus was sampled every ~6 hours with increased sampling around calving events. Calving losses were calculated by comparing front positions immediately before and after calving, summing the number of pixels lost to calving, and then multiplying by the area of each pixel (225 m^2). The result is a record of calving losses that is well constrained in time and two-dimensional space, but neglects submarine calving events. The record of terminus positions was supplemented

with Landsat panchromatic images (band 8) to extend the record in time, albeit with decreased temporal resolution.

2.3 Results

2.3.1 Short-term Variations in Speed

Speeds along a central flow line varied from 65 m d^{-1} at the terminus to 35 m d^{-1} two kilometers upglacier (Figure 4a). Thirteen calving events were observed (black vertical lines in Figure 4), and most produced no obvious change in speed. However, a calving event at 23:10 on 2 Aug resulted in a very small retreat of the calving front (black diamonds), and led to an immediate step change in flow. Speeds increased by as much as 30%, remained high for several days, and then gradually slowed to pre-calving speeds. A time-series sampled at 0.5-km steps along the same profile shows

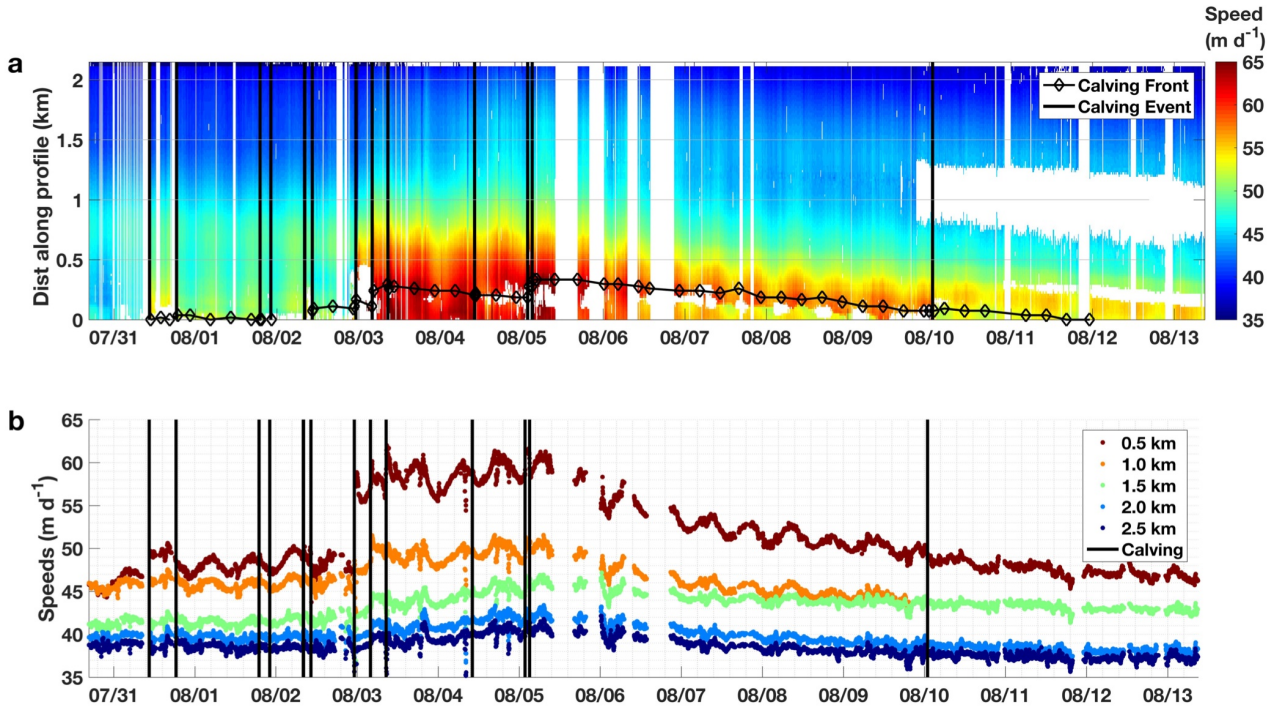

Figure 4: Variations in speed. (a) Time series of speed along a flow line of Jakobshavn Isbræ's southern branch; the timing of calving events is indicated by black lines. (b) Speed at 0.5-km intervals along the profile. Location of the flow line is shown in Figure 6.

that the response was not uniform along the terminus (Figure 4b). Rather, the change in speed was largest at the calving front and attenuated a short distance upglacier (~0.5 - 1 km upglacier).

A semi-diurnal signal was observed in the data, indicating that ice flow was tidally modulated. Furthermore, the 2 Aug 23:10 calving event enhanced this signal; speeds 0.5 km along the profile varied ~2 m d^{-1} peak-to-peak prior to calving (dark red in Figure 4b), but then increased to ~4 m d^{-1} peak-to-peak immediately after calving.

2.3.2 Response in Speed to Calving

Of the thirteen calving events observed, only a few affected glacier speed significantly (Figure 4). To investigate this behavior, we sampled speeds three hours before and after calving at a pixel 0.5 km along the profile, and found that speeds increased following five calving events: 31 Jul 10:30, 2 Aug 23:10, 3 Aug 3 03:58, 3 Aug 8:36, and 5 Aug 01:44 (Figure 5c). The 31 Jul 10:30 (1.43 km^2), 3 Aug 03:58 (0.56 km^2), and 5 Aug 1:44 (1.31 km^2) events were among the largest in the record, and all increased speeds by ~10%. In contrast, the 2 Aug 23:10 (0.08 km^2) event was eighteen times smaller than the largest event and resulted in a 30% increase in speed. Similarly, the smallest of all events, 3 Aug 8:36 (0.01 km^2), resulted in a 12% increase in speed. The remaining calving events were predominately small and produced negligible changes in speed.

We found no correlation between calving area loss and the change in glacier speed (Figure 5d). However, all five events that impacted speed calved ice in a highly-localized region, near the center of the terminus (Figure 5a, b). Furthermore, the 2 Aug 23:10 (main event), 3 Aug 3 03:58, 3 Aug 8:36 events all occurred within a 10-hour span. Of these, two were exceptionally small, resulting

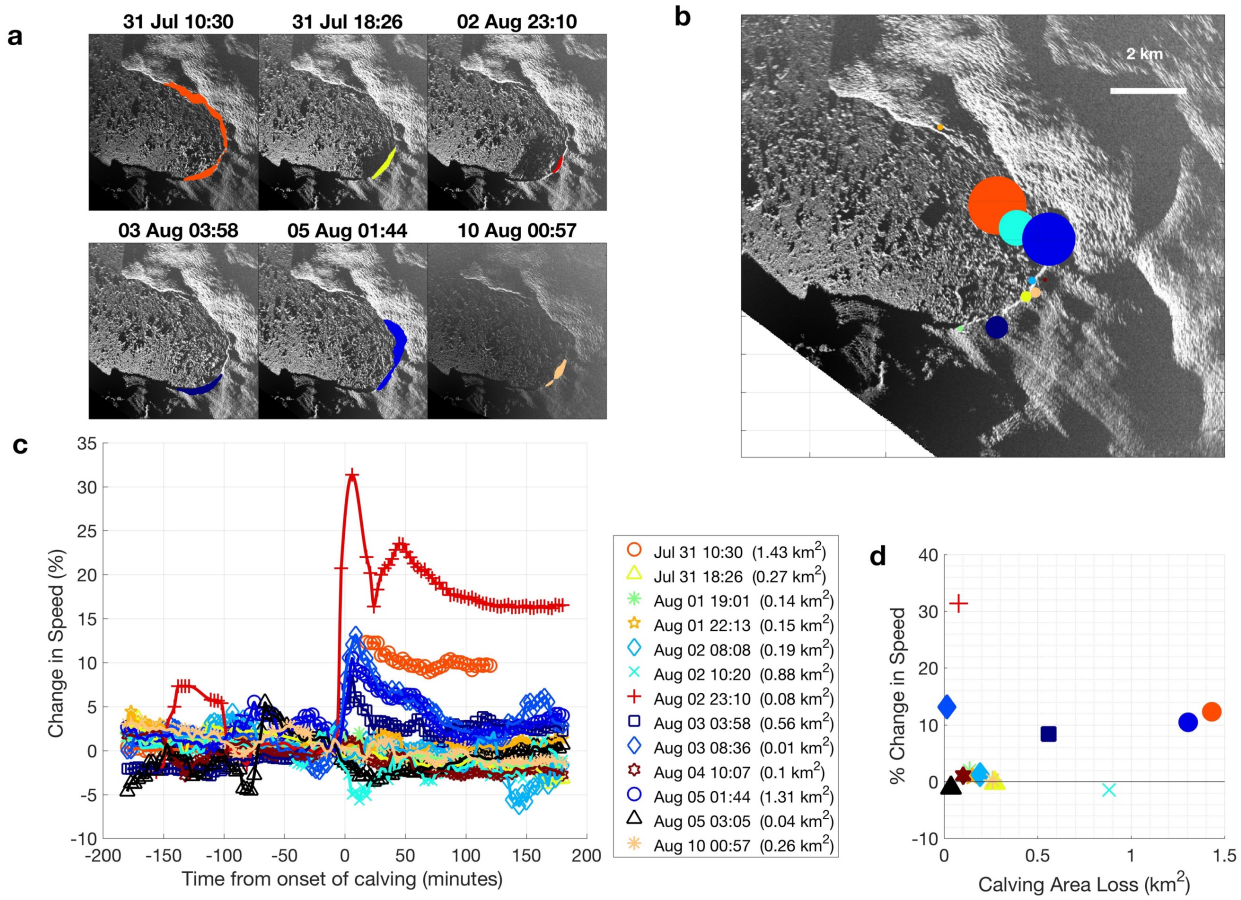

Figure 5: Characterization of calving events. (a) Polygons highlighting calving area losses for select events; (b) the distribution and relative size of all calving events mapped by the centroid; (c) change in speed during calving events; legend indicates the time and areal size of events; (d) instantaneous change in speed versus calving area loss.

in little change in terminus position and shape. The 31 Jul 10:30 and 5 Aug 1:44 events calved significantly more ice, including ice from near the center of the glacier (Figure 5a).

2.3.3 Dynamic Changes in Surface Elevation

Profiles of surface elevation show large, dynamic variations along the terminus (Figure 6b). Initially, the calving face measured 105 m in elevation (30 Jul, green), then decreased to 71 m on 1 Aug (purple), after a 100-m retreat. By 3 Aug (yellow), the calving face retreated 260 m and elevations reduced to 45 m. The glacier retreated to a minimum position on 5 Aug (red), but the

calving face increased to 67 m. By 7 Aug (blue), the terminus re-advanced, and the elevation of the calving face reduced to 48 m.

Farther upglacier, the pattern of elevation change was much different; ice thicknesses between 600 m and 900 m along the profile (inset in Figure 6) steadily increased with time. A reverse surface slope, indicative of impending calving events [*Rosenau et al.*, 2013; *James et al.*, 2014; *Xie et al.*, 2016], was observed along the terminus in the early profiles and was absent in later measurements.

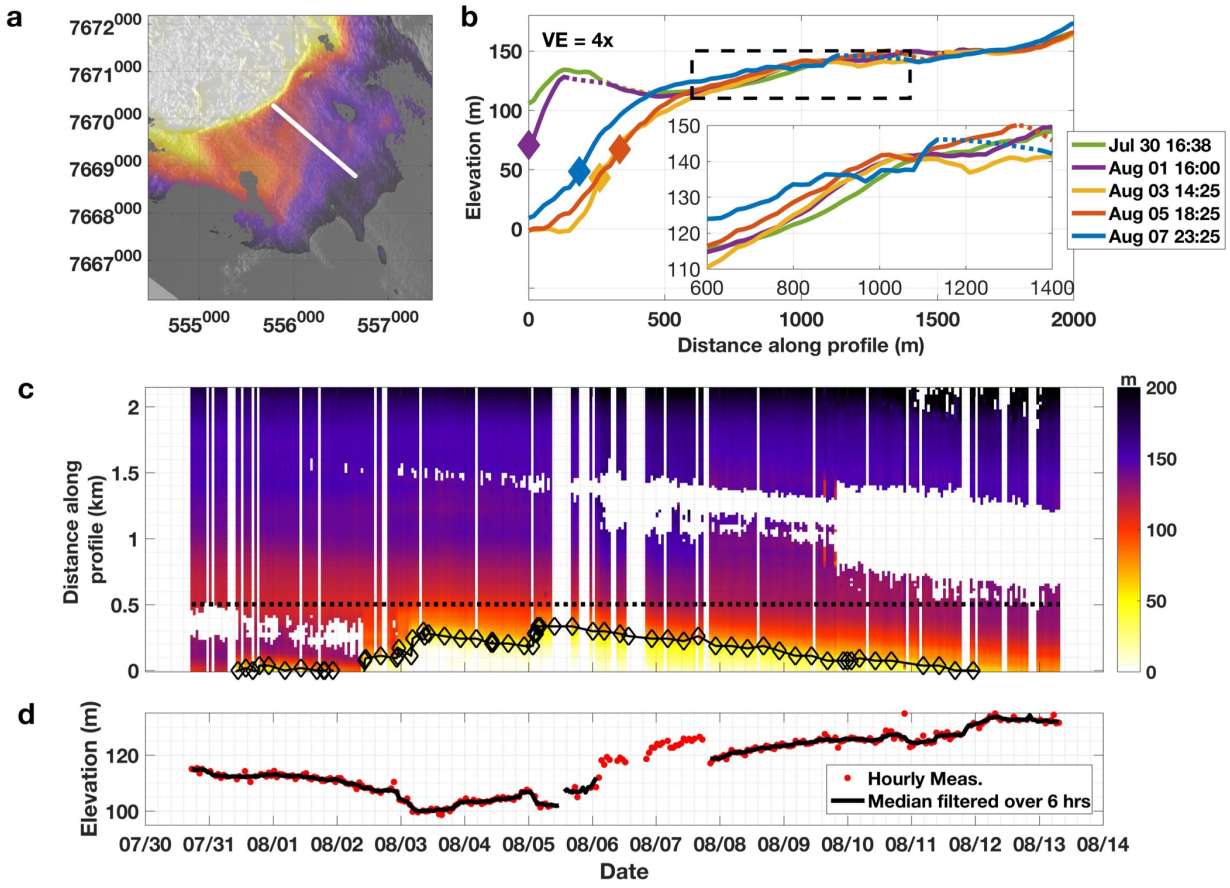

Figure 6: Variations in surface elevation. (a) Map of surface elevations with the location of a profile (white line) sampled in (b-d). (b) Cross-sections of surface elevations along the profile for five different epochs, dashed lines show interpolated values for missing data; note the reverse surface slope prior to calving in the early record. (c) A time-series of surface elevations along the profile. (d) Time-series of elevations 0.5 km along the profile. Diamonds in (b) and (c) indicate the location of the calving front.

A downward shift from dark to light colors in the time-series of surface elevations (Figure 6c) shows surface elevations along the lower terminus increased with time. This pattern emerged in the middle of the record and continued through the end. It coincided with a re-advance of the terminus, and implies the advection of thicker ice towards the calving front. Finally, a time-series sampled 0.5 km along the profile shows that elevations were generally stable during the first few days (Figure 6d), started to decrease on 2 Aug, and then abruptly decreased ~10 m on 3 Aug. Surface elevations then increased for 2 days before a second abrupt decrease in surface elevation occurred on 5 Aug. Noise precludes assessment on 6-7 Aug, but surface elevations were much higher by 8 Aug and continued to increase.

2.4 Discussion

Answering why some small calving events triggered step changes in speed and dynamic thinning while other larger events do not is fundamental to our understanding of glacier dynamics. To address this question, we investigate the conditions leading up to the 2 Aug 23:10 event and the spatiotemporal variations in speed, strain rates, surface elevations, and tidal response along the terminus. Finally, we compare our results with satellite-based observations to provide context for our study.

2.4.1 A Trigger for Fast Flow

Few of the thirteen calving events observed were of the large, full glacier width calving styles previously described at Jakobshavn Isbræ (e.g. *Amundson et al, [2008; 2010]*. Instead, most were confined to localized regions that removed small portions of the terminus (Figure 5a).

Furthermore, the timing and spatial coincidence of small events that led to step changes in speed suggests that bed topography represents an important control on the response to calving.

A small-scale retreat of the terminus behind a bedrock obstruction could have reduced basal and lateral resistance, which would lead to an increase in speed. TRI-derived surface strain rates show a compressional band (Figure 7a, green) within a predominately extensional zone (Figure 7a, b - purple). The compressional band briefly switched to extensional following the 31 Jul 10:36 calving, but remained compressional for several days thereafter. Compression in the patch increased after the 2 Aug 8:08 calving, then reversed to an extensional regime following the 2 Aug 23:10 calving event (Figure 7b). It remained extensional for several days before it gradually

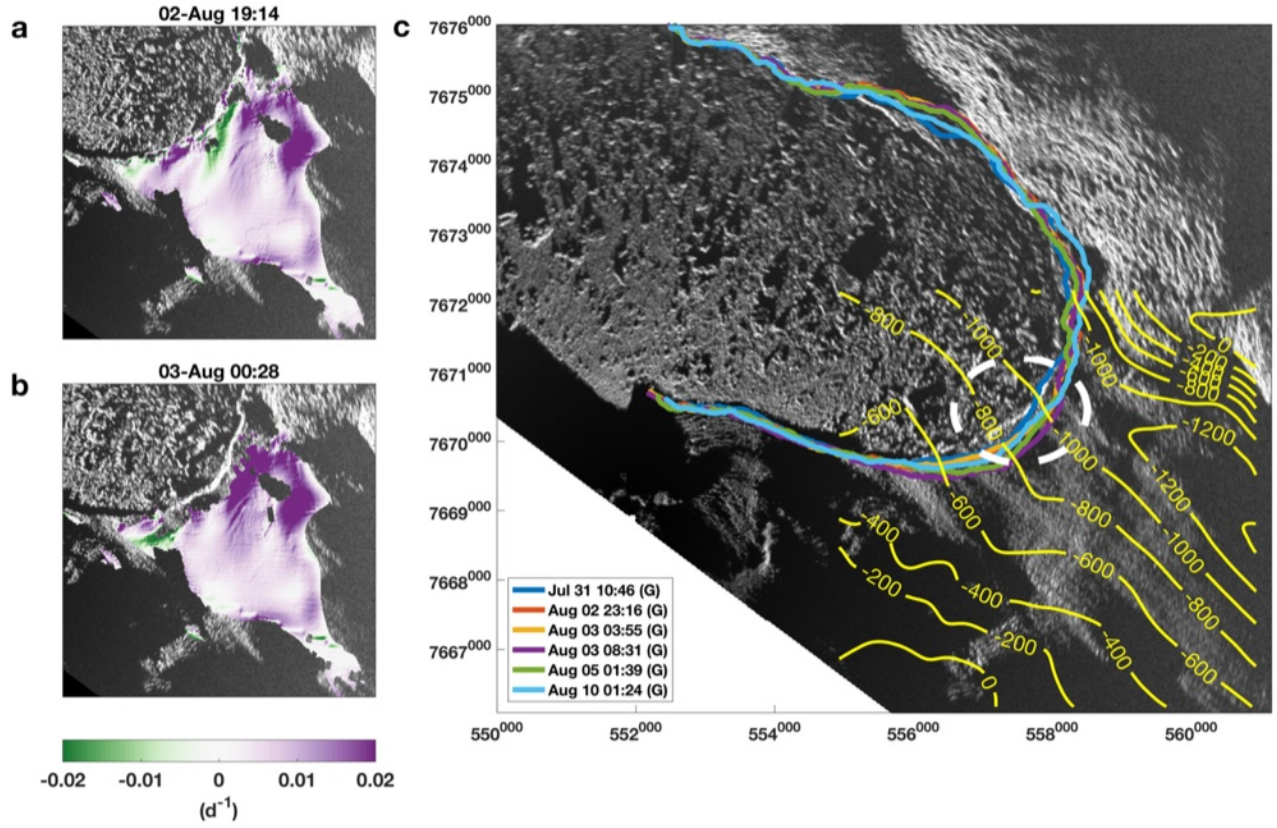

Figure 7: Bed topographic trigger to fast flow. Longitudinal strain rates (a) before and (b) after the 2 Aug 23:10 calving event; purple indicates extension, green compression. (c) Front positions (colors) and Morlighem et al.'s [2014] bed model (yellow contours) overlain on an MLI image. The largest step change in speed resulted from a very small retreat of the calving front into a subtly wider region in the deep, narrow channel (white dashed line). "G" represents GPRI-derived front positions.

transitioned back to a compressional patch by the end of the record. This area coincides with a tapered section of the bed near a deep trough (Figure 7c; *Morlighem et al., 2014*). This demonstrates that the series of calving events that began on the 2 Aug led to a small retreat of the terminus from a narrow constriction in the bed into a wider, less restrictive channel, which impacted the pattern of surface strain rates, and by inference basal and lateral drag along the bed. This suggests that the geometry of *Morlighem et al's* bed model is accurate in this section of the fjord, and points to the importance of bed geometry on tidewater glacier response to calving.

2.4.2 Spatiotemporal variations in speed, strain rate, and elevation

In a density-conserving fluid, such as a glacier, changes in strain rates must lead to changes in thickness, which has implications for terminus stability. We now look at the spatiotemporal variability in maps of speed, strain rates, surface elevation (ice thickness), and the height above flotation (HAF; Figure 8); section 2.4.3 compares these patterns against maps of tidal forcing (Figure 8e, f).

Speeds showed spatiotemporal variability throughout the record. Overall, speeds were fastest near the calving front (Figure 8, row a) and within the deep, narrow channel in *Morlighem et al's.* [2014] bed model. They were moderate during the early record, peaked after 2 Aug 23:10 calving, then gradually decreased and the region of fast flow became more localized through the end of the record. A slow patch of ice appeared behind the calving front near the glacier center, where the bed widens upstream. It disappeared following the 2 Aug 23:10 calving event, but a second patch emerged farther upglacier and advected toward the calving front.

Longitudinal surface strain rates accentuate the spatial variations in speed (Figure 8, row b). As discussed in 2.4.1, most of the terminus was under extension while compressional bands

ephemerally appeared near the calving front. The highest extensional rates occurred within the narrow channel, and intensified after the 2 Aug 23:10 calving event. Weak bands of extensional strain also appeared near the glacier center; the magnitudes varied but decreased overall as the terminus re-advanced into the narrow constriction. Small variations in terminus position led to

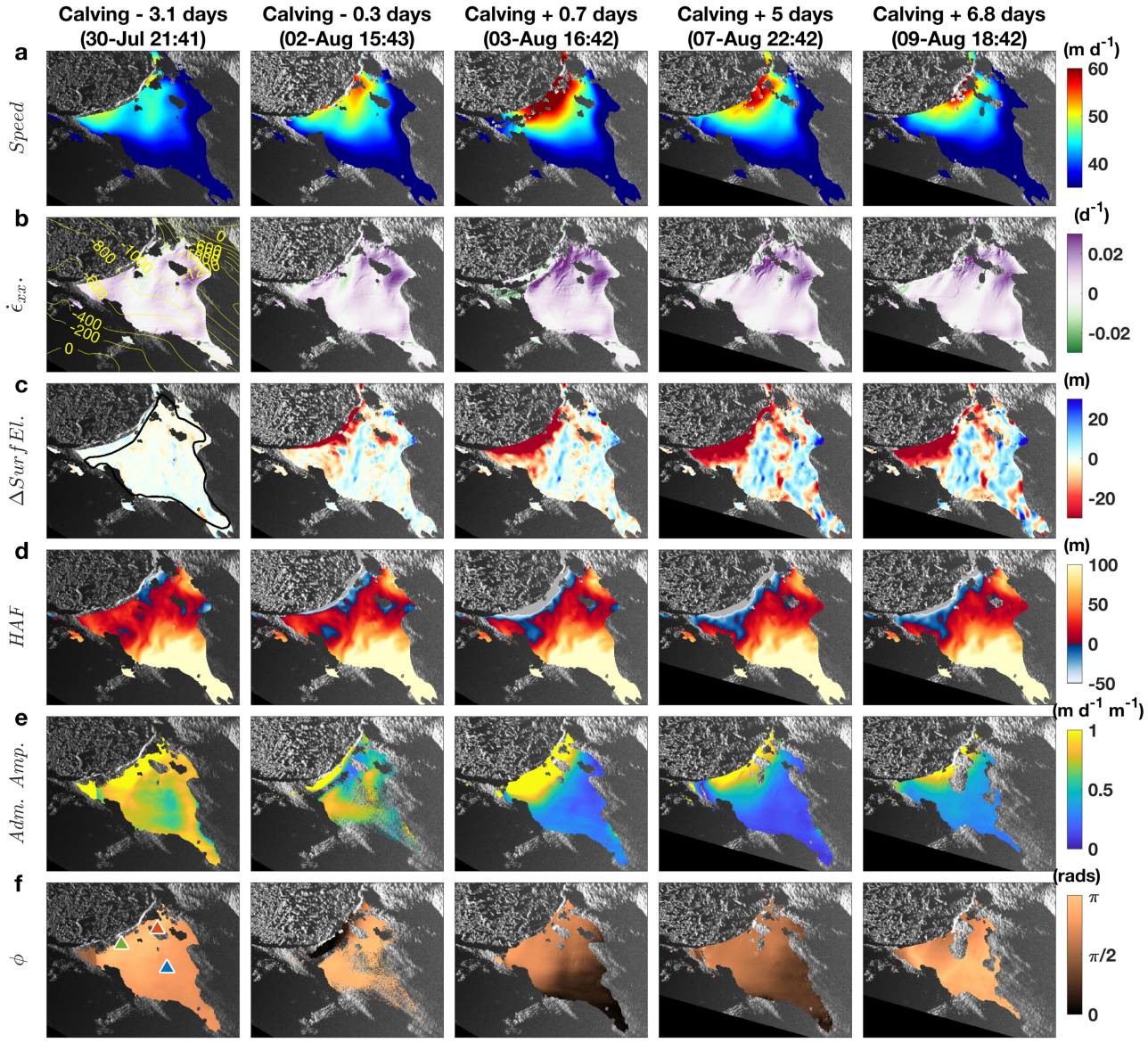

Figure 8: Spatiotemporal variations around 2 Aug 23:10 calving event. (a) speeds, (b) longitudinal strain rates with purple indicating extension and green compression, (c) surface elevation changes, (d) height above flotation (HAF), (e) tidal admittance amplitude, and (f) tidal admittance phase lag. Contours in (b) represent bed elevations from Morlighem et al, [2014]; polygon in (c) indicates 9-km^2 sample area shown in time-series in Figure 9b; colored triangles in (f) show the location of tidal admittance sampled in time-series in Figure 9.

significant changes in strain rate.

The largest decrease in surface elevation occurred at the mélange-glacier boundary and represents calving retreat (Figure 8c). The remaining elevation changes reflect the spatiotemporal pattern in strain rates and advection. Large reductions were observed behind the calving front, within a patch behind the fast-flowing region, and along a thin band that extended south from this patch. In contrast, adjacent areas show an increase in elevation (blue), which created a hummocky surface topography with the same oblique orientation as the strain rates. These observations, specifically - variations in strain rate imposed by bed geometry that resulted in large changes in surface topography, demonstrate the high sensitivity of Jakobshavn Isbræ to small variations in bed topography. Finally, the majority of ice thickened by the end of the record, indicating a strong advective effect.

Spatiotemporal variations in ice thickness have important ramifications for the height-above-flotation (HAF), a parameter often used to assess basal coupling and glacier calving (e.g. *van der Veen, [1996])*. A glacier that is well above flotation has significant overburden pressure that exceeds subglacial water pressure, and enhances basal resistance. As a tidewater glacier thins and overburden is reduced, the terminus approaches buoyancy, which reduces basal traction. Early in the observational period, large extensional strain rates thinned the glacier and decreased the HAF in two key areas: the region coinciding with the deep, narrow section of the fjord (Figure 8b, d), and a patch behind the southwest calving front. The 3 Aug 03:58 calving event removed considerable ice along the southwestern calving front (Figure 5a), and connected the calving face

to the patch of ice below flotation. As a result, a greater portion of the terminus, including the entire calving face, experienced reduced basal coupling, which helped sustain high speeds for several days. Eventually, thicker ice advected towards the calving front (Figure 8c), which increased the height above flotation, enhanced basal coupling, and reduced speeds (Figure 8a). Two localized patches had the greatest impact on basal coupling, highlighting the importance of spatial variations in the HAF. The results demonstrate that behavior of glaciers close to flotation are sensitive to small variations in ice thickness.

2.4.3 Changes in tidal-induced flow

The time-series of speed (Figure 4) showed an increase in semi-diurnal variations following the 2 Aug 23:10 calving event. Changes in basal coupling, as indicated above, should manifest in the glacier's response to ocean tides. We calculated the tidal admittance to characterize tidal forcing. Tidal admittance is a harmonic analysis performed between the ice speed and ocean tides [*Walters*, 1987; *O'Neel et al.*, 2001; de Juan et al., 2010; *Podrasky et al.*, 2014]. It is expressed as a ratio of the amplitudes of ice speed and the tide in units of m d^{-1} m^{-1}, and the difference in phase in radians (tides minus ocean). Admittance amplitude quantifies the tidal forcing, here the M2 principal lunar semi-diurnal tide, the dominant tidal constituent in the fjord. A phase lag of zero indicates glacier speeds that correlate with the tides (high tide = fast flow), while a phase lag of π indicates anticorrelation (low tide = fast flow). Changes in the admittance phase have important implications for basal drag and therefore coupling along the bed. We used t_tide [*Pawlowicz et al.*, 2002], a MATLAB-based harmonic analysis tool, to perform the calculations. First, we re-created the tidal record using t_predict, a tidal prediction tool packaged with t_tide. This was necessary to avoid

transient noise in the measured record related to glaciogenic ocean waves, and to account for a power failure between 5 Aug and 8 Aug. Next, we sampled 24-hr running windows of TRI speeds and passed them through t_tide to calculate the admittance amplitude and tidal phase. Pixels having a signal-to-noise ratio of less than 0.5 were removed to reduce noise. In addition, we discarded values from 5-6 Aug due to data gaps that precluded adequate sampling for the harmonic analysis. Finally, we mapped the admittance amplitude (Figure 8e) and phase lag (Figure 8b).

In general, admittance amplitudes were highest near the calving front (>1 m d^{-1} m^{-1}; Figure 8e) and decreased upglacier (~0.5 m d^{-1} m^{-1}), and phase was generally anticorrelated with the tides (Figure 8f). This implies that the terminus was grounded and that semi-diurnal changes in the water depth modulated terminus speeds by varying the height of the resisting water column along the calving face [*Hughes*, 1989]. We also observed variations in admittance amplitudes and tidal phase over time, indicating changes in terminus stability over time. For example, brief periods of higher admittance amplitudes and shifts in tidal phase were observed leading up to the 2 Aug 10:20 and 23:10 calving events, which suggests that the terminus approached flotation in the hours preceding the calving events, as has been hypothesized as a prerequisite for calving in previous studies [*van der Veen*, 1996; *Vieli et al.*, 2002; *Nick et al.*, 2007; *Xie et al.*, 2016]. Over the next several days, the admittance amplitude and the phase lag were reduced; the latter indicates the terminus moved closer to flotation. There are two ways to impact the flotation thickness of a glacier: 1) via melt and dynamic stretching of the terminus, and 2) by increasing the subglacial water pressure sufficiently to reduce the effective pressure, thereby reducing basal drag. In the next section, we explore these possibilities through multiple time-series.

2.4.4 Dynamic processes, feedbacks, and short-period instability

Despite several calving events during the first few days, the mean front position shows little variation (Figure 9a). Mean speeds (panel b, blue) and the mean change in elevation (orange) within a 9-km^2 polygon (Figure 8b) show small fluctuations, but were generally stable. The surface thinned ~1 m on 2 Aug, another ~1 m on 3 Aug, then stabilized for a couple days before it thinned an additional ~1.3 m on 5 Aug. Speeds reached peak levels between 2 – 5 Aug, coincident with a ~400-m calving retreat. The terminus then started to re-advance and speeds

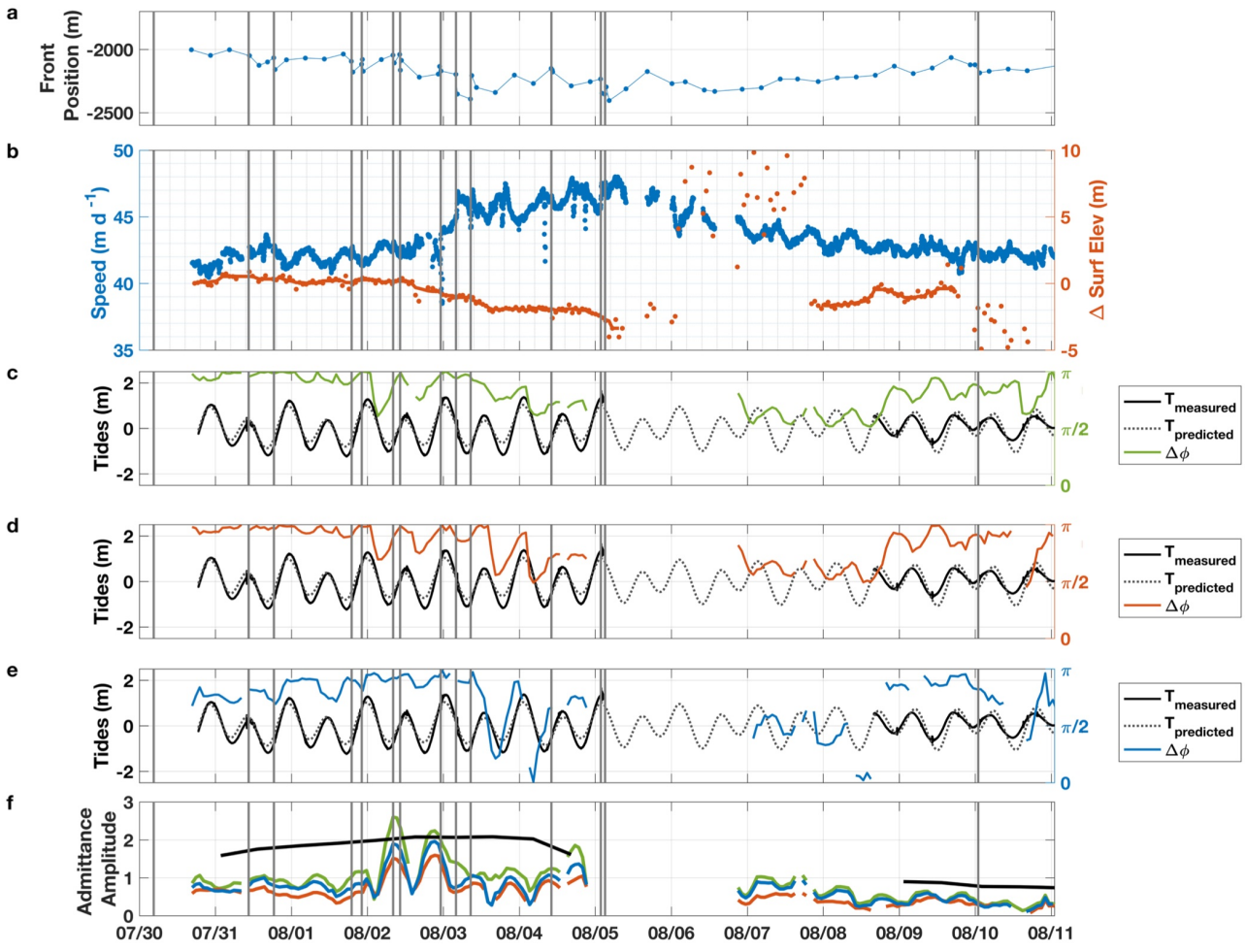

Figure 9: Variations in stability through feedbacks along the terminus. Time-series of (a) mean front position relative to 2012 maximum, (b) speed and surface elevation changes measured from beginning of the record over a 6.5-km^2 patch of the ice stream (Figure 8), (c-e) the phase lag between tides and ice speeds, and (f) admittance amplitude for three locations along the terminus (Figure 8f); black lines in (f) indicate the tidal amplitude (see text). Gray vertical lines throughout indicate the timing of calving events.

began to slow. Noise in the DEM record precluded accurate surface elevation measurements on 6-7 Aug, but elevations were notably higher on 8 Aug and continued to increase as the calving front re-advanced and speeds gradually decreased. By 9 Aug, the terminus had re-advanced to its 2 Aug location and elevation changes were within 0.4 m of pre-calving elevations.

Variations in the tidal admittance sampled at three locations demonstrate a change in the stability, due to changes in ice thickness, beginning on 2 Aug. Phase lag at all 3 locations (Figure 9, panels c,d,e) remained close to π for the first several days, indicating the terminus was well coupled to the bed. However, a dip in phase and subsequent increase in admittance amplitude indicate the terminus moved closer to flotation leading up to the 2 Aug 10:20 and 23:10 calving events (decreased coupling), but immediately moved away from flotation (enhanced coupling) after the calving event (Figure 9f). Then, coincident with the onset of rapid thinning on 3 Aug, the phase reduced and stayed low for several days (decreased coupling), which moved the terminus close to flotation. By 9 Aug, the calving front re-advanced to its 2 Aug position, the mean change in surface elevation (thickness) returned to 2 Aug levels, and the phase lag moved closer to π. However, the tidal admittance also showed greater variability with the tides. Admittance amplitude was lower and the terminus was further from flotation during low tide (enhanced coupling at the bed), while high tide produced higher admittance amplitudes and moved the terminus closer to flotation (reduced basal coupling).

The change in tidal admittance represents a shift in the tidal forcing mechanism. Semi-diurnal variations in water depth still affect the balance of forces along the calving face, but now subglacial water pressure plays a more dominant role. High tides increased the subglacial water pressure that

lowered basal friction and favored flow, while low tides led to lower subglacial water pressures that increased basal friction and retarded flow. Thus, sliding became asymptotically sensitive to changes in effective pressure as the glacier approached flotation. These variations in tidal admittance demonstrate an evolution in terminus stability that is directly related to feedbacks between ice thickness and speed variations over 15 days.

Large-scale changes in ice thickness that occur over short time periods (e.g. daily) can only be explained by ice dynamics. The rapid thinning on 3 Aug occurred because of an abrupt shift in strain rates from an alternating pattern of compressional and extensional regimes to purely extensional (Figure 7a, b), which led to dynamic thinning (Figure 9b) and sustained high flow rates. Several days later, surface elevations (ice thickness) began to increase as the calving front re-advanced. This implies a strong advective component helped reduce speeds and re-stabilize the terminus. A large overdeepening in the bed upglacier of the calving front (e.g. Figure 7c) coupled with the lack of a surface depression suggests that thick ice was located a short distance upglacier of the calving front, which could quickly and easily be advected towards the calving front to help stabilize the terminus after rapid dynamic thinning events.

The majority of calving occurred during a spring tide, which is indicated by the high tidal amplitudes (black line in Figure 9f), the range between mean high and mean low tides over a semidiurnal cycle, between 30 Jul and 5 Aug. This suggests a tidal influence on calving. In contrast, these observations could also reflect a more complex relationship between the tides, the proglacial ice mélange, and calving.

2.4.5 Transient perturbations and long-term change

Podrasky et al [2012] showed that short-term perturbations in flow can impact Jakobshavn Isbræ's behavior over much longer time scales. We compared our results with satellite and time-lapse camera observations to understand how the calving-induced step change in speed influenced the long-term record of change.

Jakobshavn Isbræ retreated ~18 km between 2002 and 2012 (Figure 10a, b), and then another ~1 km by 2013. Since then, the calving front has seasonally varied ~3 km, but maintained the same approximate position in the fjord. Satellite-derived terminus positions (Figure 10c, orange) show

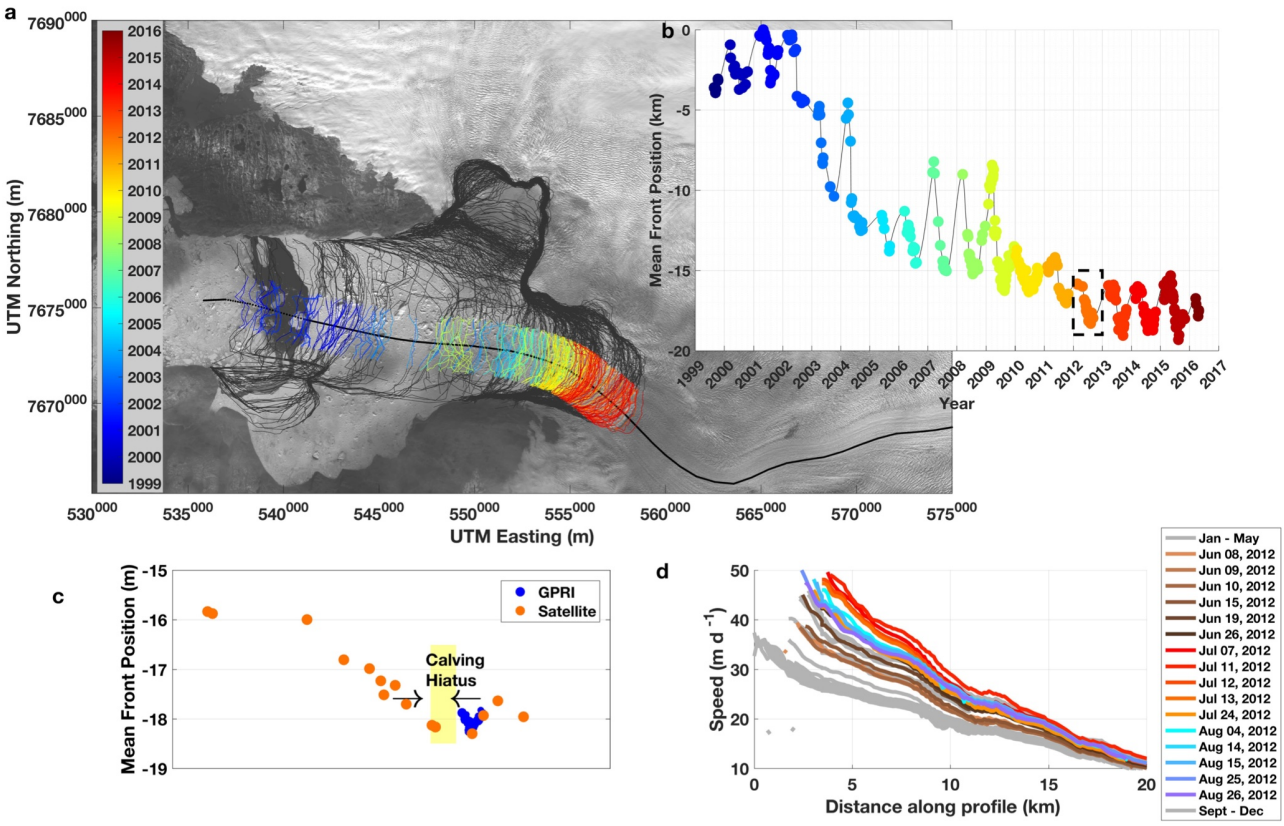

Figure 10: Impact of short-term perturbations. (a) 17-year history of terminus positions with a time-series of mean front positions in (b); (c) closer look at 2012 mean front positions from satellite and GPRI; (d) time-series of satellite-derived speeds from NASA MEaSUREs.

a progressive retreat in 2012 that peaked in July; this was the most retreated position since before the Little Ice Age (1500-1900 A.D.) [*Sohn et al.*, 1998; *Weidick et al.*, 2004] and perhaps the mid-Holocene [*Weidick and Bennike*, 2007; *Briner et al.*, 2010; *Young et al.*, 2011]. Time-lapse cameras show a calving hiatus between 11 Jul and 27 Jul, and the terminus advanced 400-m. Single calving events occurred on 28 Jul and 30 Jul before a series of calving events in early August, coincident with our TRI observations. The 2 Aug 23:10 calving event put the calving face 100 m downfjord of the 11 Jul minimum (Figure 10c), and several additional events over the next three days forced a retreat to the 11 Jul position. Calving ceased on 5 Aug, and the terminus re-advanced.

TerraSAR-X speed profiles from the NASA MEaSUREs data set *[Joughin et al, 2014]* were sampled along a center flowline and plotted by center date (Figure 10d). Speeds were at a minimum between Jan and May (gray), and ranged from 35 m d^{-1} at the calving face to 10 m d^{-1} 20 km upglacier. Speeds increased through Jun (copper profiles) and peaked at 50 m d^{-1} by 7 Jul (red profile). Speeds were slightly lower on 12 Jul (dark orange), followed by a significant reduction by 24 Jul (orange). By 4 Aug (cyan), speeds increased to a second peak that summer, then slowed in late August (purple and blues), and remained low for the remainder of the year (gray).

The satellite and camera records show that Jakobshavn Isbræ experienced two peaks in speed that summer, which coincide with a retreat of the calving front to the same bed constriction in the fjord (e.g. Figure 7c). The records also show a small re-advance between the two peaks returned the terminus into the narrow bed constriction. Serendipitously, our TRI measurements coincide with TSX radar acquisitions on 30 Jul and 10 Aug; therefore, our measurements of a small calving event that triggered a step increase in speed captured the second peak in speed that summer. As the calving front re-advanced into a narrow section of the bed on 9 Aug, speeds slowed, and the terminus moved further from flotation to enhance basal coupling. Based on these observations, we

infer that a similar and perhaps larger dynamic response likely occurred during the July peak in speed, which produced the highest speeds ever recorded along this glacier [*Joughin et al.*, 2014]. Extrapolating our results further, similar processes may explain the recent stagnation in retreat. Beginning in 2012, calving started to occur further into the deep channel where very thick ice (> 1 km) occupies overdeepened sections of the fjord (e.g. Figure 7c). If the seasonal speedup of Jakobshavn Isbræ also enhances advection, as suggested here, then ice dynamics are likely stabilizing the terminus by delivering enough ice to sufficiently increase the height above flotation following perturbations in speed. By compensating for the strain-induced increases, advection processes stabilize the terminus, which decrease speeds, and prevents further retreat.

2.5 Implications for tidewater glacier stability

Our study has several implications for tidewater glacier stability. First, a *small perturbation to a tidewater glacier terminus can generate large variations in speed and therefore ice thickness and stability*. While episodic events such as large calving events [*Scambos et al.*, 2004; *Amundson et al.*, 2008; *Nettles et al.*, 2008; *de Juan et al.*, 2010] or the loss of a floating tongue [*Joughin et al.*, 2004] are known to trigger dynamic changes along the terminus, we show that a small calving event initiated a return to peak flow. This is likely specific to glaciers that are close to flotation, and represents a consequence of the continued drawdown along Jakobshavn Isbræ. However, many of Greenland's tidewater glaciers have been thinning since the early 2000s [*Pritchard et al.*, 2009], and may be susceptible to similar large scale response to small perturbations.

A second implication is that *bed topography plays an important role in the response of a tidewater glacier to perturbations along the terminus*. The influence of bed geometry on fast tidewater

glacier flow has long been recognized [*Meier et al.*, 1979]; the funneling of ice from vast, unconfined regions of the interior through long, narrow, bedrock channels generates large driving stresses along outlet glaciers. Our study demonstrates that even subtle changes in terminus position (e.g. a few hundred meters) can have a profound effect on speed.

Third, *advection processes can stabilize a tidewater glacier by counteracting dynamic thinning losses due to enhanced strain rates.* Increases in strain rate enhance dynamic thinning, which promotes faster flow, additional thinning, and greater instability via a positive feedback loop. However, an increase in speed also increases the rate of advection. Depending on the geometry of the bed and the thickness of ice that occupies it, higher advection rates can exceed dynamic thinning by moving thicker ice into the terminus relatively quickly. The result is an increase in basal traction that creates a negative feedback to help re-stabilize the terminus. This is particularly noteworthy because since 2012, summer speeds have remained elevated but below peak levels [*Joughin et al.*, 2014], and the terminus has shown only a small retreat (Figure 10). Seasonal increases in speed are likely driven by the dynamic responses explained here and in previous studies [*Joughin et al.*, 2012; *Podrasky et al.*, 2012]. The advection of thick ice into the terminus from an overdeepening a short distance upglacier of the calving front may indeed be compensating for the seasonal increase in longitudinal stretching, and could explain at least part of the seasonal slowdown in speed and the lack of continued large-scale retreat of the terminus. However, a recent thinning trend [*Joughin et al.*, 2012], sinuous and hummocky bed geometry throughout the fjord [*Morlighem et al.*, 2014], and the recent decline in Greenland's mass balance [*Van den Broeke et al.*, 2009; *Enderlin et al.*, 2014] will limit the ability of advection processes to stabilize the terminus. Left uncompensated, seasonal accelerations in speed and dynamic thinning will continue

unabated, further enhancing speed and drawdown through positive feedbacks that will lead to large scale terminus retreat [*Pfeffer*, 2007].

2.6 Conclusions

We used terrestrial radar interferometric observations to show that a small calving event at Jakobshavn Isbræ in August 2012 forced a return to a historic peak in speed, which enhanced strain rates and led to rapid dynamic thinning. As a result, the terminus moved closer to flotation, which reduced basal coupling and sustained high speeds for several days. A small re-advance coupled with the advection of thick ice increased basal coupling, which slowed speeds and re-stabilized the terminus. Our findings are consistent with previous studies [*Vieli and Nick*, 2011; *Joughin et al.*, 2012; *Motyka et al.*, 2017] on the relationship between tidewater glacier thickness and speed; however, the short time scales shown here highlight the impact that small-scale perturbations can have on tidewater glacier termini.

Our study demonstrates the importance of bed and surface topography in tidewater glacier response to calving. Small-scale variations in bed and surface topography can lead to large dynamic changes following perturbations to the calving front. In contrast, overdeepened sections of the fjord that contain thick ice can re-stabilize a terminus through advection processes, which may help slow the rate of retreat. Any such effects are likely to be temporary, however, as elevated rates of advection are unsustainable over long time scales and ultimately deplete the reservoir of ice far upglacier. Coupled with the reduction in Greenland's mass balance and a recent thinning trend, the long-term stabilization of the glacier via advection is likely to be minimized, and the large scale, rapid retreat of Jakobshavn Isbrae that occurred over the last decade will continue until the glacier has retreated far into the interior of the ice sheet.

3 THE BIMODAL CHARACTER OF GRANULAR ICE MÉLANGE AND THE INFLUENCE ON CALVING AT JAKOBSHAVN ISBRÆ

3.1 Introduction

Ice mélange is an assemblage of icebergs and sea ice found in many tidewater glacier fjords. Ice mélange can contribute significant freshwater to fjord surface layers [*Enderlin and Hamilton*, 2014; *Moon et al*., 2017], and suppress ocean waves [*MacAyeal et al*., 2012], and thus affect fjord circulation [*Mortensen et al*., 2013; 2014]. Ice mélange can also influence iceberg calving [*Amundson et al*., 2010], which can affect the location [*Cassotto et al*., 2015], speed, and thickness (chapter 2) of a glacier terminus. Variations in the strength and resistance of ice mélange remains a leading hypothesis to explain recent changes along Greenland's tidewater glaciers [*Straneo et al*., 2013]; however, a paucity of field observations hinders validation. The granular composition and mobility of ice mélange, especially during summer months, make traditional survey techniques dangerous and satellite observations difficult. Consequently, little is known about ice mélange rheology and the mechanism(s) by which it can impede calving. Here, we present observations of speed and strain rates of Jakobshavn Isbræ's granular ice mélange acquired in Aug 2012 to evaluate the variability between calving events.

Previous studies have demonstrated a relationship between a rigid ice mélange and terminus advance in winter. Satellite observations have shown that the weakening or disintegration of ice mélange has led to dynamic changes along glacier termini [*Reeh et al.*, 2001; *Howat et al.*, 2010; *Walter et al.*, 2012; *Sundal et al.*, 2013; *Cassotto et al.*, 2015]. Numerical models have found a correlation between the presence of an ice mélange, calving cessation, and terminus advance [*Vieli*

and Nick, 2011; *Todd and Christoffersen*, 2014; *Krug et al*., 2015]. The models typically prescribe a seasonally rigid or semi-rigid ice mélange that imposes stress and inhibits calving. These ice shelf analogs apply to cold, winter ice mélange conditions [*Cassotto et al.*, 2015]; however, they do not account for the granular behavior of summer ice mélange.

Recent studies invoke granular mechanics to suggest that force chains and iceberg contact forces within the mélange can support sufficient stress to affect calving. Peters et al, [2015] used radar backscatter images to show that Jakobshavn Isbræ's proglacial ice mélange dynamically jams during calving events, which indicates a granular mélange can support stress. Robel [2017] further illustrated this phenomenon with a discrete element model, and demonstrated the importance of sea ice bonds and irregularly shaped fjord walls (rough surface) in imposing stress to the terminus. Most recently, Burton et al (in review) calibrated laboratory and numerical models with limited field observations to quantify stress in a granular mélange.

Jakobshavn Isbræ (Figure 11) produces some of the highest iceberg discharge rates along the margin of the Greenland Ice Sheet [*Rignot and Kanagaratnam*, 2006; *Enderlin et al.*, 2014]. As a result, the densely packed ice mélange persistently extends >10 km from the glacier. We used terrestrial radar interferometers (TRI) to observe short-term variability in granular ice mélange in August 2012. Earlier studies by Peters et al. [2015] and Burton et al. (in review) utilized feature tracking techniques on a subset of the TRI backscatter images to derive velocity fields during calving events and mean velocity fields between calving events, respectively. Here, we use the complete record of phase-derived measurements to evaluate short-term variations in speed and strain rates. Specifically, we seek to determine: 1) the spatial and temporal scales over which

granular ice mélange varies, 2) what do variations in strain rate indicate about the rheology of the ice mélange, and 3) if the interferometric data shows a change in mélange behavior prior to calving. We find the mélange exhibits two modes of behavior: 1) slow, coherent, quasi-plug style deformation during periods of terminus quiescence (no calving); and 2) episodic changes in the stress state prior to calving.

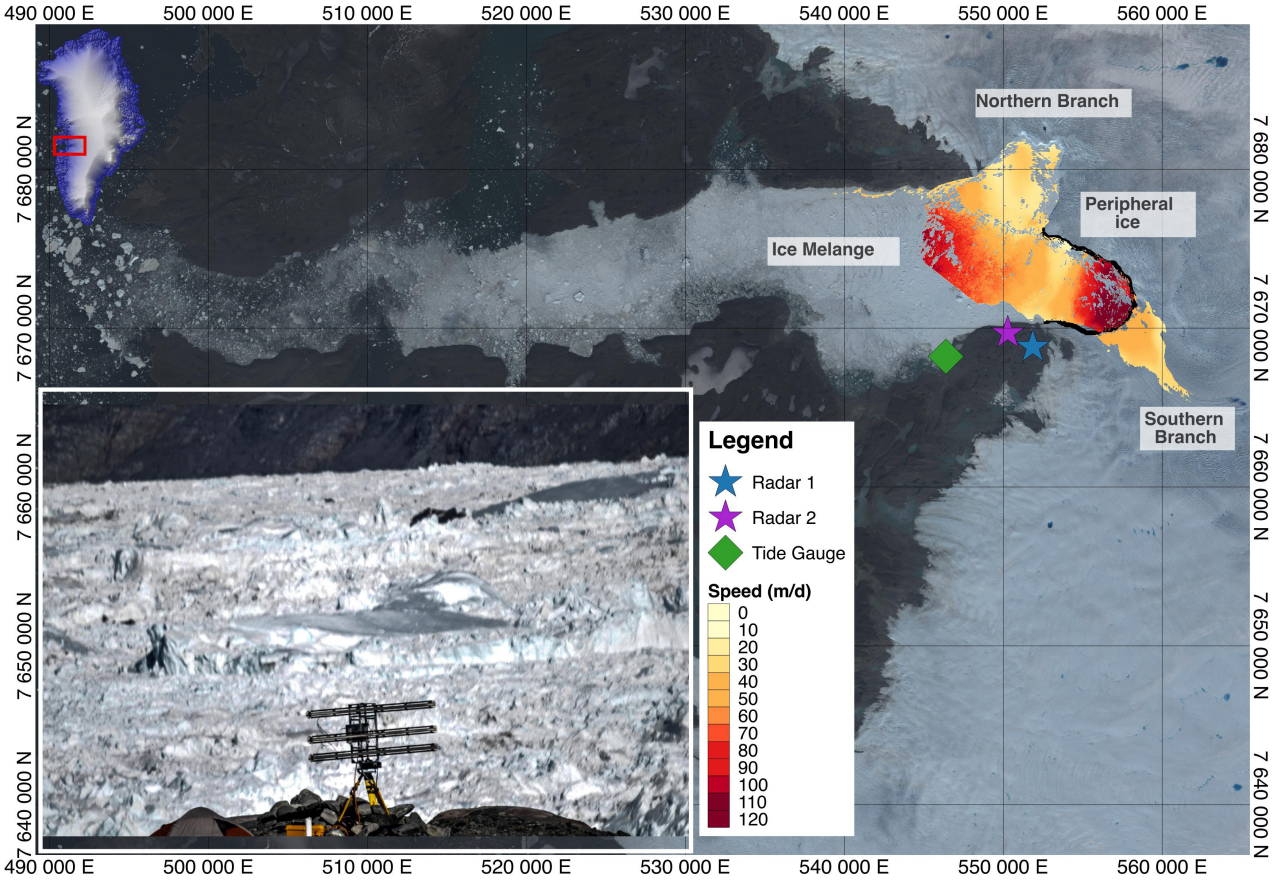

Figure 11: Landsat 8 image of Jakobshavn Isbræ and the proglacial ice mélange with TRI-derived speeds (colors) sampled ~30 minutes before a calving event on 2 Aug 2012. (Inset) Photograph of the TRI at radar site 2 with ice mélange in the background.

3.2 Methods

A field study was conducted in Aug 2012 to monitor the behavior of summer - granular ice mélange in the proglacial fjord of Jakobshavn Isbræ, Greenland. A pair of Gamma Remote Sensing

GPRI-II terrestrial radar interferometers were configured on bedrock along the southern fjord and separated by 1.9 km (Figure 11). The radars scanned the terminus and proglacial ice mélange every 3 minutes between 1 and 12 Aug with limited breaks. Each instrument used a 180º scan in azimuth, a 16-km range radius, and both radars were synchronized using GPS time codes.

Data from each radar was processed independently and then combined to create two-dimensional velocity fields. Raw data was processed to single-look complex images, multi-looked by 15 in range (to an effective range resolution of 11.25 m), and used to create 3-minute displacement interferograms. Due to instrument issues, a reduction in signal strength limited observations in the late record (10 - 12 Aug); however, useful data with lower signal to noise ratios were acquired and are presented here. Interferograms were filtered using an adaptive filter [*Goldstein and Werner*, 1998] and then unwrapped using a minimum cost flow (mcf) method [*Goldstein et al.*, 1988].

The mcf unwrapper cleanly unwrapped phase measurements for the majority of the record; however, unwrapping errors of 1- 2 integer cycle slips still occurred. Since our objective was to produce a continuous velocity field free of unwrapping errors while also preserving phase jumps related to calving events, we applied a smoothing spline through time for each pixel in the mélange. Splines were calculated over the shorter of daily intervals or inter-calving periods. This approach produces smoothly varying speeds free of cycle slips, but obscures transient signals due to rolling icebergs or calving events from the northern terminus (Figure 11).

After correcting for phase unwrapping errors, we converted displacements to line-of-sight (LOS) speeds. A total of 3163 interferogram pairs (in LOS geometry) were used to create two-

dimensional velocity fields using the methods of Voytenko et al, [2017]. The method produced northing and easting velocity components that were used to: 1) calculate speeds in the direction of flow (i.e. non-LOS), and 2) rotate the geometry for proper strain rate derivations. To derive strain rates, we used the components to calculate the flow direction at each time step and for each pixel. These angles were used to rotate the local reference frame to derive the spatial derivatives along-flow using the methods of Fastook et al [1995]. Finally, the divergence of the velocity field ($\nabla \cdot \vec{u}$) and shear strain rates were calculated and analyzed for variations in time, and compared with the timing of calving events observed in the TRI backscatter images (see 2.2.3).

3.3 Observations

3.3.1 Two-dimensional Mélange Speeds

Overall, mélange speeds were much slower near the calving front than downfjord (Figure 12a), though there was considerable variability due to calving and tides. Speeds increased prior to calving (Figure 12b), then slowed to almost 0 m d^{-1} immediately after (Figure 12c). A time-series along a longitudinal profile (Figure 12e) shows semi-diurnal variations, which is most evident between 8 and 12 km. There was a distinct change in the structure of the velocity field halfway through the record. Between 1 and 5 Aug, mélange speeds nearest the terminus were faster than speeds 2 - 4 km downfjord, which created a patch of slow moving ice mélange in this region (Figure 12a, b, e). Following the 5 Aug calving event, the slow patch disappeared in the mélange, and the longitudinal profile shows mélange speeds increasing steadily away from the calving front (Figure 12c-e). The speed and location of the glacier varied considerably during

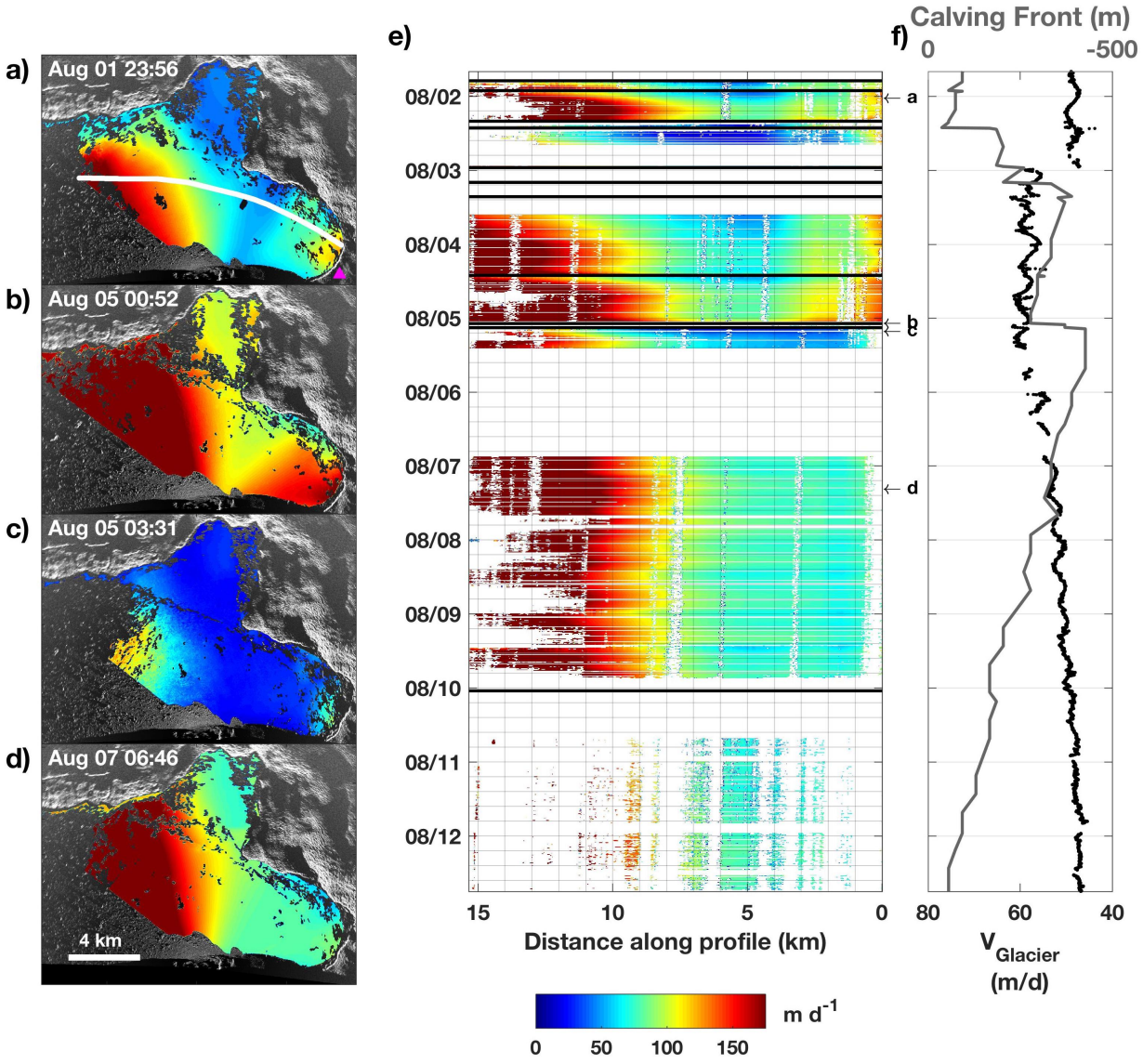

Figure 12: (a-d) Mélange speeds at different times in the record, (e) a time-series of speed sampled along the profile (white line in a), with the timing of calving events indicated by horizontal black lines. (f) the speed and location of the glacier terminus (see 2.3.1). Magenta triangle in (a) shows location of glacier speeds sampled.

this time. The mélange nearest the calving front was fastest on 4 Aug, when the glacier was also near peak flow rates and advancing.

3.3.2 Divergence of the velocity fields

The divergence of the velocity field, the rate at which the mélange is flowing into (convergent) or

out of (divergent) an Eulerian pixel, showed a bimodal pattern within the mélange in time. The first mode (mode 1) was characterized by coherent, smoothly-varying strain rate fields (Figure 13a) that occurred during periods of terminus quiescence. The strain rate fields were clearly delineated with mélange in the inner fjord under compression (blue), and mélange downfjord under extension (red). The second mode (mode 2) was characterized by the rapid deterioration of the

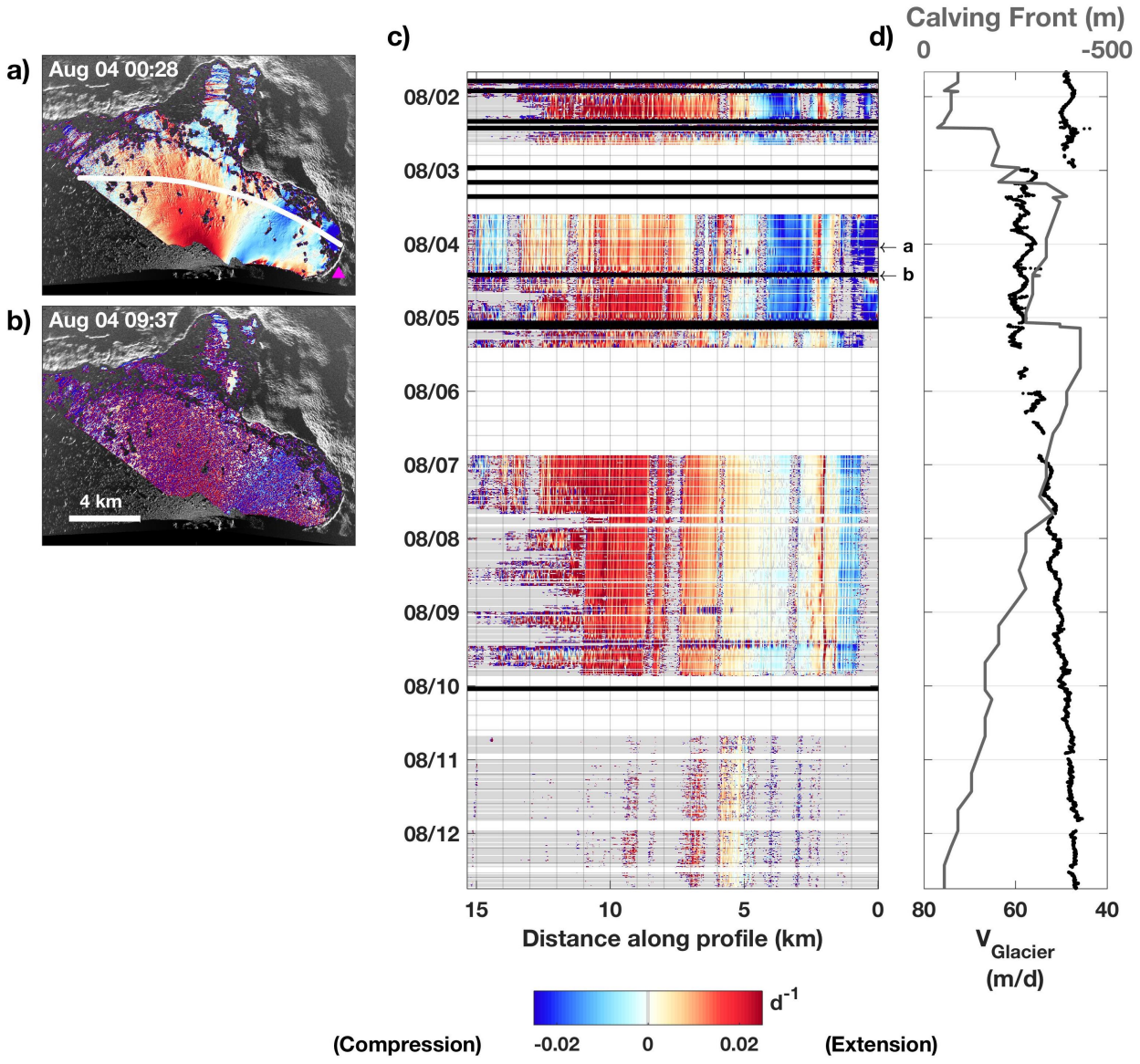

Figure 13: Bimodal strain rates: (a) Coherent, distributed strain fields between calving, and the (b) rapid deterioration of strain rates prior to calving. (c) Time-series of strain rates along the profile in (a), black lines indicate timing of calving events. (c) The speed and location of the glacier terminus (see 2.3.1). Magenta triangle in (a) shows location of glacier speeds sampled.

coherent strain rate fields into heterogeneous fields that reflect the localized strain rates within small clusters of icebergs (Figure 13b); this mode had an ephemeral existence, which initiated ~60 minutes before and terminated 60-180 minutes after calving. In contrast, mode 1 type strain rates dominated the record, though the magnitude of strain rates varied (Figure 13c). Compression rates were highest in the inner fjord (0 – 5 km) between 1 and 5 Aug when the terminus was slowly advancing downfjord (Figure 13d, gray), and when it retreated and experienced a step increase in speed (Figure 13d, black). Beginning on 7 Aug, the compression rates were lower when the terminus was slowing and in a retreated position.

3.3.3 Shear strain rates

The mélange exhibited quasi-plug flow, wherein shear strain rates were minimal near the mélange center and were greatest along lateral margins nearest to the fjord and glacier walls; this is most evident in the mélange nearest the calving front (Figure 14a, b). The northern margin showed a positive or clockwise rotation (red), while the southern margin showed a negative or counterclockwise rotation (blue) of angles within shear margins. A time-series sampled along a transverse profile (Figure 14a, black line) shows significant variability in shear margins (Figure 14c) over time. Following calving, large areas of the northern margin experienced negative shearing before eventually transitioning back to a positive shear angle (Figure 14a, c). Shear was highest along both margins between 2 and 4 Aug, concurrent with multiple shear bands along the north margin (purple arrows). The northern margin also showed a southward migration with time (downward shift in red).

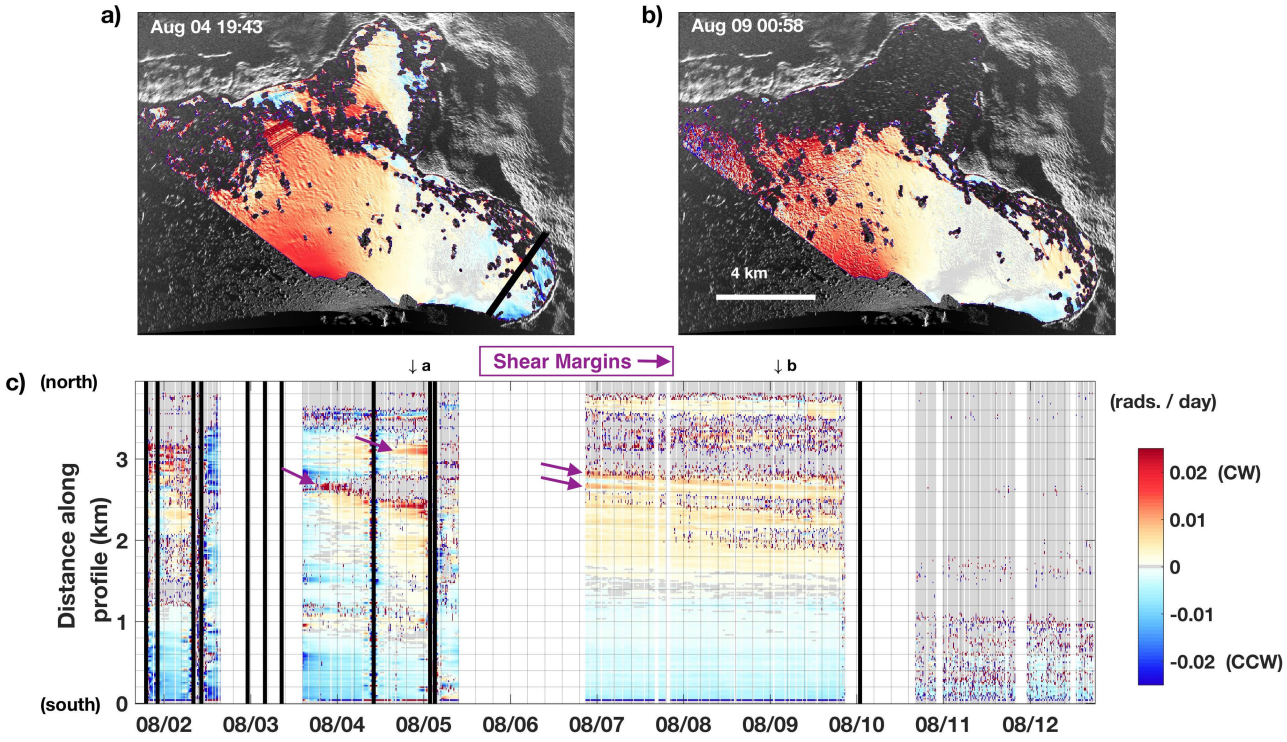

Figure 14: Maps of shear strain rates (a,b) show clockwise (CW) or opening of shear margins downfjord (red), where the fjord widens and the mélange is less confined. Alternating patterns of red (CW) and blue (CCW or closing of the shear margin) appear near the glacier, where the fjord narrows. (c) Time-series of shear strain rates sampled along a transverse profile (black line in a) show the dynamic character of the shear margins. Shear margins are clearly defined along the northern margin and move towards the mélange center between calving events (black lines).

3.4 Discussion

Jakobshavn Isbræ's granular ice mélange occurs along the fjord surface of Greenland's most dynamic tidewater glaciers, and thus is subjected to several forcing mechanisms that occur over a variety of spatial and temporal scales. Ocean tides, iceberg calving, the speed and location of the glacier terminus, wind (e.g. katabatic), subglacial meltwater discharge, and iceberg contact forces are all likely to impose varying level of control on the granular ice mélange. Here, we assess the influence of these mechanisms using our 11-day record of observations.

3.4.1 Wind and subglacial discharge

High velocity, directional winds can force sea ice [*Oltmanns et al.*, 2014] and ice mélange [*Cassotto et al.*, 2015] away from a glacier, and thus could influence mélange speed. For the orientation of the glacier terminus and its proglacial ice mélange during our observation period (Figure 11), winds that originated from the south to southeast may have imposed such an influence. Meteorological data acquired from an all-weather station situated on a bedrock outcrop near the norther terminus of Jakobshavn Isbræ (~12 km north of camp) report winds consistently originated from the northwest to the northeast (Figure 15) over our observation period *[Holland and Holland, 2016]*. Thus, winds do not appear to be a factor during our field study.

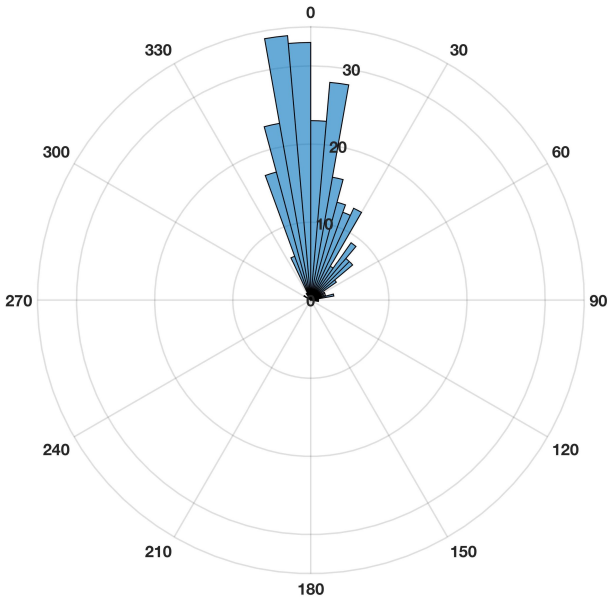

Figure 15: Polar histogram showing the origination direction of winds in the fjord sampled from a weather station near the northern terminus of Jakobshavn Isbræ [Holland and Holland, 2016].

Subglacial discharge of meltwater can create buoyant freshwater plumes [*Motyka et al*., 2003; 2013] that erode melt channels along the basal layers of floating ice tongues [*Rignot and Steffen*, 2008; *Motyka et al*., 2011]. Surface melt was exceptionally high in 2012 [*Nghiem et al*., 2012], which suggests that meltwater discharge could have forced the mélange away from the terminus, and therefore influenced speed. To access this influence requires extensive knowledge of the subglacial hydrology and mélange subsurface conditions (e.g. roughness), neither of which is well known.

3.4.2 Iceberg calving and terminus dynamics

Dynamic changes at the glacier terminus were a dominant control on mélange speed, especially within the first ~7 km from the terminus. The speed and location of the calving front imposed a first order control on mélange speed nearest the glacier. The mélange was fast when the glacier was in an advanced position and/or flowing fast, and slow when the terminus was in a retreated position and slowing. Mélange speeds at the glacier terminus were also consistently higher than the glacier, indicating the glacier terminus was not the sole control on speed. This is an important distinction from winter conditions when a cold, rigid ice mélange is pushed downfjord at the speed of the terminus [*Joughin et al.*, 2008; *Foga et al.*, 2014; *Cassotto et al.*, 2015].

Iceberg calving also influenced mélange speed, and the effects scaled with calving size. Speeds were consistently slower after all calving events (Figure 12c, e); however, the reduction in speed was pronounced both in spatial extent and duration after the 2 Aug and 5 Aug calving events. These were the two largest calving events (0.88 and 1.31 km^2; see Figure 5 in 2.3.2) for which velocities were obtained. A data gap inhibits a thorough assessment of speeds after the 3 Aug 03:58 event (0.56 km^2, Figure 5); however, speeds midfjord (3.5 – 8 km) were still quite low on 3 Aug

14:13, suggesting this calving event also led to lower speeds there. In contrast, the remaining events were quite small (<0.19 km^2, Figure 5) and reduced speeds for short durations (e.g. minutes vs hours). Thus, small events minimally impact mélange speeds, while large events imposed greater influence. This is because large events introduce more ice to the immediate proglacial mélange than smaller events, which leads to greater displacement within the mélange. This is supported by time-lapse observations of radar backscatter images that show the displacement of icebergs within the mélange after calving; large calving events forced displacements throughout the entire width of the mélange, while the effect was much more localized for small events.

3.4.3 Tidal forcing

A semi-diurnal signal observed in the time-series of speeds (Figure 12e) suggests a tidal influence. We evaluated this influence using a harmonic analysis, commonly referred to as a tidal admittance calculation [*Walters and Dunlap*, 1987; *O'Neel et al.*, 2003; *Podrasky et al.*, 2014]. Tidal admittance quantifies the response of a system to ocean tides and is expressed as: 1) an admittance amplitude, expressed as the ratio between a system response (e.g. mélange) and the tidal forcing in units of m d^{-1} per m of tide, 2) a phase lag in units of radians. We used t_tide [*Pawlowicz et al.*, 2002] to calculate the admittance of the M2 component – the principal lunar semi-diurnal constituent, over a 24 hour period beginning on 7 Aug, a period with no calving and steady flow. Admittance amplitude was smallest near the calving front (~1 m d^{-1} m^{-1}) and increased downfjord (>10 m d^{-1} m^{-1}; Figure 16a). The small response upfjord is likely a consequence of the compressive, resistive mélange there (Figure 13a), but also smaller tidal flux. In contrast, extensional strain rates downfjord (Figure 13a) suggest the mélange is less coherent there, and therefore more susceptible to tidal fluctuations. Overall, mélange speeds lagged the tides by ~$\pi/2$ radians (Figure 16b), which indicates that tidal transitions imposed the greatest influence on mélange speed. The influence was

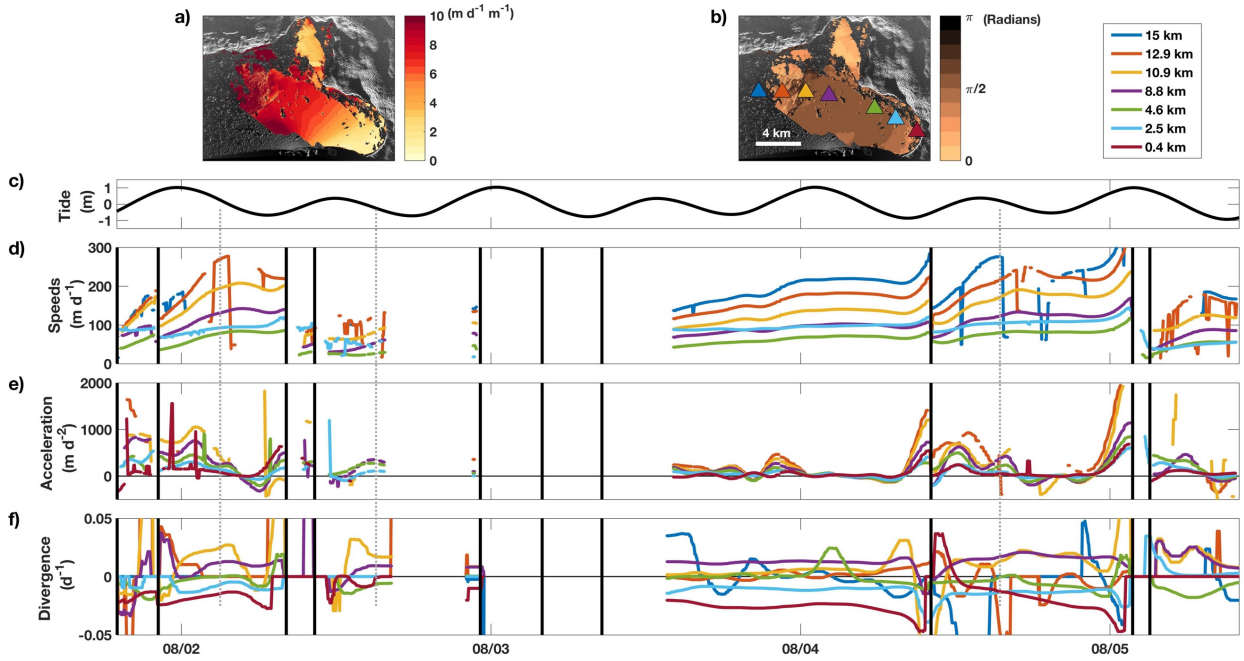

Figure 16: (a) Admittance amplitude and (b) phase lag of mélange speeds on 7 Aug. Time-series of (c) ocean tides, (d) speeds, (e) acceleration, and (f) divergence at discrete points in the mélange. The colors in (d-f) correlate to the colored triangles in (b

apparent in time-lapse sequences of radar backscatter images that show icebergs along the western margin of the observation window repeatedly pulled downfjord with the falling tide. This influence can also be observed in the time-series in Figure 16. At high tide (Figure 16e), the mélange began to accelerate (Figure 16e), speeds peaked during mean tides (gray vertical dashed lines in Figure 16c,d), and then decelerated at low tide (Figure 16e).

3.4.4 Internal controls with granular ice mélange

In contrast to mélange downfjord and the region nearest the calving front, speeds in the central fjord lacked significant diurnal variability and appeared independent of changes at the glacier (e.g. 5 - 8 km along profile in Figure 12e). The time-series of speeds (Figure 12e) suggests a region of converging flow that was highest in the early portion of the record, coincident with an advanced position and step increase in speed of the terminus (Figure 13). The large area of

compression implies jamming and therefore some internal dynamics within the granular ice mélange. This also implies resistance within the mélange, and the proximity to the calving front suggests that the ice mélange could influence calving.

The region under compression occurs within a narrow section of the fjord (~4km; Figure 11), while extension occurs where the fjord is wide (~9 km). This suggests that fjord width has a first order control on mélange resistance, which is consistent with numerical simulations and laboratory experiments of sea ice [*Hopkins and Tuhkuri*, 1999] and ice mélange [Robel, [2017]; *Burton et al (in review)*] that show an inverse relationship between fjord width and stress in the mélange. An important distinction between the observations and the models is the unidirectional stress applied in the models. At Jakobshavn Isbræ, ice flow exerts pressure on the mélange from many directions - from the peripheral ice to the north, all the way down to the main branch in the southeast (Figure 11), which likely bolsters compression in this region. The ompression observed in the mélange nearest the terminus implies a resistive mélange that is capable of supporting stress.

Two general modes were exhibited in the maps of divergence, which implies a bimodal stress state in the mélange. The first mode, distributed stress, is interpreted as having force chains and iceberg-contact forces that produce a smoothly-varying and coherent stress field. The observations show the mélange remained in this mode for the majority of the record (~85% of observation period). The second mode, incoherent stress, occurred when contact forces and force chains rapidly deteriorated and resulted in localization of stress in the mélange; this mode was transient and episodic, and always preceded calving. Peters et al, [2015] showed that Jakobshavn Isbræ's mélange dynamically jams during calving events and concluded that the mélange is close to the

jamming point just before calving. What remained uncertain, however, was whether this phenomenon was associated with calving only, or if jamming occurs between calving events. The coherently distributed patterns of strain rate in mode 1 indicate that the mélange is at the jamming point during periods of terminus quiescence. A short transition time between the two states further supports this and indicates that the mélange unjams prior to calving, then quickly re-jams soon after.

Prominent shear bands were observed along the mélange margins (Figure 14a, b) that coincide with the compressional region (Figure 13). Multiple bands and intervals of negative values (a closing of the shear margin) indicate a wide plug with extensive shearing through one or more bands along the northern margin. The inward migration of the northern shear margin towards the mélange center (Figure 14c) indicates an evolution of stress from large-scale compression of a wide plug in the early record (Figure 13, Figure 14) to small-scale compression of a narrow plug beginning on 6 Aug. The plug narrows until force chains are broken, the stress field breaks down, and calving commences, which further perturbs the mélange, and resets the stress field.

The size of the calving events affected the severity of the perturbation to the mélange. The 5 Aug 1:44 event was the second largest event in the study (1.31 km^2; see Figure 5 in 2.3.2) and occurred in front of the northern shear margin. This caused a major perturbation in the mélange that reset the stress field and resulted in lower compressional (Figure 13) and shear strain rates (Figure 14). Likewise, the 2 Aug 10:20 event (0.88 km^2) was also quite large and had a similar impact on the stress fields. In contrast, calving on 4 Aug (0.1 km^2) was ~8% the size of the 5 Aug event, and only briefly disturbed the stress field. These strain rate observations suggest that small calving

events contribute ice to the mélange, which bolsters the mélange fabric and enhances stress (e.g. Aug 4), while large calving events perturb the mélange and reset the stress field.

3.4.5 Downfjord initiation of ice mélange variability

Tidal-induced variations in mélange flow are initiated downfjord, where weak extensional strains are susceptible to perturbations in flow, and then propagate toward the glacier terminus. We found a similar sequence of events prior to calving on 2 Aug, 4 Aug, and 5 Aug. An acceleration of the downfjord mélange (Figure 16e) led to faster speeds in the mélange upfjord (Figure 16d). As a result, extensional strain rates increased downfjord (Figure 16f) and the compressional mélange near the terminus shifted to an extensional regime (divergence became less negative), which led to calving (black vertical lines in Figure 16). The process initiated downfjord ~2-3 hours prior to calving, led to a transition from a distributed to an incoherent stress field ~60 minutes before calving (see section 3.3.2), and eventually loss of compressive strain rates at the calving front ~6-9 minutes prior to calving (Figure 16f). The sequence of events implies that perturbations in mélange speed, and consequently strain rates, are triggered downfjord and propagate upfjord soon after.

The downfjord initiation of perturbations in mélange speed, coupled with the strong tidal influence there suggests a complex relationship between ocean tides, ice mélange, and glacier calving. The majority of calving occurred during the first week of observations, coincident with a spring tide (see Figure 9 in *2.4.3),* while only a single calving event occurred in the second week (neap tide). The short record makes it difficult to further discern a definitive relationship. Nonetheless, extensional strain rates in the outer mélange indicate that the granular interactions

there are weak and thus susceptible to perturbations. The evacuation of the outer mélange increases mélange speeds near the terminus, which lowers stress in the mélange, and if large enough, can lead to catastrophic failure and calving.

3.5 Conclusions

We present the first known observations of short-term flow variability of granular ice mélange from a terrestrial radar interferometric study along Jakobshavn Isbræ, Greenland. In general, the mélange was slower near the glacier terminus than it was downfjord, though there was considerable variability in mélange speed over the study. Several factors influenced speeds within the mélange. Ice dynamics exerted a dominant control on mélange speeds nearest the glacier, while ocean tides had the greatest influence downfjord. The confining fjord geometry and complex ice flow patterns in the middle of the fjord, coupled with the inability of small calving events to evacuate ice from the inner fjord, led to a convergence of ice mélange and a reduction in speeds there, which led to a large area of compression within the mélange near the glacier.

Overall, we observed strain rates within the mélange to exhibit bimodal characteristics. For the majority of the record, the mélange remained in a distributed stress state characterized by smoothly-varying strain rates likely facilitated through force chains and iceberg-iceberg contact forces. The second mode, incoherent stress, occurred ~1 hour before and after calving and represents the deterioration of contact forces, which reduced stress and led to calving. The rapid remobilization of the mélange and redistribution of stress following calving suggests that Jakobshavn Isbræ's proglacial summer ice mélange remains close to the jamming point during periods of terminus quiescence. Mélange motion was accommodated along lateral shear bands in a quasi-plug style deformation. The channel of the deforming mélange narrowed in time until a

large calving event displaced icebergs within the mélange, which reset the shear margins and re-organized shear strain rate fields; we observed that calving events >0.19 km^2 were sufficient reset the shear margins. Our observations show that compressive strain rates in the divergence of the velocity fields were greatest when the deforming mélange margin was most narrow; this is consistent with numerical models of ice mélange [*Robel*, 2017] and laboratory experiments of sea ice [*Hopkins and Tuhkuri*, 1999] that show narrow channels support higher stress levels.

Finally, our observations show that variations in strain rates of ice mélange can influence calving along a tidewater glacier. We observed multiple occurrences of a speedup in ice mélange that preceded calving. Changes in mélange speed initiated downfjord >60 minutes before calving, propagated up the mélange, and led to a loss of compressive strain rates at the terminus ~6-9 minutes before calving. These findings validate a hypothesis: that variations in ice mélange can trigger dynamic changes at tidewater glacier termini [*Straneo et al*., 2013]. Our observations are the first in-situ evidence of such an influence from summertime, granular ice mélange conditions. Our findings have implications for calving rates, terminus speed [*Nettles et al.*, 2008; *de Juan et al.*, 2010], ice thickness and stability (see 2.4). Future studies would benefit from longer observation periods that include multiple tidal cycles and the evolution of granular ice mélange and its influence on calving dynamics over seasonal time scales. Future efforts should also be dedicated to characterizing the viscosity of the mélange, which would be most useful for the modeling community.

4 LARGE VELOCITY RESPONSE TO PRECIPITATION AND TIDAL FORCING AT COLUMBIA GLACIER, ALASKA – EVIDENCE FOR LATE SUMMER CHANGES IN SUBGLACIAL HYDROLOGY

4.1 Introduction

Columbia Glacier is an Alaskan tidewater glacier that stretches from the high peaks of the Chugach Mountains to Prince William Sound (Figure 17). A calving retreat that initiated in the 1970s has resulted in a 22 kilometer retreat [*McNabb and Hock*, 2014]), reduced the ice volume by half [*McNabb et al.*, 2012], and split the glacier into two branches. The lower 10 kilometers of the main branch are grounded below sea level at depths up to 300 m [*McNabb et al.*, 2012; *Rignot et al.*, 2013a], which suggests additional retreat is likely. Speeds along the lower termini vary seasonally, with fast flow (~10 m d^{-1}) during winter months and slow speeds (~2 m d^{-1}) during the mid-to-late summer. Similar observations have been observed along Alaskan tidewater glaciers, including Columbia [*Vaughn et al.*, 1985; *Krimmel and Vaughn*, 1987; *Walters and Dunlap*, 1987] and Hubbard Glaciers [*Trabant et al.*, 2003; *Ritchie et al.*, 2008]; however, the pronounced seasonal slowdown of the lower glacier has not (~20% of annual maximum, Figure 18b). Such large decreases in speed and low summer speeds suggest a change in hydrology driven by seasonal variations in precipitation and meltwater. To better understand these uncharacteristically low speeds, we conducted a field study to investigate short-term variations in speed during a slow period of flow.

Pioneering work by Austin Post and Mark Meier led them to develop the idea of the Tidewater Glacier Cycle [*Post*, 1975], and consequently a prediction of Columbia Glacier's impending retreat

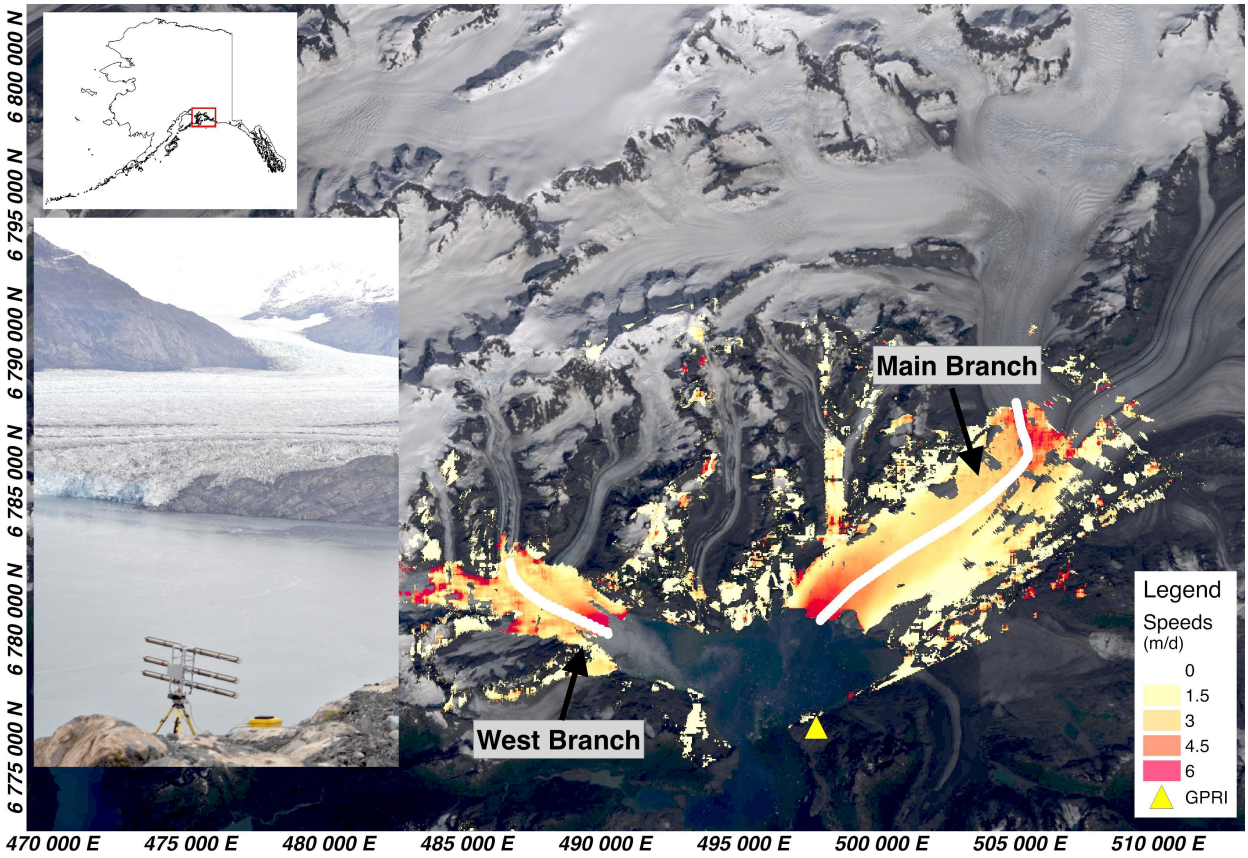

Figure 17: Landsat 8 image from the study area with TRI-derived speeds from Oct 2014; white lines indicate the location of the profiles sampled in Figures 18 - 20. (Inset) TRI instrument deployed at a bedrock camp ~4 km from the Main Branch.

[*Meier et al.*, 1979]. Their work motivated numerous studies that have documented Columbia Glacier through its historic retreat, many of which highlight the importance of subglacial water on fast tidewater flow [*Meier and Post*, 1987]. For example, Walters and Dunlap [1987] showed that tidal forcing, precipitation, and surface melt dominates Columbia Glacier's flow variations; the latter two indicating that sliding is the primary mechanism of flow [*Rasmussen*, 1988]. Walters [1989] then demonstrated that the impact of tidal forcing was localized to the lower 2 kilometers of the terminus. Further upglacier, drilling expeditions discovered that flow was controlled by insolation and precipitation effects [*Kamb et al.*, 1994; *Meier et al.*, 1994], and that the storage and

subsequent release of water in subglacial cavities led to "extra-slowdown" events [*Meier et al.*, 1994]. More significantly, Kamb et al. [1994] showed that increases in glacier speed had a stronger correlation with a peak in meltwater storage as opposed to the timing of meltwater input and output. Later on, glacial seismic and photographic evidence suggest the terminus went afloat in 2007 [*Walter et al.*, 2010], as thinning led to lower effective pressure along the bed. Throughout its retreat, tidal forcing, precipitation, and the input and storage of meltwater have continued to impact flow along Columbia Glacier.

Speeds along grounded tidewater glacier termini are often inversely related to tidal fluctuations [*Walters*, 1989; *O'Neel et al.*, 2001; *Podrasky et al.*, 2014]. Diurnal fluctuations in ocean tides affect the height of the resistive water column, which leads to faster flow during low tides [*Hughes*, 1989]. However, subglacial water pressures along tidewater glacier termini are also directly related to seawater pressure at the calving face [*Meier and Post*, 1987]; therefore, high tides lead to higher basal water pressure along the terminus. Walters [1989] noted that fluctuations of the resistive water column was the dominant mechanism of tidal-induced flow variations along Columbia Glacier in the 1980s. Since then, the large retreat of Columbia Glacier has significantly altered the glacier's geometry, which could affect the glacier's response to tides.

Columbia Glacier has a history of fast speeds in the winter and spring and slow speeds in late summer and early fall. Between 1983 and 1985, speeds along the lower several kilometers of the terminus ranged from 7 m d^{-1} in summer [*Vaughn et al.*, 1985; *Krimmel and Vaughn*, 1987; *Walters and Dunlap*, 1987] to 15 m d^{-1} in winter [*Krimmel and Vaughn*, 1987]. In 1987, summer speeds were >6 m d^{-1} over the lower 6 km, even after the meltwater evacuation of subglacial conduits led

to "extra slowdown" events [*Meier et al.*, 1994]. More recently, the glacier has continued the pattern of a late summer reduction in flow, though the seasonally low speeds are now slower and approach 2 m d^{-1} (e.g. Figure 18c) in fall.

Here, we present terrestrial radar interferometric (TRI) observations of short-term variability from Oct 2014 (red box in Figure 18), a period that coincided with low insolation (Figure 18a) and the onset of seasonally low speeds (Figure 18c). The remnants of Tropical Storm Phanfone entered from the southwest mid-way through our study, which altered velocity patterns. We observed both branches to be highly sensitive to precipitation and tidal forcing, consistent with earlier studies. We used these observations to investigate: 1) how precipitation and tidal forcing affect Columbia

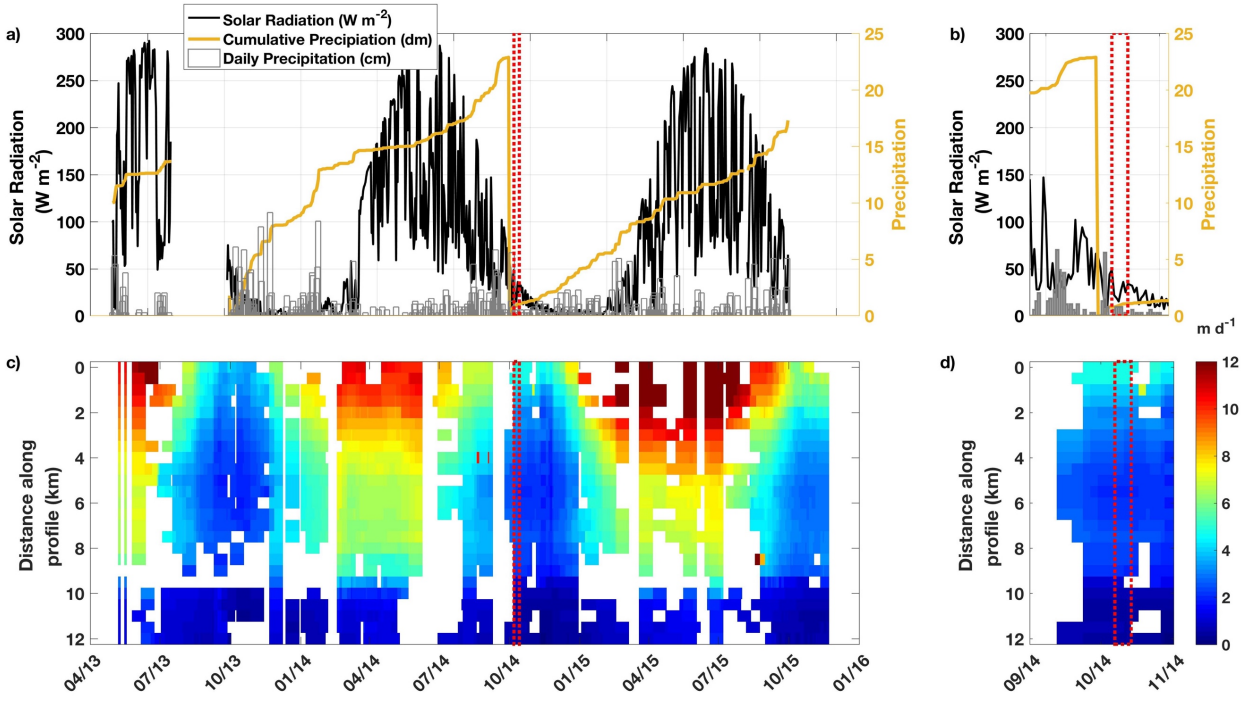

Figure 18: (a) Precipitation and insolation records from a Natural Resources Conservation Service weather station in nearby Valdez. (c) Satellite record of speeds from Fahnestock et al, (2015) sampled along the profile in Figure 17. Red dashed boxes indicate the time of our field study. (b) and (d) same as (a) and (c) but for Sep – Nov 2014. Units of precipitation are centimeters for daily and decimeters for cumulative.

Glacier's flow in its present state; 2) how the spatial patterns of the response to precipitation relate to recent bed maps of topography and what they suggest about stability along the termini of both branches; and 3) what the short-term variations in speed suggest about the causes of seasonal transitions in flow.

4.2 Methods

We performed a field study at Columbia Glacier from 7-14 Oct 2014 to monitor short-term variations in speed. We deployed a Gamma Remote Sensing GPRI-II terrestrial radar interferometer at a bedrock camp ~4 km from the Main Branch terminus and ~8 km from the West Branch terminus (Figure 17). The radar scanned 180º in azimuth and 16 km in range every 3 minutes with limited breaks due to high winds. Raw radar data were processed to single-look complex (SLC) images and then co-registered to the first SLC in the record to account for subtle azimuth offsets due to winds. Differential motion interferograms were generated to observe changes in speed. The interferograms were multi-looked by 10 pixels in range and filtered with an adaptive filter [*Goldstein and Werner*, 1998] to reduce noise. We used a minimum cost flow (mcf; Goldstein et al, [1988]) phase unwrapper to convert relative phase differences to true phase displacements. We reduced phase unwrapping errors by subtracting a phase reference map prior to unwrapping, unwrapped using the mcf tool, and then added the reference phase back to the interferogram. This approach reduced phase differences to within 1 integer cycle throughout each scene, minimizing erroneous jumps in phase during unwrapping. Next, we stacked interferograms in 15-minute intervals to reduce atmospheric effects. Finally, we converted line-of-sight displacements to speeds in the direction of flow using PyCorr-derived flow vectors as outlined in

section 2.2.1.3. All results were projected into local UTM coordinates, and all times are presented in UTC.

We compared TRI-derived speeds with the tidal record from Valdez, ~30 km due east of Columbia Glacier. We used data from a Natural Resources Conservation Service Snow Telemetry (SNOTEL) site to assess air temperatures and precipitation. SNOTEL maintains multiple sites throughout the region, including Valdez (closest to Columbia Glacier); however, the site on Esther Island was chosen due to its location, ~60 km southwest (238º) of Columbia Glacier, and the southwesterly trajectory of Tropical Storm Phanfone. The air temperatures from Esther Island (elevation: 15 m) were reduced by 2.4º to account for an adiabatic lapse rate of 2ºC per 308 m (1000 ft) at an elevation of 380 meters, the mean elevation of both glacier surfaces within the far range of the TRI viewing geometry.

4.3 Results

Initially, speeds were low, which indicated the glaciers had already transitioned to seasonally slow flow. However, speeds increased midway through our observation period, coincident with the arrival of precipitation from Tropical Storm Phanfone from the southwest.

4.3.1 Speeds along the Main Branch

Between 8 and 10 Oct, speeds along the Main Branch varied from 2-4 m d^{-1} at the terminus and 1-2 m d^{-1} upglacier (Figure 19a). The semi-diurnal variations in speed indicated the lowermost 1.5 km of the glacier was tidally modulated with low tides (Figure 19c) resulting in fast flow (Figure 19a). Minimal precipitation occurred during the early record, including some snow (Figure 19d). However, the remnants of Tropical Storm Phanfone arrived late on 10 Oct, which increased air temperatures and delivered considerable rain to the region (Figure 19d). Speeds started to increase,

but did not peak until 13 Oct (Figure 19a, c) when speeds at the terminus reached 5 m d^{-1} and the ice upglacier flowed 2-3 m d^{-1}. The largest change occurred behind the calving front. Speeds 4 – 8 km along the profile increased to 200% of original speeds, whereas speeds at the terminus only increased ~50% (Figure 19b). The precipitation and resultant increase in speed also increased the extent of the upglacier response to the tidal forcing to at least 2 km. This occurred as the tidal amplitude, the difference between the daily mean high and low tides [*O'Neel et al.*, 2003], had decreased (Figure 19c, gray line), indicating a transition from spring to neap tides.

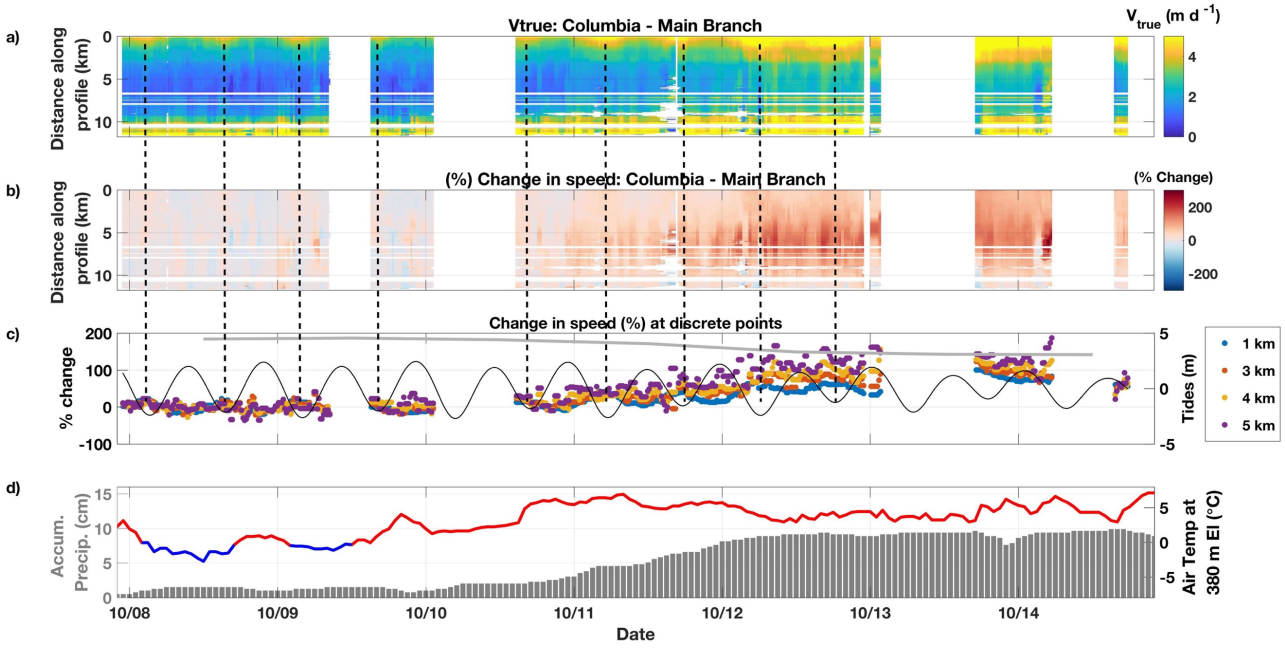

Figure 19: Time-series of speeds for the centerline profile along the Main Branch shown in Figure 17. (a) speeds, (b) the percent change in speed, and (c) speeds (colors) at discrete pixels along the profile with the tides (black) and tidal amplitude (gray). (d) accumulated precipitation (gray) and temperatures (red/blue) at 380 m elevation, the mean elevation of glacier surfaces within far range of TRI geometry; blue indicates temperature below freezing.

4.3.2 Speeds along the West Branch

The change in speed along the West Branch was larger and occurred earlier than on the Main Branch. Between 8 and 10 Oct, speeds within 0.5 km of the calving front were ~8 m d^{-1}, while speeds upglacier were slower and ranged between 0.5 and 2 m d^{-1}; only the first 0.5-km of the glacier was tidally modulated (Figure 20a, c). Speeds started to increase late on 10 Oct, coincident with the arrival of rain (Figure 20d), and then peaked on 11 Oct. Speeds at the calving front increased to 13 m d^{-1}, while speeds >2 km upglacier ranged from 2-5 m d^{-1}. Once again, the largest percent change in speed occurred >2 km behind the calving front and increased >300%. During and after the precipitation, the extent of the glacier that experienced tidal modulations increased to ~3.0 km (Figure 20c). Similar to the Main Branch, the change in tidal forcing occurred as the tidal amplitude was decreasing.

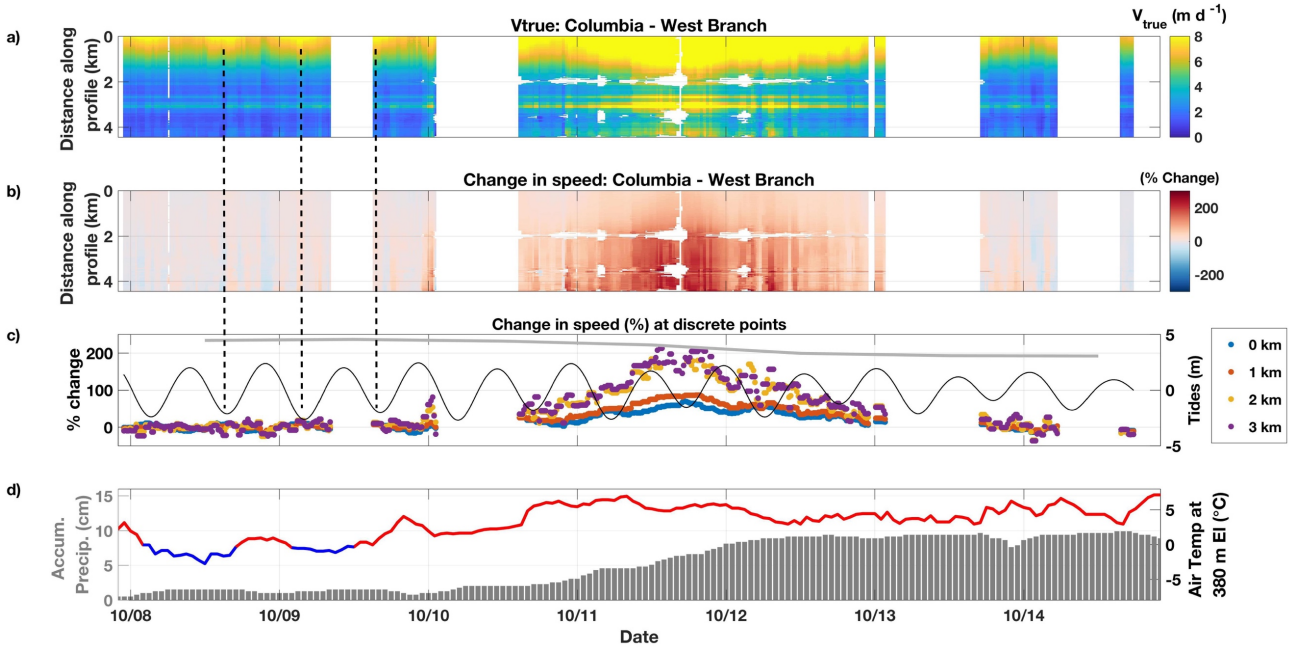

Figure 20: Time-series of speeds along a centerline profile along the West Branch shown in Figure 17. (a) speeds, (b) the percent change in speed, and (c) speeds (colors) at discrete pixels along the profile with the tides (black) and tidal amplitude (gray). (d) accumulated precipitation (gray) and temperatures (red/blue) at 380 m elevation; blue indicates temperature below freezing.

4.4 Discussion

Columbia Glacier has historically exhibited a strong response to precipitation, surface melt, and tidal forcing [*Walters and Dunlap*, 1987; *Walters*, 1989; *Kamb et al.*, 1994; *Meier et al.*, 1994], all of which invoke changes in subglacial hydrology. We observed significant increases in speed (Figure 19, Figure 20) coincident with the arrival of Tropical Storm Phanfone, which suggests a hydrologic control on the speedup. Here, we take a closer look at the spatial variations in the response to precipitation (section 4.4.1) and the coincident change in tidal forcing (section 4.4.2). In section 4.4.3, we evaluate changes in sliding through variations in effective pressure. Finally, in section 4.4.4, we discuss the implications for seasonal variations in subglacial hydrology and speed.

4.4.1 Response to precipitation

To evaluate the response to precipitation along the Main Branch, we compared the mean speeds calculated on 8 Oct (Figure 21a - before precipitation) with those on 12 Oct (Figure 21b – after precipitation). The fastest speeds were consistently observed nearest the terminus, and further upglacier (Figure 21a; 6788 km N, 505 km E) where the Main Branch converges with the East Branch in a submarine channel and surface slopes along the Main Branch are steep. In contrast, speeds were slower in the intermediate region and showed greater response to precipitation. Here, early on, flow was quite uniform across the glacier, and speeds ranged from 0.5 to 1.0 m d^{-1} (Figure 21a). After the precipitation, speeds doubled and were representative of fast tidewater glacier flow through a submarine channel (Figure 21b, c). Bed elevations range from 50 – 250 m below sea level along the lower 10 km [*McNabb et al.*, 2012; *Rignot et al.*, 2013a]. Our data demonstrate that the hydrological impacts were most profound in deepest portions of the submarine channel.

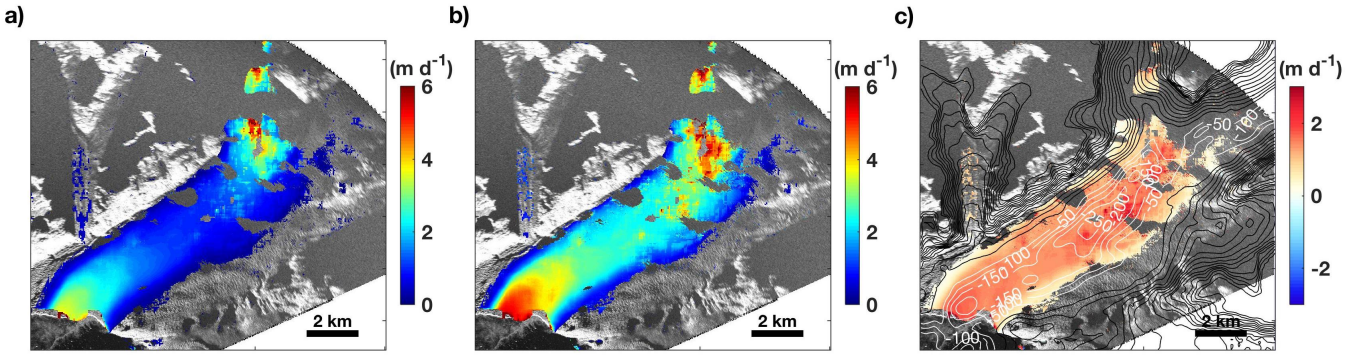

Figure 21: Response to precipitation along Main Branch. Mean speeds (a) before and (b) after precipitation event. (c) The change in speed after precipitation; white (black) contours are bed elevations below (above) sea level from McNabb et al, 2012.

The West Branch showed a similar response to precipitation. Prior to the event, speeds were fastest nearest the calving front (Figure 22a; 5-7 m d^{-1}), and slower upglacier (~1 m d^{-1}). The mean speeds between 11-12 Oct (after precipitation) increased to ~11 m d^{-1} at the terminus, and ~5 m d^{-1} upglacier (Figure 22b). Once again, the greatest increase in speed occurred behind the calving front (Figure 22c). Such a large-scale response implies a change in the subglacial hydrology similar to that along the Main Branch. Although a bed elevation model based on mass conservation [*McNabb et al.*, 2012] shows bed elevations along the West Branch that are above sea level, recent retreat of the West Branch terminus and subsequent re-occupation with sea water indicates that bed elevations in this region are grounded below sea level for some distance upglacier from the terminus. Furthermore, hydrographic work sampled at the time of the TRI survey shows depths at the calving front are ~300 m below sea level *[Campbell, 2014]*. Radar sounding of Columbia Glacier's bed has been conducted, but has been limited to the Main and East Branches (e.g. *Rignot et al*, [*2013]*), and thus provides no estimate for the West Branch. Nonetheless, the fast flow rates observed (>10 m d^{-1}) are typical of tidewater glaciers and are an order of magnitude higher than rates observed for non-surging terrestrial glaciers with similar slopes. The characteristically fast

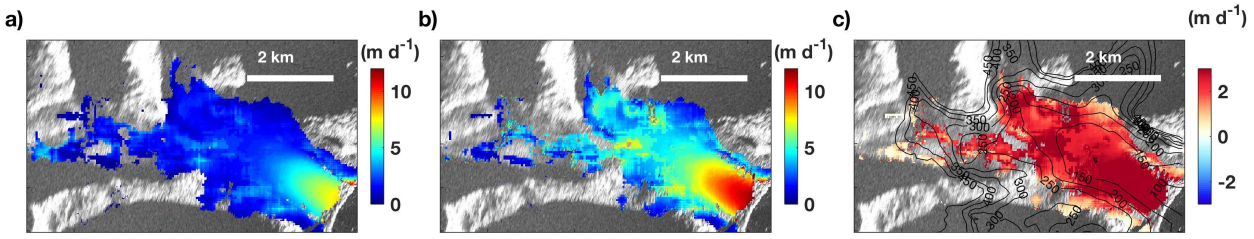

Figure 22: Response to precipitation along the West Branch. Mean speeds (a) before and (b) after precipitation event. (c) The change in speed due to precipitation; contours are bed elevations above sea level from McNabb et al, (2012).

flow of tidewater glaciers is due, in large part, to the high-pressure environments of their submarine beds; high basal water pressures are necessary to counter basal marine water pressures and facilitate the subglacial discharge of meltwater [*Meier and Post*, 1987]. Some terrestrial glaciers can reach high speeds (m d^{-1}) during surge phases [*Kamb et al.*, 1985; *Truffer and Harrison*, 2006; *Harrison et al.*, 2008]; however, Columbia Glacier is not known to be a surge-type glacier. The large response to precipitation, the high speeds (m d^{-1}) observed *before* precipitation, and the hydrography along the calving front all suggest a submarine bed. This implies calving retreat along the West Branch may continue, and further suggests that efforts to characterize Columbia Glacier's bed topography should include refined estimates along the West Branch.

These observations show an increase in glacier speed that coincided with onset of precipitation. Earlier records from Valdez show significant precipitation events between 9 and 16 Sep and again on 4 Oct (Figure 18b) with little precipitation in between. The records show solar radiation values were >1 order of magnitude lower than peak rates in Jun and Jul and approaching an annual minimum (Figure 18a). Cool air temperatures on 8 and 9 Oct produced snow prior to the arrival of the tropical storm (Figure 19d); field notes indicate 10-15 cm of snow in camp (elevation 399 m). Tropical Storm Phanfone arrived from the southwest on 10 Oct, which advected warm air and

moisture into the region (Figure 19d). Assuming a temperature lapse rate of 2ºC per 308 m, and using the record from Esther Island, the snow/rain transition likely occurred at ~1500 m, which approximately coincides with the snow line in Figure 17. Therefore, hydrologic inputs were seasonally low at the start of our field season. Glaciers speeds increased on 11 Oct (Figure 20; West Branch) and 13 Oct (Figure 19; Main Branch), which suggests the addition of water to the glacial hydrologic system led to the increase in speed. However, previous studies show that speed variations along Columbia Glacier correlate better with peaks in storage of meltwater than with input of water to the system [*Kamb et al.*, 1994; *Meier et al.*, 1994]. Such a mechanism could explain the discrepancy in the timing of the response between the branches. The West Branch responded to precipitation within several hours, while the peak in speeds along the Main Branch occurred almost 2 days after the precipitation event.

4.4.2 A change in tidal forcing

The time-series in Figure 19 and Figure 20 showed evidence of semi-diurnal variations in speed coincident with the tides. More significantly, the magnitude and areal extent of tidal influence increased later in the record when a transition to neap tide should have resulted in reduced tidal forcing. Therefore, the additional precipitation may have increased speeds and enhanced tidal forcing along both glaciers. We performed a tidal admittance analysis [*Walters and Dunlap*, 1987; *O'Neel et al.*, 2003; *Podrasky et al.*, 2014] along both branches to characterize the change in tidal response. We used the methods outlined in section 2.4.3 to calculate the admittance amplitude (units: m d^{-1} m^{-1}) and difference in phase (units: radians) from the M2 tidal constituent (principal lunar semi-diurnal). We evaluated the tidal admittance during the first half of the record (7 Oct 22:55 – 10 Oct 00:55) and again during the second half (10 Oct 15:18 – 14 Oct 17:48), when

enhanced flow resulted from heavy precipitation. Pixels with a signal-to-noise ratio (SNR) less than 0.5 were considered unreliable and were removed.

4.4.2.1 Main Branch

Early on, a tidal influence was detected near the calving front and upglacier near the convergence between the Main and East Branches. SNR levels were too low in the area in between to determine admittance. The highest amplitudes occurred near the calving front (Figure 23a; dark purple) and decayed upglacier (white). The difference in phase (Figure 23b) shows that speeds along the lower terminus were anti-correlated with the tides, while the phase upglacier correlated with the tides. Tidal response was strongest in the lowermost 1.5 km of the glacier, wherein semi-diurnal modulations in water depth impacted speeds nearest the calving front through variations in the height of the water column that resisted flow along the calving face [*Hughes*, 1989]. Low tides shortened the resistive column and led to faster flow, which is consistent with earlier studies [*Walters and Dunlap*, 1987].

Tidal forcing was different later in the record. Admittance amplitude decreased at the calving front, but increased upglacier, including the center of the glacier where noise levels previously impeded detection of a tidal signal. Phase differences reduced along the calving front, but were still out of phase with the tides (Figure 23d, orange), while phase differences upglacier were closer to 0. This suggests that speeds along the entire lower 10 km of the Main Branch showed a response to the tides (Figure 23c) as a result of the precipitation; though, the low admittance amplitudes indicate tidal forcing was minimal.

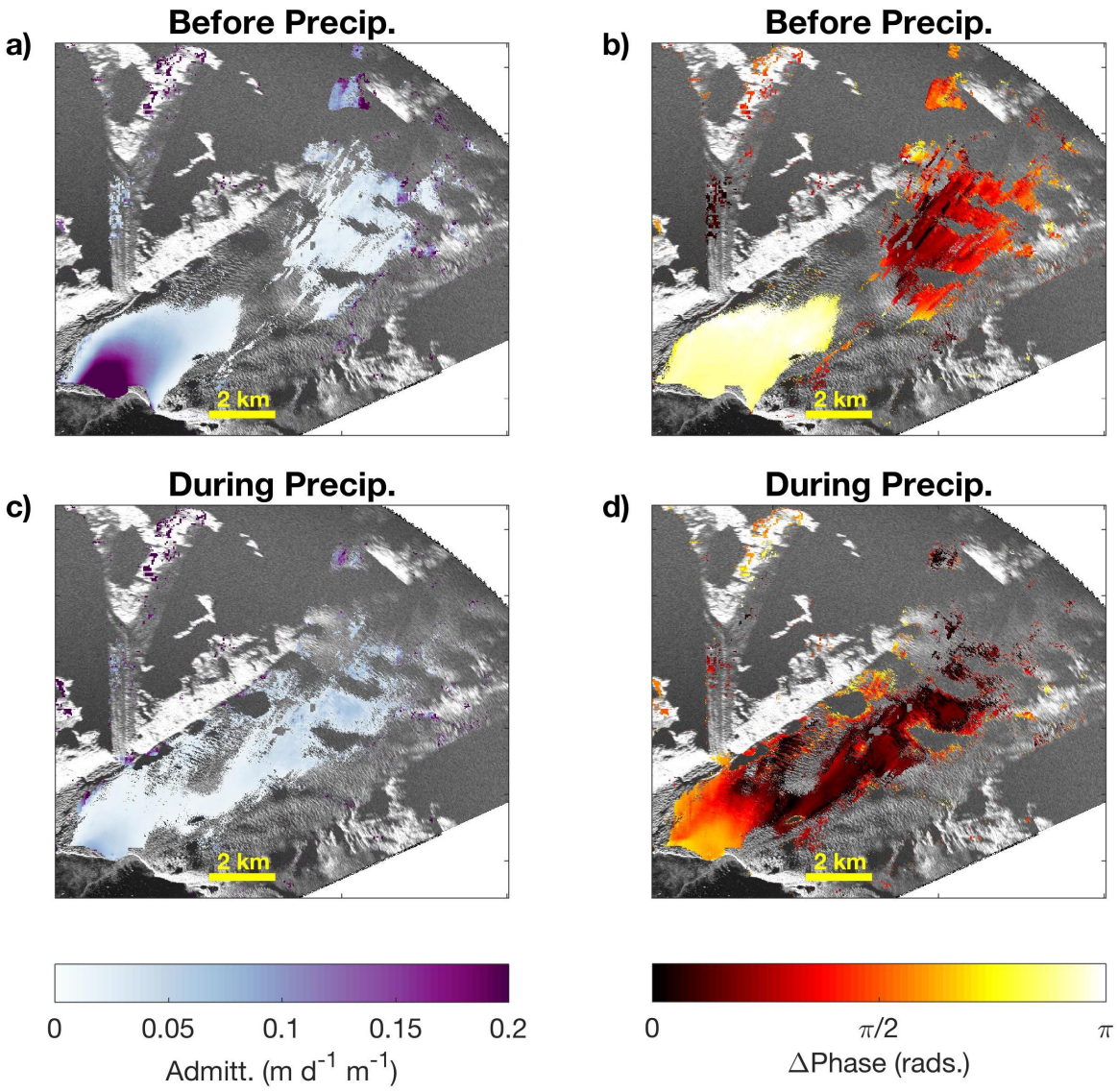

Figure 23: Change in tidal forcing along Main Branch. (a) admittance amplitude and (b) phase difference before precipitation, and the (c) admittance amplitude and (d) phase difference during precipitation.

The most significant finding is the reduction in admittance amplitude nearest the calving front, which suggests a change in the tidal forcing mechanism in response to the influx of water to the subglacial hydrology. Walters [1989] identified the two different ways in which ocean tides modulate glacier speeds: 1) through variations in the height of the resistive water column [*Hughes*, 1989] at the calving face that results in an anticorrelation between glacier speeds and tidal height,

and 2) through the pressurization of the basal water system where speed variations and tidal height correlate. Walters further identified the former as the dominant tidal forcing mechanism at Columbia Glacier from data collected over 30 days in the summers of 1984, 1985, and 1986 [*Walters and Dunlap*, 1987; *Walters*, 1989]. The reduction in phase to some intermediate value (~$\pi/2$) after the rain event suggests the pressurization of the basal water system was equally as significant as the change in height of the resistive water column.

A second possibility for the change in tidal admittance is that pulses of water from the addition of rainwater that reached the bed along the Main Branch may have coincided with high tides. The timing of the water reaching the bed is unknown, and thus may have biased the harmonic analysis if one or more pulses occurred during high tide. The Main Branch analysis is complicated by a smaller signal than what was observed along the West Branch (see below). Furthermore, the perturbation only covers ~2.5 tidal cycles and peaked on 13 Oct when a large gap in data appears due to high winds.

4.4.2.2 West Branch

The change in tidal admittance along the West Branch was similar to the Main Branch, though the effect following the addition of water was greater. Before precipitation (7 Oct 22:55 – 10 Oct 00:55), only the ice within 1 km of the calving front showed any response (Figure 24a; admittance amplitude 0.1-0.2 m d^{-1} m^{-1}). The calving front was anti-correlated with the tides (Figure 24b); thus, low tides led to faster speeds. Further upglacier, SNR levels were too low to discern any tidal influence. After precipitation, the SNR increased and the admittance amplitude approached 0.2 m

d^{-1} m^{-1} along the entire 4.5 km of the viewable terminus (Figure 24c), and phase differences approached 0 (Figure 24d); high tides led to faster flow.

The change in tidal admittance suggests a switch in the tidal forcing mechanism similar to that along the Main Branch. Prior to the precipitation, the highly localized and anticorrelated response to tides suggest that the variations in the height of the resistive water column along the calving front was the dominant tidal forcing mechanism. However, the increase in admittance amplitude and correlated response after precipitation suggests that pressurization of the basal hydrology was the dominant tidal forcing. Subglacial water pressures are directly tied to sea-water pressure

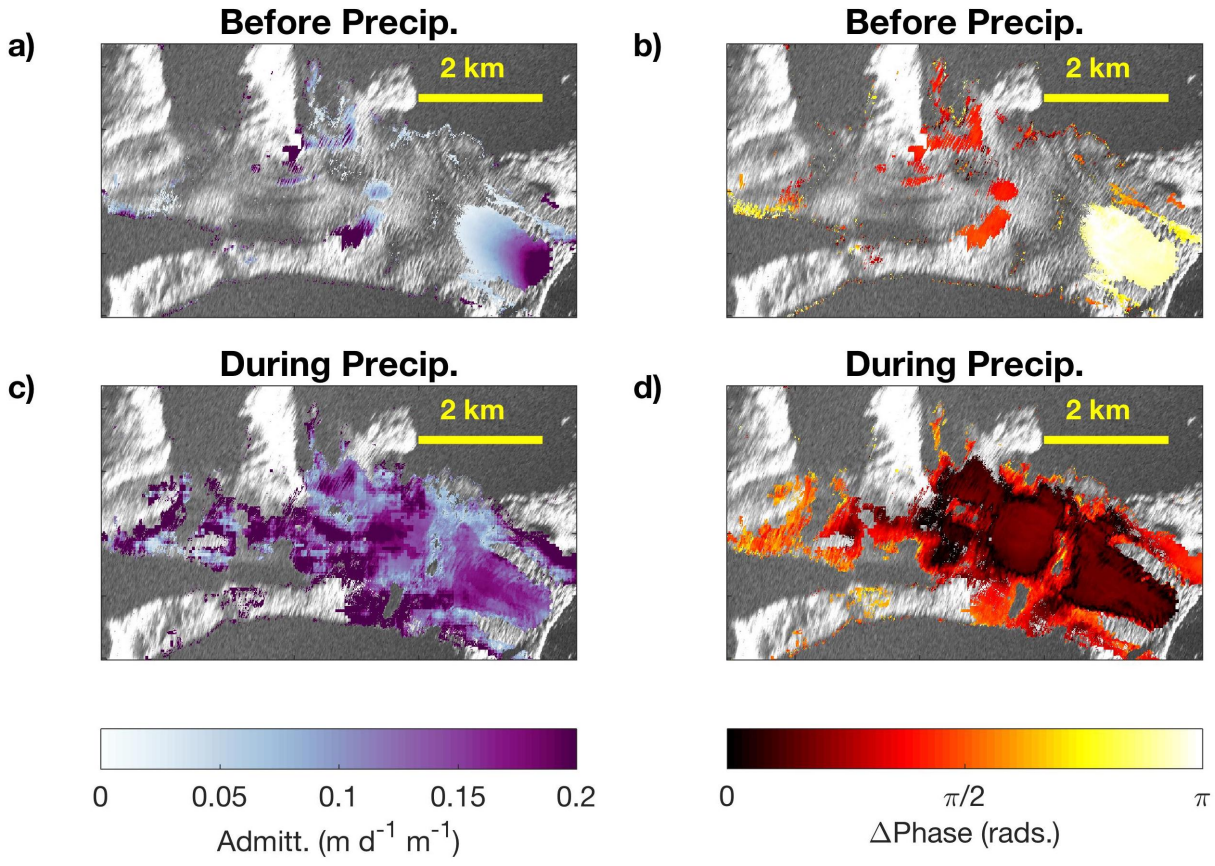

Figure 24: ***Change in tidal forcing along West Branch. (a) admittance amplitude and (b) phase difference before precipitation, and after (c) and (d), respectively.***

[*Meier and Post*, 1987]. The influx of precipitation increased basal water pressures. Soon after, the rising tide increased water pressures further, which evoked the large response observed. Such observations were not observed in earlier studies [*Walters and Dunlap*, 1987; *Walters*, 1989] when Columbia Glacier was much thicker [*McNabb et al.*, 2011]. Thus, the change in tidal forcing mechanism may be a consequence of thinner ice and lower effective pressures. Finally, the large spatial and in-phase response of speeds with tides suggests that the West Branch is grounded in a submarine bed for at least the first 4.5 kilometers.

4.4.3 Change in effective pressure

We observed that a significant precipitation event coincided with large increases in speed and appears to have impacted the tidal forcing along both branches. Such large changes in speed over short time periods are indicative of changes in basal conditions, and specifically sliding. Variations in effective pressure, the difference between the glaciostatic and subglacial water pressures, have a significant effect on sliding. This is illustrated in conventional sliding laws (equation 1; Budd et al, [1979], Bindschadler [1983]), where u is the sliding speed, P_e is the effective pressure, n is Glen's flow law parameter, m is a constant, and k is a dimensional scaling parameter; τ_d is the driving stress defined as the product of ice density (ρ_i), gravity (g), ice thickness (h), and the sine of the surface slope (α).

$$u = k\tau_d^n P_e^{-m} \qquad (1)$$

For tidewater glaciers, Pfeffer [2007] expanded equation 1 to include the flotation thicknesses ($h_f = D_w\rho_w/\rho_i$), which is the critical thickness where ice becomes buoyant; D_w is the water depth and ρ_w is the density of sea water (Equation 2). Following Pfeffer's approach, we use the flotation

thickness in a representation of effective pressure to produce an estimate of sliding along a submarine bed.

$$u = k(\rho_i g)^{n-m} \frac{(\alpha h)^n}{(h-h_f)^m} \qquad (2)$$

We begin by arranging equation 2 to define the scaling parameter *k.* We make general assumptions for constant parameters (Table 2), and calculate the surface slope (α) from a digital elevation model [*Kienholz et al.,* 2015]. Bed elevations, ice thickness, and surface speeds are evaluated for each pixel. Bed elevations were derived from *McNabb et al, [2012]*. Ice thicknesses are calculated by differencing the bed topography from the DEM ice surface. We use measurements from 7 Oct (before precipitation) for *u* to determine a value for *k,* which we evaluate at each pixel to account for spatially varying parameters not accounted for in the sliding law (equation 1), such as bed roughness and longitudinal and lateral stress. *K* has been shown to vary temporally in response to the opening and closing of conduits on seasonal time-scales [*Iken and Truffer,* 1997]; however, variations in *k* are likely to be negligible over the few days of our study.

Table 2: List of constants used in model

Parameter	Value
ρ_i	917 kg m^{-3}
ρ_ω	1030 kg m^{-3}
n	3
m	1
α	1.48
g	9.8 m s^{-2}

Next, we plug the values of *k* in equation 2 and calculate a sliding speed for the Main Branch. Because of our local solution for *k,* the results produced the 7 Oct values (Figure 25a); thus, the values represent sliding speeds in the pre-perturbed state. The assumption is that basal water

pressure was at its lowest and therefore fixed by the depth of the bed below sea level. We further assume that the influx of precipitation to the subglacial hydrology increased basal water pressure, which consequently impacted effective pressure. To simulate this, we subtracted an additional term, H_{pert}, in the denominator (equation 3). We iterated H_{pert} until the difference between the measured and predicted speed was small along the glacier. The calculation was confined to the Main Branch because the depths of the submarine portion of the West Branch are unknown.

$$u = k(\rho_i g)^{n-m} \frac{(\alpha h)^n}{(h - h_f - H_{pert})^m} \qquad (3)$$

We found a value of 32.5 m applied over the whole domain (Figure 25b) produced reasonable results with the measured rates on 14 Oct (Figure 25c). This is equivalent to 328 kPa, or about 10% of the ice overburden pressure along the terminus. This represents the additional water pressure necessary for the increased flux of water to exit the subglacial terminus. This simple model assumes a uniform increase in pressure over the lower 10 km of the terminus, which is unlikely given the varying bed topography and ice thicknesses over the large area (~17 km^2). It also oversimplifies changes in the subglacial hydrology and neglects resistance along the lateral margins, which is illustrated in the error map (Figure 25d). The greatest errors occur along the margins where the bed is shallow *[McNabb et al, 2012*], the ice is thin, and shear stress along the bedrock (north) and slow ice (south) resist flow. In contrast, errors are low in the center of the channel where lateral stresses are minimal, and changes in the subglacial hydrology are likely to have the greatest effect. Despite the large errors, this simple model illustrates how changes in effective pressure, such as a sudden increase in subglacial water pressures due to a higher flux of water being introduced to the system, can influence sliding and therefore speed along Columbia Glacier.

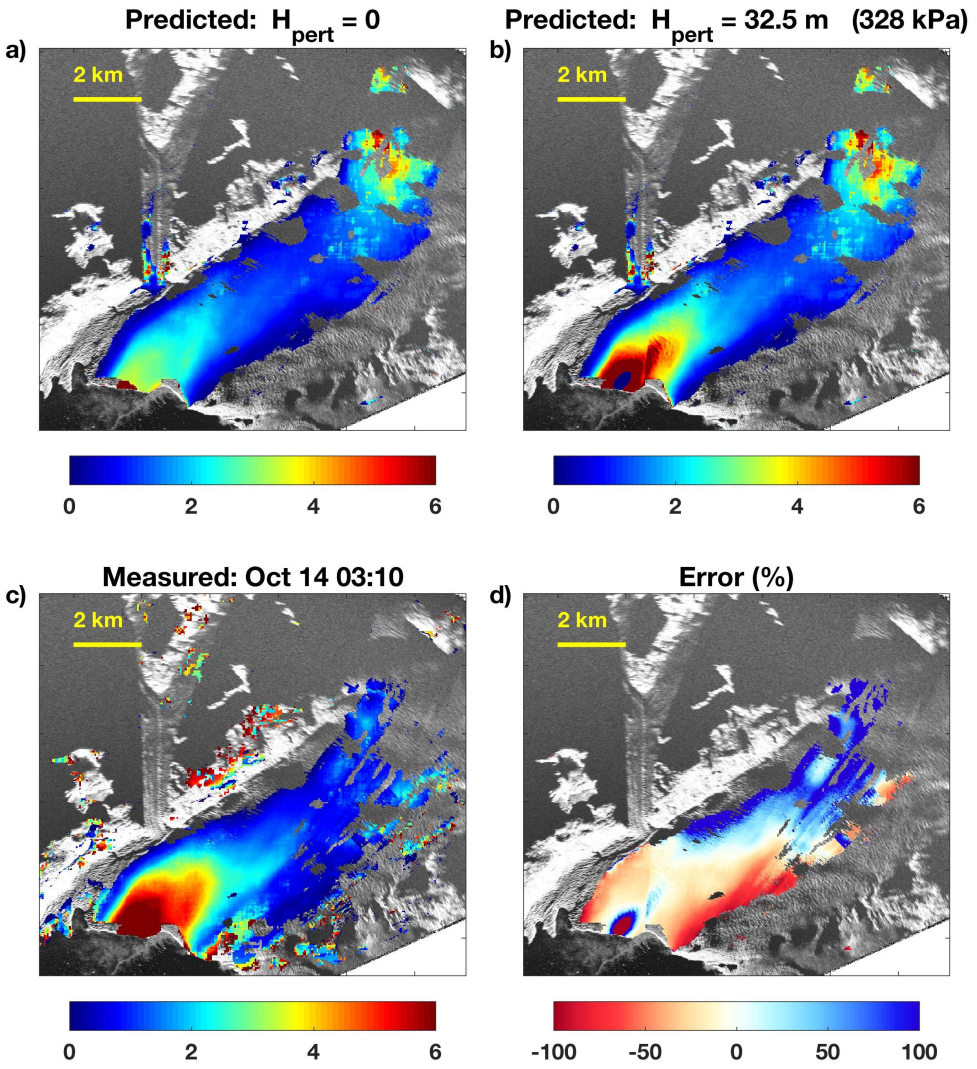

Figure 25: Speed variations due to changes in effective pressure. Predicted sliding speeds (a) before and (b) after a perturbation in effective pressure caused an influx of precipitation; (c) Observed measurements from 14 Oct (after precipitation); (d) error between (b) and (c).

4.4.4 Subglacial change and the Implications for seasonal variations in speed

Our observations were made in October (red dashed box in Figure 18c) during a period of seasonally low flow. Surface melt had been decreasing since July and only a couple precipitation events had occurred within the previous month; thus, hydrologic inputs were at an annual

minimum (see also 4.4.1). Tropical Storm Phanfone delivered rain, which added water to the subglacial hydrologic system and invigorated glacier flow.

These observations have implications for the seasonal variations in glacier speed. The combined effects of precipitation in late spring followed by an increase in summer insolation (e.g. Figure 18a) provides significant meltwater to the subglacial hydrologic system. Initially, this increases water pressure in subglacial cavities, which drives effective pressures lower. However, the sustained increase in meltwater through the summer leads to a reduction in basal water pressure due to the inverse relationship between flux and subglacial water pressure in a steady state channelized system [*Rothlisberger*, 1972]. The reduction in insolation in late summer lowers meltwater inputs, which lowers basal water pressures, and consequently increases effective pressures that slow the glacier in the summer (e.g. Columbia Glacier in September). A similar process works in reverse as water pressure drops. The continued reduction of meltwater later in the year initially raises effective pressures because the large conduits accommodate reduced water flow with low pressure gradients.

Large-scale thinning along Columbia Glacier's submarine terminus has reduced ice thicknesses, and therefore ice overburden stress, by approximately half [*McNabb et al.*, 2012]. The subsequent reduction in effective pressure has led to an increased sensitivity of basal motion to changes in basal water pressure, which might explain the large response to precipitation in Oct 2014. Furthermore, because the rate of tunnel closure scales with the cube of the effective stress [*Nye*, 1953], thinner ice along the lower terminus leads to longer closure times of subglacial conduits.

This results in extended periods of low water pressure during periods of reduced insolation, and therefore very slow speeds in fall (e.g. pre-precipitation flow rates).

4.5 Conclusions

We performed a terrestrial radar interferometric study along Columbia Glacier in October 2014 to investigate short-term perturbations in speeds during a period of seasonally slow flow. We observed a significant change in speed following a fall precipitation event, with the largest changes occurring a few kilometers behind the calving fronts. The precipitation also impacted the tidal response along both branches.

Along the Main Branch, the precipitation-induced speed effects had the greatest influence along the submarine portions of the bed. An analysis of effective pressure demonstrates that the addition of water to the subglacial hydrologic system could have reduced effective pressure, which enhanced sliding and permitted faster flow. The change in basal hydrology also increased the extent of the glacier that experienced tidal influence. The West Branch showed a similar response to precipitation. An analysis of effective pressure was not performed as bed elevations here were inferred to be above sea level in the current bed model [*McNabb et al.*, 2012], but this is likely to be incorrect. However, the low (several meters per day) flow rates observed before the precipitation, the large response in precipitation, a strong response to tidal forcing, and a recent hydrography study in front of the calving face all indicate Columbia's West Branch is grounded below sea level. Our results indicate that the submarine bed extends at least 4.5 km of the present terminus, and thus suggests the glacier will continue to experience dynamic changes.

The large response to precipitation suggests changes to the subglacial hydrology beneath both glacier termini. The occurrence of these events during a seasonally slow flow implies that conduit systems beneath the glaciers were ill-equipped to accommodate the surge of water. As a result, the reduction in effective pressure moved the glaciers closer to flotation and enhanced speeds. Based on these observations and invoking Rothlisberger's [1972] theoretical work, we infer that large seasonal variations in Columbia Glacier's speed are the result of variations in the basal hydrology, specifically the size of subglacial conduits.

5 CONCLUSIONS

Characterizing the response of tidewater glaciers to perturbations along their calving fronts is imperative for predictions of tidewater glacier evolution and the resultant impact to sea level. Our understanding is hindered by a lack of high resolution observations that measure the response to dynamic processes along the terminus. Iceberg calving, ocean tides, and variations in ice mélange are dynamic processes that influence tidewater glacier flow, but they occur on spatial and temporal scales that are difficult to observe with traditional measurement techniques. The results presented in this thesis demonstrate that terrestrial radar interferometers (TRI), a relatively new tool, can be used to acquire high-resolution time-series of these processes; the techniques and results presented establish TRI as a viable tool in future studies.

The observations and analysis presented in Chapter 2 show that the large dynamic response to a small calving retreat of Jakobshavn Isbræ is indicative of a tidewater glacier that is close to flotation, and therefore sensitive to small variations in bed topography. A subsequent re-advance of the terminus, coupled with the advection of thick ice from an overdeepening a short distance upglacier, reduced speeds and restabilized the terminus. The response demonstrates the competing effects of dynamic thinning and ice thickening through advection processes. Thick ice that occupies a deep fjord can restabilize a terminus following a perturbation to the calving front, which may slow the rate of retreat. However, such processes are likely to be unsustainable over long time scales as recent thinning and negative mass balance trends deplete ice upglacier, which will reduce stabilizing effects of advection processes. The results also emphasize the need for refined bed

models and estimates of ice thickness for predictions of tidewater glacier evolution. Several efforts are underway to map the bed and surface topography of the Greenland and Antarctic ice sheets, including the scheduled launch of NASA's ICESat-2 in 2018. Combining these new records with TRI observations of tidewater glacier response to short-term perturbations in flow will enable comprehensive predictions of tidewater glacier evolution.

The observations presented in Chapter 3 provide the first known evidence of a granular ice mélange impeding calving along a tidewater glacier, a phenomenon that has been hypothesized but not observed in the field. Previous studies have shown a mélange influence on calving that is highly dependent on a robust winter sea ice matrix. However, summer ice mélange is typically an agglomeration of icebergs that lack a sea ice matrix. Laboratory experiments and numerical models show that a granular ice mélange can support stress through the development of grain bridges and iceberg contact forces. Our results suggest this does and has occurred at Jakobshavn Isbræ, whose densely packed, perennial ice mélange represents one end member in the ice mélange spectrum. Future advances will be made by studies that focus on the characteristics of a granular ice mélange that can impede calving. For example, what is the required packing density of icebergs in the mélange necessary to impose stress? What is the residence time of icebergs in the mélange? How does the subglacial melt impact stress fields? How does the mélange character vary seasonally? Additionally, the greatest advances will be made by expanding observations to other fjord systems, which will help constrain the conditions by which granular ice mélange influences calving; fjord systems with reasonably high iceberg calving and retention rates are most favorable.

In chapter 4, I showed that a precipitation event forced a large response in speed along Columbia Glacier, and for the West Branch, a change in tidal forcing; both indicate a change in the subglacial hydrology. This has important implications for basal sliding due to the impact on effective pressure, as was demonstrated with a simple sliding model. These results, coupled with Columbia Glacier's substantial thinning history and subsequent decrease in overburden stress, suggest that longer subglacial conduit closure times keep basal water pressures low in fall. As a result, sliding rates along Columbia Glacier's submarine bed are seasonally slow in the fall. Future work should include attempts to map the evolution of the subglacial conduit(s) through the hydrologic year.

Columbia Glacier is unique in that the current retreat has occurred in modern times and has been well documented. As a result, numerous tidewater glacier studies can be traced back to Columbia Glacier. Many Greenlandic tidewater glaciers are now in retreat. If Columbia Glacier serves as an example, then efforts should be made to conduct extensive, long-term field campaigns at a few candidate sites around the Greenland Ice Sheet, as has been suggested by Straneo et al [2013].

The field of glaciology has evolved from theodolite studies to GPS and radar surveys. The addition of terrestrial radar interferometry to the glaciologist's arsenal has increased our temporal and spatial sampling capabilities. This has clear advantages for monitoring tidewater glacier response to short-term perturbations, which can complement longer observational records to provide a more comprehensive understanding of rapid, dynamic changes along tidewater glacier termini. The challenge that remains is to understand the influence that short-term perturbations in glacier flow have on the long-term evolution of tidewater glacier retreat.

REFERENCES

Amundson, J. M. (2016), A mass-flux perspective of the tidewater glacier cycle, *Journal of Glaciology*, *62*(231), 82–93, doi:10.1017/jog.2016.14.

Amundson, J. M., Fahnestock M, M. Truffer, J. Brown, M. P. L. U. thi, and R. J. Motyka (2010), Ice m\'elange dynamics and implications for terminus stability, Jakobshavn Isbræ, Greenland, *J. Geophys. Res. Earth Surf.*, *115*, F01005.

Amundson, J. M., M. Truffer, M. P. Lüthi, Fahnestock M, M. West, and R. J. Motyka (2008), Glacier, fjord, and seismic response to recent large calving events, Jakobshavn Isbræ, Greenland, *Geophysical Research Letters*, *35*(22), L22501, doi:10.1029/2008GL035281.

Bamber, J. L. et al. (2013), A new bed elevation dataset for Greenland, *The Cryosphere*, *7*(2), 499–510, doi:10.5194/tc-7-499-2013.

Bamber, J. L., D. G. Vaughan, and I. Joughin (2000a), Widespread Complex Flow in the Interior of the Antarctic Ice Sheet, *Science*, *287*(5456), 1248–1250, doi:10.1126/science.287.5456.1248.

Bamber, J. L., R. J. Hardy, and Joughin I (2000b), An analysis of balance velocities over the Greenland ice sheet and comparison with synthetic aperture radar interferometry, *Journal of Glaciology*, *46*(152), 1–8.

Bartholomaus, T. C., C. F. Larsen, and S. O′Neel (2013), Does calving matter? Evidence for significant submarine melt, *Earth and Planetary Science Letters*, *380*, 21–30, doi:10.1016/j.epsl.2013.08.014.

Bindschadler, R. (1983), The importance of pressurized subglacial water in separation and sliding at the glacier bed, *Journal of Glaciology*, *29*(101), 3–19.

Briner, J. P., N. E. Young, R. Thomas, H. A. M. Stewart, S. Losee, and S. Truex (2011), Varve and radiocarbon dating support the rapid advance of Jakobshavn Isbræ during the Little Ice Age, *Quaternary Science Reviews*, *30*(19-20), 2476–2486, doi:10.1016/j.quascirev.2011.05.017.

Brinkerhoff, D., M. Truffer, and A. Aschwanden (2017), Sediment transport drives tidewater glacier periodicity, *Nature Communications*, 1–8, doi:10.1038/s41467-017-00095-5.

Budd, W. F., P. L. Keage, and N. A. Blundy (1979), Empirical studies of ice sliding, *Journal of Glaciology*, *23*, 157–170.

Caduff, R., F. Schlunegger, A. Kos, and A. Wiesmann (2014), A review of terrestrial radar interferometry for measuring surface change in the geosciences, *Earth Surf. Process.*

Landforms, *40*(2), 208–228, doi:10.1002/esp.3656.

Campbell (2014). Hydrographic Survey of Columbia Bay, October 8-11, 2014. A report prepared for the Regional Citizen's Advisory Council Prince William Sound Science Center, Cordova, AK

Cassotto, R., M. Fahnestock, J. M. Amundson, M. Truffer, and I. Joughin (2015), Seasonal and interannual variations in ice melange and its impact on terminus stability, Jakobshavn Isbræ, Greenland, *Journal of Glaciology*, *61*(225), 76–88, doi:10.3189/2015JoG13J235.

Clarke, T. S., and K. Echelmeyer (1996), Seismic-reflection evidence for a deep subglacial trough beneath Jakobshavns Isrbrae, West Greenland, *Journal of Glaciology*, *43*(141), 1–14.

Das, S. B., Joughin I, M. D. Behn, I. M. Howat, M. A. King, D. Lizarralde, and M. P. Bhatia (2008), Fracture Propagation to the Base of the Greenland Ice Sheet During Supraglacial Lake Drainage, *Science*, *320*(5877), 778–781, doi:10.1126/science.1153360.

de Juan, J. et al. (2010), Sudden increase in tidal response linked to calving and acceleration at a large Greenland outlet glacier, *Geophysical Research Letters*, *37*(12), L12501, doi:10.1029/2010GL043289.

Dixon, T. H., D. Voytenko, C. LEMBKE, S. Peña, I. Howat, N. GOURMELEN, C. Werner, and B. ODDSSON (2012), Emerging technology monitors ice-sea interface at outlet glaciers, *EOS*, *93*(48), 497–498, doi:10.1029/2012EO480001.

Enderlin, E. M., and G. S. Hamilton (2014), Estimates of iceberg submarine melting from high-resolution digital elevation models: application to Sermilik Fjord, East Greenland, *Journal of Glaciology*, *60*(224), 1084–1092, doi:10.3189/2014JoG14J085.

Enderlin, E. M., I. M. Howat, S. Jeong, M.-J. Noh, J. H. van Angelen, and M. R. ven den Broeke (2014), An improved mass budget for the Greenland ice sheet, *Geophysical Research Letters*, *41*, 866–872.

Fahnestock, M., T. Scambos, T. Moon, A. Gardner, T. Haran, and M. Klinger (2015), Rapid large-area mapping of ice flow using Landsat 8, *Remote Sens Environ*, *185*, 1–11, doi:10.1016/j.rse.2015.11.023.

Fastook, J. L., H. H. Brecher, and T. J. Hughes (1995), "Derived Bedrock Elevations, Strain Rates and Stresses from Measured Surface Elevations and Velocities - Jakobshavns Isbrae, Greenland, *Journal of Glaciology*, *41*(137).

Foga, S., L. A. Stearns, and C. J. van der Veen (2014), Application of Satellite Remote Sensing Techniques to Quantify Terminus and Ice Mélange Behavior at Helheim Glacier, East Greenland, *Marine Technology Society Journal*, *58*(5), 81–91.

Goldstein, R. M., and C. L. Werner (1998), Radar interferogram filtering for geophysical applications, *Geophysical Research Letters*, *25*(21), 4035–4038, doi:10.1029/1998GL900033.

Goldstein, R. M., H. A. Zebker, and C. L. Werner (1988), Satellite radar interferometry: Two-dimensional phase unwrapping, *Radio Science*, *23*(4), 713–720, doi:10.1029/RS023i004p00713.

Hanssen, R. F. (2001), *Radar Interferometry. Data Interpretation and Error Analysis*, Kluwer Academic Publishers, Hingham, US.

Harrison, W. D., R. J. Motyka, M. Truffer, O. Eisen, M. T. Moran, C. F. Raymond, and M. A. Fahnestock (2008), Another surge of Variegated Glacier, Alaska, USA, 2003/04, *Journal of Glaciology*, *54*(184), 192–194, doi:10.1594/PANGAEA.655702.

Holland, D., R. Thomas, B. D. Young, M. H. Ribergaard, and B. Lyberth (2008), Acceleration of Jakoshavn Isbrae triggered by warm subsurface ocean waters, *Nature Geoscience*, *1*, 659–664.

Holland, David M.; Holland, Denise (2016). AIR TEMPERATURE, RELATIVE HUMIDITY, and others collected from Automatic Weather Station installed on rock outcrop in Jakobshavn Glacier Ice Front from 2007-10-13 to 2016-02-14 (NCEI Accession 0148760). Version 1.1. NOAA National Centers for Environmental Information. Dataset. 5 Dec 2017

Hopkins, M. A., and J. Tuhkuri (1999), Compression of floating ice fields, *Journal of Geophysical Research*, *104*(C7), 15815–15825.

Howat, I. M., J. E. Box, A. Yushin, A. Harrington, and E. M. McFadden (2010), Seasonal variability in the dynamics of marine-terminating outlet glaciers in Greenland, *Journal of Glaciology*, *56*(198), 601–613.

Hughes, T. (1989), Calving Ice Walls, *Annals of Glaciology*, *12*, 74–80.

Iken, A., and M. Truffer (1997), The relationship between subglacial water pressure and velocity of Findelengletscher, Switzerland, during its advance and retreat, *Journal of Glaciology*.

James, T. D., T. Murray, N. Selmes, K. Scharrer, and M. O'Leary (2014), Buoyant flexure and basal crevassing in dynamic mass loss at Helheim Glacier, *Nature Geoscience*, *7*(8), 593–596, doi:10.1038/ngeo2204.

Joughin, I., B. Smith, I. Howat, and T. Scambos. 2014. *MEaSUREs Greenland Ice Velocity: Selected Glacier Site Velocity Maps from InSAR.* [WCoast-69.10N, 2012]. Boulder, Colorado USA: NASA National Snow and Ice Data Center Distributed Active Archive Center. http://dx.doi.org/10.5067/MEASURES/CRYOSPHERE/nsidc-0481.001.

Joughin, I., B. E. Smith, D. E. Shean, and D. Floricioiu (2014), Brief Communication: Further summer speedup of Jakobshavn Isbræ, *The Cryosphere*, *8*(1), 209–214, doi:10.5194/tc-8-209-2014.

Joughin, I., B. E. Smith, I. M. Howat, D. Floricioiu, R. B. Alley, M. Truffer, and M. Fahnestock (2012), Seasonal to decadal scale variations in the surface velocity of Jakobshavn Isbrae,

Greenland: Observation and model-based analysis, *Journal of Geophysical Research*, *117*(F2), doi:10.1029/2011JF002110.

Joughin, I., B. E. Smith, I. M. Howat, T. Scambos, and T. Moon (2010), Greenland flow variability from ice-sheet-wide velocity mapping, *Journal of Glaciology*, *56*(197), 415–430.

Joughin, I., I. M. Howat, M. Fahnestock, B. Smith, W. Krabill, R. B. Alley, H. Stern, and M. Truffer (2008), Continued evolution of Jakobshavn Isbrae following its rapid speedup, *Journal of Geophysical Research*, *113*(F4), F04006, doi:10.1029/2008JF001023.

Joughin, I., W. Abdalati, and M. Fahnestock (2004), Large fluctuations in speed on Greenland's Jakobshavn Isbrae glacier,, *432*, 608–610.

Kamb, B., C. F. Raymond, W. D. Harrison, H. Engelhardt, K. A. Echelmeyer, N. F. Humphrey, M. M. Brugman, and W. Pfeffer (1985), Glacier surge mechanism: 1982–1983 surge of Variegated Glacier, Alaska, *Science*.

Kamb, B., H. Engelhardt, M. A. Fahnestock, N. F. Humphrey, M. Meier, and D. Stone (1994), Mechanical and hydrologic basis for the rapid motion of a large tidewater galcier. 2. Interpretation, *J geophys Res*, *99*(B8), 15231–15244.

Kienholz, C., S. Herreid, J. L. Rich, A. A. Arendt, R. Hock, and E. W. Burgess (2015), Derivation and analysis of a complete modern-date glacier inventory for Alaska and northwest Canada, *Journal of Glaciology*, *61*(227), 403–420, doi:10.3189/2015JoG14J230.

Krabill, W. et al. (2004), Greenland Ice Sheet: Increased coastal thinning, *Geophysical Research Letters*, *31*(24), doi:10.1029/2004GL021533.

Krimmel, R. M., and B. H. Vaughn (1987), Columbia Glacier, Alaska: Changes in velocity 1977-1986, *Journal of Geophysical Research*, *92*(B9), 8961–8968.

Krug, J., G. Durand, O. Gagliardini, and J. Weiss (2015), Modelling the impact of submarine frontal melting and ice mélange on glacier dynamics, *The Cryosphere*, *9*, 989–1003, doi:10.5194/tc-9-989-2015.

Luckman, A., and T. Murray (2005), Seasonal variation in velocity before retreat of Jakobshavn Isbræ, Greenland, *Geophysical Research Letters*, *32*(8), doi:10.1029/2005GL022519.

Luthi, M., M. Funk, A. Iken, S. Gogineni, and M. Truffer (2002), Mechanisms of fast flow in Jakobshavn Isbrae, West Greenland: Part III. Measurements of ice deformation, temperatureandcross-boreholeconductivityinboreholes to the bedrock, *Journal of Glaciology*, *48*(162), 369–385.

MacAyeal, D., J. Freed-Brown, W. W. Zhang, and J. M. Amundson (2012), The influence of ice melange on fjord seiches, *Annals of Glaciology*, *53*(60), 45–49, doi:10.3189/2012/AoG60A027.

McNabb, R. W. et al. (2012), Using surface velocities to calculate ice thickness and bed

topography: a case study at Columbia Glacier, Alaska, USA, *Journal of Glaciology*, *58*(212), 1151–1164, doi:10.3189/2012JoG11J249.

McNabb, R. W., and R. Hock (2014), Alaska tidewater glacier terminus positions, 1948-2012, *J. Geophys. Res. Earth Surf.*, *119*(2), 153–167, doi:10.1002/2013JF002915.

McNabb, R. W., R. M. Hock, S. O'Neel, and A. Rasmussen (2011), A New Bed Topography Map for Columbia Glacier, *AGU Fall Meeting Abstracts*, *-1*, 0677.

Meier, M. F., A. Post, L. A. Rasmussen, W. G. Sikonia, and L. R. Mayo (1979), *Retreat of Columbia Glacier, Alaska*, United States Geological Survey.

Meier, M. F., and A. Post (1987), Fast Tidewater Glaciers, *Journal of Geophysical Research*, *92*(B9), 9051–9058.

Meier, M., S. Lundstrom, D. Stone, B. Kamb, H. Engelhardt, N. F. Humphrey, W. W. Dunlap, M. Fahnestock, R. M. Krimmel, and R. Walters (1994), Mechanical and hydrologic basis for the rapid motion of a large tidewater glacier, *Journal of Geophysical Research*, *99*(B8), 15–219–15–229.

Moon, T., and I. Joughin (2008), Changes in ice front position on Greenland's outlet glaciers from 1992 to 2007, *Journal of Geophysical Research*, *113*, 1–10, doi:10.1029.

Moon, T., D. A. Sutherland, D. Carroll, D. Felikson, L. Kehrl, and F. Straneo (2017), Subsurface iceberg melt key to Greenland fjord freshwater budget, *Nature Geoscience*, 1, doi:10.1038/s41561-017-0018-z.

Morlighem, M., E. Rignot, J. Mouginot, H. Seroussi, and E. Larour (2014), Deeply incised submarine glacial valleys beneath the Greenland ice sheet, *Nature Geoscience*, *7*(6), 418–422, doi:10.1038/ngeo2167.

Mortensen, J., Bendtsen J, K. Lennert, and Rysgaard S (2014), Seasonal variability of the circulation system in a west Greenland tidewater outlet glacier fjord, Godthåbsfjord (64°N), *J. Geophys. Res. Earth Surf.*, *119*(12), 2591–2603, doi:10.1002/2014JF003267.

Mortensen, J., Bendtsen J, R. J. Motyka, K. Lennert, M. Truffer, Fahnestock M, and Rysgaard S (2013), On the seasonal freshwater stratification in the proximity of fast-flowing tidewater outlet glaciers in a sub-Arctic sill fjord, *J. Geophys. Res. Oceans*, *118*(3), 1382–1395, doi:10.1002/jgrc.20134.

Motyka, R. J. et al. (2017), Asynchronous behavior of outlet glaciers feeding Godthåbsfjord (Nuup Kangerlua) and the triggering of Narsap Sermia, *Journal of Glaciology*, 1–21, doi:10.1017/jog.2016.138.

Motyka, R. J., L. Hunter, K. A. Echelmeyer, and C. Connor (2003), Submarine melting at the terminus of a temperate tidewater glacier, LeConte Glacier, Alaska, U.S.A, *Annals of Glaciology*, *36*, 57–65.

Motyka, R. J., M. Truffer, M. Fahnestock, J. Mortensen, S. Rysgaard, and I. Howat (2011), Submarine melting of the 1985 Jakobshavn Isbræ floating tongue and the triggering of the current retreat, *J. Geophys. Res. Earth Surf.*, *116*(F), F01007–n/a, doi:10.1029/2009JF001632.

Motyka, R. J., W. P. Dryer, J. Amundson, M. Truffer, and M. Fahnestock (2013), Rapid submarine melting driven by subglacial discharge, LeConte Glacier, Alaska, *Geophysical Research Letters*, *40*(19), 5153–5158, doi:10.1002/grl.51011.

Motyka, R., M. Fahnestock, and M. Truffer (2010), Volume change of Jakobshavn Isbrae, West Greenland: 1985 - 1997 - 2007, *Journal of Glaciology*, *56*(198), 635–646.

Nettles, M. et al. (2008), Step-wise changes in glacier flow speed coincide with calving and glacial earthquakes at Helheim Glacier, Greenland, *Geophysical Research Letters*, *35*(24), L24503, doi:10.1029/2008GL036127.

Nghiem, S. V., D. K. Hall, T. L. Mote, M. Tedesco, M. R. Albert, K. Keegan, C. A. Shuman, N. E. DiGirolamo, and G. Neumann (2012), The extreme melt across the Greenland ice sheet in 2012, *Geophysical Research Letters*, *39*(20), n/a–n/a, doi:10.1029/2012GL053611.

Nick, F. M., C. J. van der Veen, and J. Oerlemans (2007), Controls on advance of tidewater glaciers: Results from numerical modeling applied to Columbia Glacier, *Journal of GeoPHYSICAL …*, *112*.

Nye, J. F. (1953), The flow law of ice from measurements in glacier tunnels, laboratory experiments and the Jungfraufirn borehole experiment, *Proceedings of the Royal Society of London. Series A, Mathematical and Physical Sciences*, *219*(1139), 477–489.

O'Neel, S., K. A. Echelmeyer, and R. J. Motyka (2001), Short-term flow dynamics of a retreating tidewater glacier: LeConte Glacier, Alaska, U.S.A, *Journal of Glaciology*, *47*(159), 567–578, doi:10.3189/172756501781831855.

O'Neel, S., K. A. Echelmeyer, and R. J. Motyka (2003), Short-term variations in calving of a tidewater glacier: LeConte Glacier, Alaska, U. S. A, *Journal of Glaciology*, *49*(167), 587–598, doi:10.3189/172756503781830430.

Oltmanns, M., F. Straneo, G. W. K. Moore, and S. H. Mernild (2014), Strong Downslope Wind Events in Ammassalik, Southeast Greenland, *Journal of Climate*, *27*(3), 977–993, doi:10.1175/JCLI-D-13-00067.1.

Pawlowicz, R., B. Beardsley, and S. Lentz (2002), Classical tidal harmonic analysis including error estimates in MATLAB using T_TIDE, *Computers & Geosciences*, *28*(8), 929–937, doi:10.1016/S0098-3004(02)00013-4.

Peters, I. R., J. M. Amundson, R. Cassotto, M. Fahnestock, K. N. Darnell, M. Truffer, and W. W. Zhang (2015), Dynamic jamming of iceberg-choked fjords, *Geophysical Research Letters*, 1–8, doi:10.1002/(ISSN)1944-8007.

Pfeffer, W. T. (2007), A simple mechanism for irreversible tidewater glacier retreat, *Journal of Geophysical Research*, *112*(F03S25), 1–12, doi:10.1029/2006JF000590.

Podlech, S., and A. Weidick (2004), A catastrophic break-up of the front of Jakobshavn Isbrae, West Greenland, 2002/03, *Journal of Glaciology*, *50*(168), 153–154.

Podrasky, D., M. Truffer, M. Fahnestock, J. Amundson, R. Cassotto, and I. Joughin (2012), Outlet glacier response to forcing over hourly to interannual timescales, Jakobshavn Isbræ, Greenland, *Journal of Glaciology*, *58*(212), 1212–1226, doi:10.3189/2012JoG12J065.

Podrasky, D., M. Truffer, M. Luthi, and M. Fahnestock (2014), Quantifying velocity response to ocean tides and calving near the terminus of Jakobshavn Isbræ, Greenland, *Journal of Glaciology*, *60*(222), 609–621, doi:10.3189/2014JoG13J130.

Post, A. (1975), *Preliminary hydrography and historic terminal changes of Columbia Glacier, Alaska*, U.S. Geological Survey Hydrologic Atlas.

Post, A., S. O'Neel, R. J. Motyka, and G. Streveler (2011), A Complex Relationship Between Calving Glaciers and Climate, *EOS*, *92*(37), 305–307.

Pritchard, H. D., R. J. Arthern, D. G. Vaughan, and L. A. Edwards (2009), Extensive dynamic thinning on the margins of the Greenland and Antarctic ice sheets,, *461*, 971–975, doi:10.1038/nature08471.

Rasmussen, L. A. (1988), Bed Topograpy and Mass-Balance Distribution of Columbia Glacier, Alaska, USA, Determined from Sequential Aerial Photography, *Journal of Glaciology*, *34*(117), 208–216.

Reeh N, Thomsen HH, Higgins AK, and A. Weidick (2001), Sea ice and the stability of north and northeast Greenland floating glaciers, *Annals of Glaciology*, *33*, 474–480.

Rignot, E., and K. Steffen (2008), Channelized bottom melting and stability of floating ice shelves, *Geophysical Research Letters*, *35*(2), L02503, doi:10.1029/2007GL031765.

Rignot, E., and P. Kanagaratnam (2006), Changes in the Velocity Structure of the Greenland Ice Sheet, *Science*, *311*, 986–990, doi:10.1126.

Rignot, E., J. Mouginot, C. Larsen, Y. Gim, and D. Kirchner (2013a), Low-frequency radar sounding of temperate ice masses in Southern Alaska, *Geophysical Research Letters*, *40*(20), 5399–5405, doi:10.1002/2013GL057452.

Rignot, E., M. Koppes, and I. Velicogna (2010), Rapid submarine melting of the calving faces of West Greenland glaciers, *Nature Geoscience*, *3*(3), 187–191, doi:10.1038/ngeo765.

Rignot, E., S. Jacobs, J. Mouginot, and B. Scheuchl (2013b), Ice-Shelf Melting Around Antarctica, *Science*, *341*(6143), 266–270, doi:10.1126/science.1235798.

Ritchie, B. J., C. S. Lingle, R. J. Motyka, and M. Truffer (2008), Seasonal fluctuations in the

advance of a tidewater glacier and potential causes: Hubbard Glacier, Alaska, USA, *Journal of Glaciology*, *54*(186), 401–412.

Robel, A. A. (2017), Thinning sea ice weakens buttressing force of iceberg me ́lange and promotes calving, *Nature Communications*, *8*, 1–7, doi:10.1038/ncomms14596.

Rosenau, R., E. Schwalbe, H.-G. Maas, M. Baessier, and R. Dietrich (2013), Grounding line migration and high-resolution calving dynamics of Jakobshavn Isbrae, West Greenland, *J geophys Res*, n/a–n/a, doi:10.1029/2012JF002515.

Rothlisberger, H. (1972), Water Pressure in Intra- and Subglacial Channels, *Journal of Glaciology*, *11*(62), 177–203, doi:10.3189/S0022143000022188.

Scambos, T. A., J. A. Bohlander, C. A. Shuman, and P. Skvarca (2004), Glacier acceleration and thinning after ice shelf collapse in the Larsen B embayment, Antarctica, *Geophysical Research Letters*, *31*(18), doi:10.1029/2004GL020670.

Sohn, H.-G., K. C. Jezek, and C. J. van der Veen (1998), Jakobshavn Glacier, West Greenland: 30 years of spaceborne observations, *Geophysical Research Letters*, *25*, 2699–2702.

Straneo, F. et al. (2013), Challenges to Understanding the Dynamic Response of Greenland's Marine Terminating Glaciers to Oceanic and Atmospheric Forcing, *Bull. Amer. Meteor. Soc.*, *94*(8), 1131–1144, doi:10.1175/BAMS-D-12-00100.1.

Straneo, F., G. S. Hamilton, D. A. Sutherland, L. A. Stearns, F. Davidson, M. O. Hammill, G. B. Stenson, and A. Rosing-Asvid (2010), Rapid circulation of warm subtropical waters in a major glacial fjord in East Greenland, *Nature Geoscience*, *3*(3), 182–186, doi:10.1038/ngeo764.

Strozzi, T., Kouraev A, A. Wiesmann, U. Wegmuller, Sharov A, and C. Werner (2008), Estimation of Arctic glacier motion with satellite L-Band SAR data, *Remote Sens Environ*, *112*(3), 636–645.

Sundal, A. V., A. Shepherd, M. Van den Broeke, J. Van Angelen, N. Gourmelen, and J. Park (2013), Controls on short-term variations in Greenland glacier dynamics, *Journal of Glaciology*, *59*(217), 883–892, doi:10.3189/2013JoG13J019.

Thomas, R. (2004), Force-pertubation analysis of recent thinning and acceleration of Jakobshavn Isbrae, Greenland, *Journal of Glaciology*, *50*(168), 57–66.

Todd, J., and P. Christoffersen (2014), Are seasonal calving dynamics forced by buttressing from ice mélange or undercutting by melting? Outcomes from full-Stokes simulations of Store Glacier, West Greenland, *The Cryosphere*, *8*(6), 2353–2365, doi:10.5194/tc-8-2353-2014-supplement.

Trabant, D. C., R. M. Krimmel, K. A. Echelmeyer, S. L. Zirnheld, and D. H. Elsberg (2003), The slow advance of a calving glacier: Hubbard Glacier, Alaska, U.S.A, *Annals of Glaciology*, *36*, 45–50.

Truffer, M., and W. D. Harrison (2006), In situ measurements of till deformation and water pressure, *Journal of Glaciology*, *52*(177), 175–182.

van der Veen, C. J. (1996), Tidewater calving, *Journal of Glaciology*, *42*(141), 375–385.

Vaughn, B. H., C. F. Raymond, L. A. Rasmussen, D. S. Miller, C. A. Michaelson, M. F. Meier, R. M. Krimmel, A. G. Fountain, W. W. Dunlap, and C. S. Brown (1985), Short-term velocity measurements at Columbia Glacier, Alaska; August-September 1984, *Open-File Report*.

Vieli, A., and F. M. Nick (2011), Understanding and Modelling Rapid Dynamic Changes of Tidewater Outlet Glaciers: Issues and Implications, *Surv Geophys*, *32*(4-5), 437–458, doi:10.1007/s10712-011-9132-4.

Vieli, A., J. Jania, and L. Kolondra (2002), The retreat of a tidewater glacier: observations and model calculations on Hansbreen, Spitsbergen, *Journal of Glaciology*, *48*(163), 592–600.

Voytenko, D., A. STERN, D. M. Holland, T. H. Dixon, K. Christianson, and R. T. Walker (2015a), Tidally driven ice speed variation at Helheim Glacier, Greenland, observed with terrestrial radar interferometry, *Journal of Glaciology*, *61*(226), 301–308, doi:10.3189/2015JoG14J173.

Voytenko, D., T. H. Dixon, D. M. Holland, R. Cassotto, I. M. Howat, M. Fahnestock, M. Truffer, and S. de la Peña (2017), Acquisition of a 3 min, two-dimensional glacier velocity field with terrestrial radar interferometry, *Journal of Glaciology*, *63*(240), 629–636, doi:10.1017/jog.2017.28.

Voytenko, D., T. H. Dixon, I. M. Howat, N. GOURMELEN, C. LEMBKE, C. L. Werner, S. de la Peña, and B. ODDSSON (2015b), Multi-year observations of Breiðamerkurjökull, a marine-terminating glacier in southeastern Iceland, using terrestrial radar interferometry, *Journal of Glaciology*, *61*(225), 42–54, doi:10.3189/2015JoG14J099.

Voytenko, D., T. H. Dixon, M. E. Luther, C. LEMBKE, I. M. Howat, and S. de la Peña (2015c), Observations of inertial currents in a lagoon in southeastern Iceland using terrestrial radar interferometry and automated iceberg tracking, *Computers & Geosciences*, *82*, 23–30, doi:10.1016/j.cageo.2015.05.012.

Walter, F., S. O'Neel, D. McNamara, W. T. Pfeffer, J. N. Bassis, and H. A. Fricker (2010), Iceberg calving during transition from grounded to floating ice: Columbia Glacier, Alaska, *Geophysical Research Letters*, *37*(15), n/a–n/a, doi:10.1029/2010GL043201.

Walter, J. I., J. E. Box, S. Tulaczyk, E. E. Brodsky, I. M. Howat, Y. Ahn, and A. Brown (2012), Oceanic mechanical forcing of a marine-terminating Greenland glacier, *Annals of Glaciology*, *53*(60), 181–192, doi:10.3189/2012AoG60A083.

Walters, R. (1989), Small-amplitude, short period variations in the speed of a tide-water glacier in South-Central Alaska, U.S.A, *Annals of Glaciology*, *12*, 187–191.

Walters, R. A., and W. W. Dunlap (1987), Analysis of time series of glacier speed: Columbia Glacier, Alaska, *Journal of Geophysical Research*, *92*(B9), 8969–8975.

Weidick, A., N. Mikkelsen, C. Mayer, and S. Podlech (2004), Jakobshavn Isbræ, West Greenland: The 2002–2003 collapse and nomination for the UNESCO World Heritage List, *Geological Survey of Denmark and Greenland Bulletin*

Xie, S., T. H. Dixon, D. Voytenko, D. M. Holland, D. Holland, and T. Zheng (2016), Precursor motion to iceberg calving at Jakobshavn Isbræ, Greenland, observed with terrestrial radar interferometry, *http://dx.doi.org/10.1017/jog.2016.104*, *62*(236), 1134–1142, doi:10.1017/jog.2016.104.

Young, N. E., J. P. Briner, H. A. M. Stewart, Y. Axford, B. Csatho, D. H. Rood, and R. C. Finkel (2011), Response of Jakobshavn Isbrae, Greenland, to Holocene climate change, *Geology*, *39*(2), 131–134, doi:10.1130/G31399.1.